Polymeric Micro- and Nanofabricated Devices for Oral Drug Delivery

by

Cade Brylee Fox

DISSERTATION

Submitted in partial satisfaction of the requirements for the degree of

DOCTOR OF PHILOSOPHY

in

Pharmaceutical Sciences and Pharmacogenomics

in the

GRADUATE DIVISION

of the

UNIVERSITY OF CALIFORNIA, SAN FRANCISCO

Acknowledgments

Thank you to my advisor, Dr. Tejal Desai, for welcoming me into her group, providing excellent advice when needed, and giving me the freedom to pursue my interests and make mistakes. The open and collaborative environment of the Desai Lab, fostered by Tejal and the other members of the lab, made the journey to completing a Ph.D. an exciting and enjoyable experience.

To all of the members of the Desai Lab. Specifically, I am grateful to Dr. Hari Chirra for teaching me so many skills and being an excellent mentor as I transitioned into the lab. I am also thankful to Long Le, Jean Kim, Cameron Nemeth, Dr. Rachel Chevalier, Hari, and everyone else in lab for your friendship, encouragement, and insight.

To the PSPG Program and Dr. Deanna Kroetz, who does an excellent job leading the program and looking out for the students' interests. I'd like to thank my PSPG classmates for all of the great times and making me feel at home immediately after joining the program.

To my qualifying exam and dissertation committee members, Dr. Deanna Kroetz, Dr. Shuvo Roy, Dr. Adam Abate, Dr. Jeffrey Lotz, and Dr. Tejal Desai for their time and valuable advice that significantly improved my research.

To my parents, James and Dara, who have given so much love and time to help me grow as a person and pursue a career in science. You continue to inspire me today.

To my brother and sister, Matayah and Landon, for your friendship, encouragement, and love.

To Jessie, the love of my life. I'd be lost without you.

Elements of this dissertation are adapted from other published work. Chapters 1 and 5 are adapted from "Micro/nanofabricated Platforms for Oral Drug Delivery," a work published in

the *Journal of Controlled Release* and authored by Cade B. Fox, Jean Kim, Long V. Le, Cameron L. Nemeth, Hariharasudhan D. Chirra, and Tejal A. Desai, and "Planar Bioadhesive Microdevices, a New Technology for Oral Drug Delivery," a work published in the *Current Pharmaceutical Biotechnology* and authored by Cade B. Fox, Hariharasudhan D. Chirra, and Tejal A. Desai. Chapter 2 is adapted from "Fabrication of Micropatterned Polymeric Nanowire Arrays for High-Resolution Reagent Localization and Topographical Cellular Control," a work published in *Nano Letters* and authored by Cade B. Fox, Jean Kim, Erica B. Schlesinger, Hariharasudhan D. Chirra, and Tejal A. Desai. Chapter 3 is adapted from "Fabrication of Sealed Nanostraw Microdevices for Oral Drug Delivery," a work published in *ACS Nano* and authored by Cade B. Fox, Yuhong Cao, Cameron L. Nemeth, Hariharasudhan D. Chirra, Rachel W. Chevalier, Alexander M. Xu, Nicholas A. Melosh, and Tejal A. Desai. Chapter 4 shows submitted work by Cade B. Fox, Cameron L. Nemeth, Rachel W. Chevalier, Joshua Cantlon, Derek B. Bogdanoff, Jeff C. Hsiao, and Tejal A. Desai.

I would like to gratefully acknowledge funding for this work, which was provided by the National Institute of Health, the Achievement Awards for College Students Foundation, and Zambon Research Venture.

Abstract

While oral drug administration is by far the most preferred route, it is accompanied by many barriers that limit drug uptake such as the low pH of the stomach, metabolic and proteolytic enzymes, and limited permeability of the intestinal epithelium. As a result, many drugs ranging from small molecules to biological therapeutics have limited oral bioavailability, precluding them from oral administration. To address this issue, microfabrication has been applied to create planar, asymmetric devices capable of binding to the lining of the gastrointestinal tract and releasing drug at high concentrations, thereby increasing oral drug uptake. While the efficacy of these devices has been validated *in vitro* and *in vivo*, modifying their surfaces with nanoscale features has potential to refine their properties for enhanced drug delivery. This dissertation first presents an approach to fabricate polymeric microdevices coated with nanowires in a rapid, high throughput manner. The nanowires demonstrate rapid drug localization onto the surface of these devices via capillary action and increased adhesion to epithelial tissue, suggesting that this fabrication technique can be used to create devices with enhanced properties for oral drug delivery. Also presented are microdevices sealed with nanostraw membranes. The nanostraw membranes provide sustained drug release by limiting drug efflux from the devices, prevent drug degradation by limiting influx of outside biomolecules, and enhance device bioadhesion by penetrating into the mucus layer of the intestinal lining. Finally, an approach that dramatically increases the capacity and efficiency of drug loading into microdevices over previous methods is presented. A picoliter-volume printer is used to print drug directly into device reservoirs in an automated fashion. The technologies presented here expand the capabilities of microdevices for oral drug delivery by incorporating

nanoscale structures that enhance device bioadhesion, tunability of drug release, and drug protection and also provide a more cost-effective and scalable approach to drug loading.

Table of Contents

List of Figures

Chapter 1

Chapter 2

Chapter 3

Chapter 4

Chapter 1 – Introduction

1.1. Abstract

The oral route of drug administration is most preferred due to its ease of use, low cost, and high patient compliance. However, the oral uptake of many small molecule drugs and biotherapeutics is limited by various physiological barriers, and, as a result, drugs suffer from issues with low solubility, low permeability, and degradation following oral administration. The flexibility of micro- and nanofabrication techniques has been used to create drug delivery platforms designed to address these barriers to oral drug uptake. Specifically, micro/nanofabricated devices have been designed with planar, asymmetric geometries to promote device adhesion and unidirectional drug release toward epithelial tissue, thereby prolonging drug exposure and increasing drug permeation. Furthermore, surface functionalization, nanotopography, responsive drug release, motion-based responses, and permeation enhancers have been incorporated into such platforms to further enhance drug uptake. This work will focus on developing techniques to incorporate nanostructures into microdevices and demonstrating that these nanostructures may enhance the properties of these devices for oral drug delivery through mechanisms including enhanced bioadhesion, improved drug loading efficiency, and protection of loaded drug.

1.2. Introduction

Oral drug administration is the most preferred and common route. As opposed to parenteral administration, the oral route typically causes neither tissue damage nor pain and

requires less patient supervision, resulting in high patient compliance and decreased cost of care.[1] Oral drug formulations may also provide advantages over intravenous drug formulations, which can involve injection of solubilizing excipients associated with toxicity and/or altered disposition of coadministered drugs.[2-4] In addition to being the primary route for systemic drug therapy, oral administration allows for localized drug treatment of gastrointestinal (GI) tissue. However, there is currently limited approaches to target diseased tissue.[5, 6] Therefore, diseases of the GI tract are often treated through formulations designed for systemic administration, resulting in system-wide side effects.[5, 7]

While oral administration is most preferred, approximately 50% of active pharmaceutical agents suffer from limited oral uptake.[8, 9] The oral route is associated with issues with 1) drug degradation, 2) low drug solubility, and 3) low drug permeability, preventing uptake of intact drug into the bloodstream.[10] Current approaches to improve drug uptake include permeation enhancers, excipients to enhance drug solubility or provide sustained drug release, micro- and nanoparticulate systems, drug conjugation and modification, enteric coating, metabolic and transporter protein inhibitors, and bioadhesive polymers and ligands, which have been reviewed in detail.[6, 11-19] While these approaches allow for control over many properties of drug delivery systems, they do not typically provide precise geometric control, which can be used to facilitate interaction with the micro- and nanoscale features of GI tract physiology for increased adhesion and tissue permeability.[20, 21]

Photolithography, soft lithography, and nanofabrication approaches can be used to fabricate oral drug delivery systems with precise control over feature geometry, symmetry, dimensions, material composition, and surface modification, allowing for design of microscale devices that specifically address physiological barriers of the GI tract. These fabrication

technologies have also been reviewed in detail previously.[6, 22-25] Application of these approaches to oral drug delivery has been expanding to utilize biocompatible and bioadhesive polymers, asymmetric geometries, nanotopographical features, and materials that respond to environmental cues to improve drug uptake. This review will highlight recent advances in the application of micro/nanotechnology to oral drug delivery and predict how current and developing technologies may be incorporated into these micro/nanofabricated platforms to improve the bioavailability of a wide range of drugs and biotherapeutics.

1.3. Physiological barriers to oral drug delivery

The comprehensive set of barriers to oral drug uptake must be considered when examining the rationale behind microdevice design. Orally administered drugs face a sequential set of barriers to systemic drug uptake as outlined in Figure 1.1. Following oral administration, drugs encounter pH values ranging from 1.5 to 3.5 and digestive enzymes in the stomach and are subsequently exposed to pH values of 5 to 7 and additional proteolytic and metabolic enzymes in the small intestine.[26] After entering the small intestine, the primary site of drug and nutrient uptake, drugs must then pass through a hydrophobic mucous membrane composed of a motile layer moving in contact with an underlying firmly adherent layer.[27] The motile mucus layer ranges between 100 and 500 μm in thickness, and the adherent mucus layer ranges from 0 to 20 μm in thickness.[28, 29] After penetrating the mucus layer, drugs must pass through the glycocalyx, an extracellular matrix approximately 0.5 to 1 μm thick composed of negatively charged glycoproteins, proteoglycans, glycosaminoglycans, and glycolipids.[30, 31]

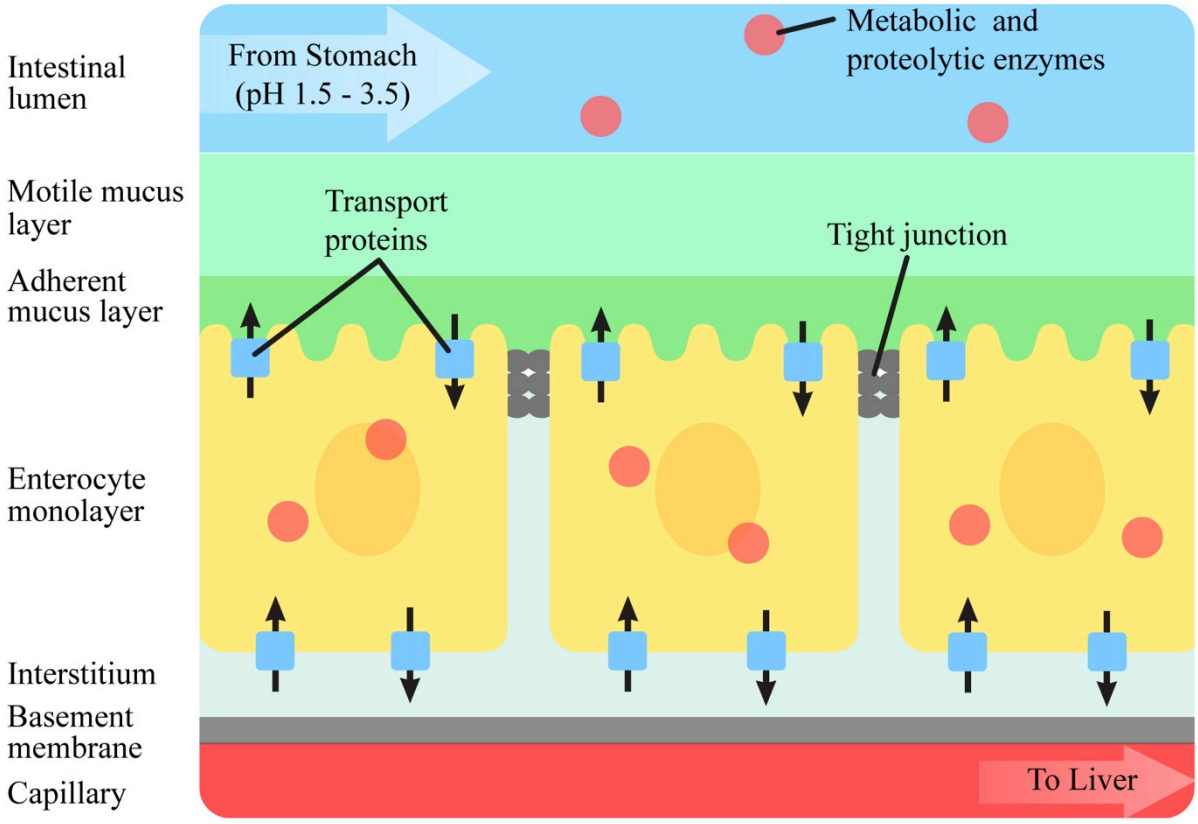

Figure 1.1. Physiological barriers to drug uptake. Drug is first exposed to the low pH of the stomach, from which it enters the small intestine where it is exposed to metabolic and proteolytic enzymes. It must then pass through the motile and adherent mucus layers and subsequently permeate through the enterocyte monolayer by either the transcellular route, where transport proteins and additional enzymes are present, or the paracellular route through tight junctions between cells. Finally, drug must pass through the basement membrane and enter blood flow to the liver.

Drugs must then pass through the polarized enterocyte monolayer by either paracytosis directly through enterocytes or transcytosis through junctions between enterocytes. Paracytosis involves permeation through the apical cell membrane into enterocytes and subsequent permeation through the basal cell membrane into the interstitium. Paracytosis occurs through both passive diffusion through the cell membrane and facilitated diffusion involving transporter

proteins or endocytosis.[32-34] Within the cytosol of enterocytes, drugs are exposed to influx and efflux protein transporters differentially expressed on the apical and basal cell membranes as well as metabolic enzymes.[35] The alternate pathway of transcytosis involves travel between cells through tight junctions, structures between closely associated cells composed of multiprotein complexes with pores approximately 1 to 3 nm in diameter.[36, 37] This small pore size presents a significant obstacle to drug uptake, particularly for high molecular weight therapeutics. These barriers present a unique set of challenges not encountered in other routes of drug administration.

1.4. Rationale for planar, asymmetric microdevices

Like most previously developed oral drug delivery microparticulate systems made via precipitation methods, microdevices are designed on a scale small enough to fit within the features of the intestinal wall, which is made up of micron-sized folds and pits of the intestinal villi.[38] Also, microdevices are designed to be large enough to prevent device uptake into cells through endocytosis. While microdevices are similar in size to many oral drug delivery particulate systems, conventional methods of microfabrication deliver precise and consistent dimensions of microdevices, resulting in much higher monodispersity in size and shape.[23] In addition to providing monodispersity, microfabrication also provides the ability to create devices with custom shapes and dimensions. This ability has been utilized to design devices with a planar design that simultaneously address drug permeability barriers, drug degradation, and low drug solubility.

To address issues with poor drug solubility and increase overall drug exposure, microdevices are designed to be relatively flat, providing multiple advantages for drug transfer. A flat shape increases the surface area in contact with the GI wall, improving adhesive properties

of the device.[6] In addition, a flat microdevice shape decreases the shear force per mass on the devices as shown in Figure 1.2, preventing detachment of the device from the intestinal epithelium and further increasing residence time.[39] To overcome a second major barrier to oral drug uptake, issues with drug permeability, microdevices are designed with reservoirs on only one side of the device, allowing drug to be released in only one direction. In addition to asymmetric shape, devices can be asymmetrically modified with targeting moieties, mucoadhesive materials, and micro- and nanotopography, providing selective binding of the device side from which drug will be selectively released.[6] Thus, microdevices are designed to adhere to the mucosal or GI epithelial layer and release drug to enterocytes in a proximal, unidirectional manner as shown in Figure 1.2. Releasing drug directly toward the epithelial barrier rather than into the lumen provides a more efficient mechanism of drug release by decreasing the loss of drug downstream through the lumen and also increasing the exposure of the enterocytes to the drug. Furthermore, the unidirectional release of drug in a localized, high concentration at the device-intestinal wall interface creates a strong concentration gradient, thereby enhancing drug permeation across the intestinal enterocytes.[39] This localized release of drug in high concentrations may also increase drug uptake through a second mechanism, as high drug concentrations may saturate metabolic enzymes and efflux transporters, in turn increasing the bioavailability of the drug.[40]

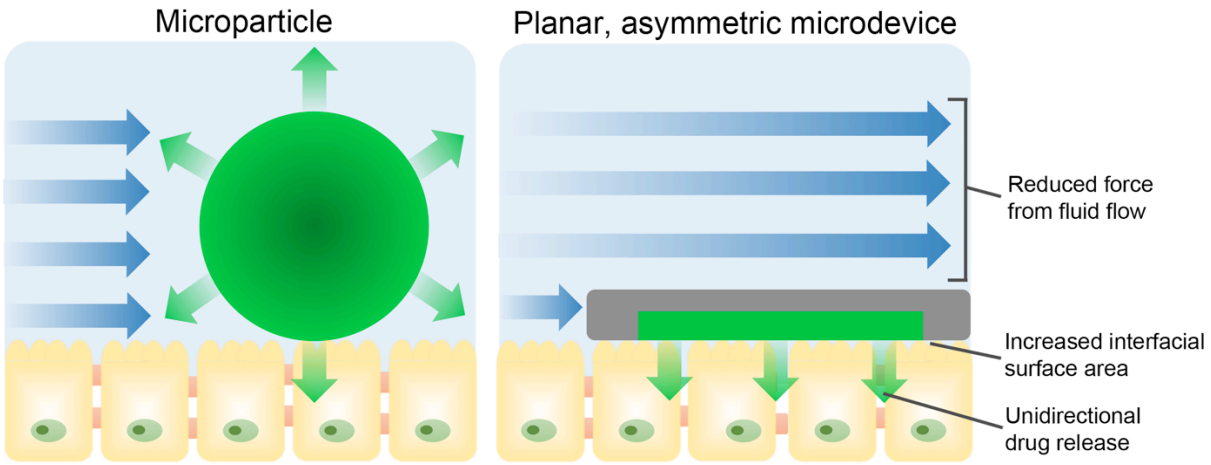

Figure 1.2. In contrast to spherical microparticles, planar, asymmetric microdevices provide proximal, unidirectional drug release and increased residence time in the GI tract. A planar microdevice shape reduces the force experienced from intestinal fluid flow (blue arrows) and increases surface area available for binding to epithelial tissue, increasing device adhesion to the lining of the GI tract and prolonging drug exposure. Devices can be asymmetrically fabricated with a drug reservoir on one side of the device, allowing for proximal, unidirectional release of drug (green) toward epithelial tissue.

Finally, to address the third major barrier to oral drug uptake - drug degradation, microdevices are fabricated to include drug reservoirs that allow for sustained release of drug, thereby decreasing the exposure of drugs to harsh conditions of the GI tract relative to a bolus dose [6]. With a variety of sustained drug release systems developed in the recent past for oral delivery, including pH-sensitive hydrogels,[41-43] enteric coating,[44] and degradable polymers, well established microfabrication techniques can be effectively used to incorporate microdevice reservoirs with these drug systems.[39, 45-47]

In addition to delivery of drugs for systemic uptake, oral microdevices have the potential to treat diseases local to the GI tract including Crohn's disease, inflammatory bowel disease (IBD), and irritable bowel syndrome (IBS). While the site of action of most therapeutics for GI

disorders is in intestinal tissue, many of these drugs in conventional large doses lead to severe systemic side effects.[48, 49] For more efficient treatment of these diseases, microdevices could be modified to adhere to only the diseased GI tissue for localized delivery of drugs directly to the therapeutic target.[50] Direct targeting of sites of inflammation could improve drug efficacy while reducing severity of side effects associated with therapies for diseases of the GI tract.

1.5. Materials utilized for microdevice structure

To prevent toxicity and inflammation, microdevices must be made from biocompatible material. The first systems of oral microdevices used standard semiconductor materials, including silicon oxide and porous silicon as the device material.[21, 51] While silicon and silicon oxide have been found to be relatively non-toxic in some studies,[52-54] they have also been associated with inflammation.[55, 56] In order to overcome this issue, microdevice fabrication shifted towards the use of relatively non-toxic polymers, including hydrogels and biodegradable materials. Poly(methyl methacrylate) (PMMA), an FDA-approved polymeric material[57] used in contact lenses and bone cement and also known to be stable at low pH values,[6] has been utilized in numerous oral microdevice designs.[45, 46, 58-61] Microdevices have also been fabricated from SU-8, an epoxy-based negative photoresist originally developed as an ultra-thick photoresist.[47, 62] While SU-8 is not currently FDA approved, studies have shown that SU-8 is non-toxic as an implantable material.[63-65] Other biocompatible polymers utilized for microdevice fabrication include chitosan,[66] gelatin,[67] poly(lactic-co-glycolic) acid (PLGA),[66-68] polypropylene (PP),[69] and poly(ethylene glycol) (PEG).[39, 62, 66] The intrinsic biocompatibility, biodegradation, hydrophobicity, and structural properties of individual polymers can be tuned by adjusting the

chemical structure of the monomer(s) used in polymer synthesis, the molecular weight of the polymer, and/or the crosslinking density. [66, 70-72]

1.6. Techniques for micro- and nanofabrication of oral drug delivery devices

A variety of fabrication methods, including photolithography, electron beam lithography, x-ray lithography, and soft lithography techniques are available for the fabrication of microdevices. The use of micro- and nanofabrication techniques for biological applications has been reviewed in detail elsewhere, [73-75] but this work will highlight a selection of techniques that are particularly useful for oral microdevice fabrication. Many studies to this date have utilized conventional photolithography techniques originally developed by the microchip industry for the fabrication of microdevices.[21, 39, 45, 47, 60-62, 72, 74-77] Photolithography involves selective UV exposure of a photosensitive material, termed a photoresist, and is often followed by an etching step to transfer the photoresist pattern to a substrate. Typically, the substrate is spin-coated to form a thin film deposition, and a photoresist layer is spin-coated onto the substrate. The photoresist is then exposed to UV light through a mask created with custom patterns by computer-aided design (CAD), transferring the mask pattern through selective polymerization or cleavage of the photoresist in regions exposed to UV light, and non-polymerized or cleaved resist is removed by chemical development. The resist pattern can then be transferred to the substrate through either wet or dry etching processes with the resist acting to selectively protect regions of the substrate. In a straightforward fabrication technique, Tao et al. applied photolithography to fabricate microdevices from SU-8 in a two-step process.[47] A layer of SU-8 was exposed to UV light to form a device base, and then a second layer of SU-8 was UV-exposed to form the walls of drug reservoirs. The use of SU-8 photoresist as the structural component of microdevices eliminates

the need for etching of a substrate material following UV exposure. To create microdevices from non-photoreactive materials, photolithography followed by reactive ion etching (RIE), a dry etching technique involving directional destruction of material by bombardment with chemically reactive plasma, has been employed. [45] As shown in Figure 1.3, Chirra and Desai used two series of steps each composed of photolithography followed by RIE with oxygen plasma to create microdevices with three reservoirs partially etched through the microdevice structure.

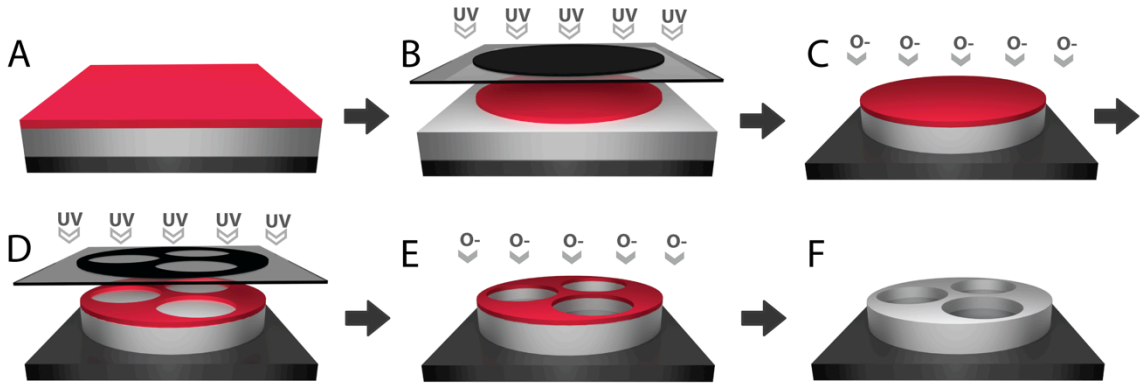

Figure 1.3. Photolithography-based techniques for microfabrication of multi-reservoir PMMA devices. A. PMMA and, subsequently, photoresist are spin-cast onto a silicon wafer. **B.** A circular pattern is transferred from a UV-blocking photomask to the photoresist through UV-induced cleavage. **C.** Reactive ion etching with oxygen plasma directionally destroys PMMA not protected by the photoresist pattern. **D.** Following photoresist removal and re-coating of a fresh resist layer, a reservoir-containing pattern is transferred to the photoresist by UV-exposure. **E.** Reactive ion etching is used to partially etch the PMMA layer to form drug reservoirs. **F.** Photoresist is chemically removed.

While photolithography techniques are often expensive and require access to cleanroom facilities, soft lithography allows for replication of a hard patterned substrate to create an inverse pattern with a soft elastomer such as polydimethylsiloxane (PDMS). The patterned elastomer can

then be used as a master mold to repeatedly pattern a wide range of materials under standard laboratory settings. These patterned elastomers can be used as either a mold, to create devices from recessed regions, or as a stamp, which can be coated with material to create devices or patterned surface modifications in regions of contact. Guan et al. have demonstrated a variety of soft lithography techniques that can be utilized to fabricate microdevices (Figure 1.4).[66, 69, 70, 78] In one study, a micropillar PDMS stamp was coated with PPMA before bringing the stamp into contact with a glass slide coated with polyvinyl alcohol (PVA), creating PPMA microdevices in regions of contact (Figure 1.4A).[69] In contrast, Guan et al. also used a microwell stamp to collect PPMA within recessed regions before bringing the stamp into contact with PVA-coated glass, creating microdevices from the wells of the microstamp (Figure 1.4B).[69] In later studies, a mixture of PEGMA and PEGDMA was applied to a PDMS microwell stamp, allowing for microdevice formation through discontinuous dewetting (Figure 1.4C).[66] As a result of the interactions at the interface of the polymer solution and the PDMS, the PEGMA/PEGDMA resin selectively collected in the microwells before UV exposure induced polymerization via a photoinitiator.[66, 79] A number of other studies have utilized similar soft lithography techniques in the fabrication of microdevices.[75, 80-84]

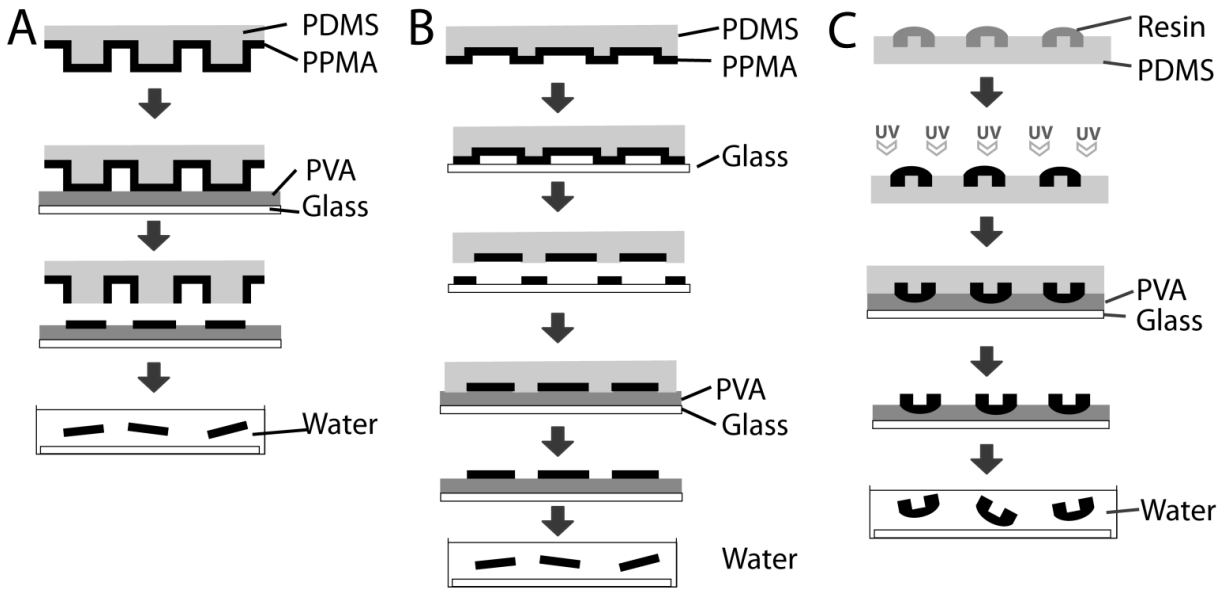

Figure 1.4. Soft lithography-based techniques for microdevice fabrication. A. Microcontact printing can be utililized for fabrication of microdevices in regions of contact of PVA with micropillar stamp with subsequent dissolution of PVA in water for device release. **B.** Fabrication of microdevices from recessed regions of microwell stamp. The stamp was brought into contact with glass to remove PPMA from non-microwell regions before bringing the remaining PPMA into contact with PVA. **C.** Discontinuous dewetting utilized to selectively collect resin before UV-induced polymerization. Microdevices were then brought into contact with PVA with subsequent dissolution in water for device release.

Currently, only a select number of microparticulate drug delivery systems have incorporated nanostructures to enhance oral drug delivery.[85-87] As microdevice design advances, future studies may apply a wide range of nanofabrication techniques to microdevice design as nanotopography has been shown to enhance muco- and cytoadhesion and interact with epithelial cells to enhance drug permeability.[87, 88] However, resolutions below 100 nm are difficult to achieve with UV-based photolithography due to the diffraction limit of light.[89] For fabrication of devices with nanoscale features, nanofabrication techniques are required. One such technique, X-

ray lithography, uses electromagnetic radiation with wavelengths ranging from 0.5 to 4 nm and is capable of achieving resolutions approaching 20 nm.[90-92] Similar to UV lithography, X-ray lithography uses an X-ray source such as a synchrotron or laser-induced plasma generator to irradiate X-ray-sensitive material through an X-ray absorbing mask.[90, 92] Maskless lithography techniques, including electron beam, ion beam, and dip-pen lithography are also available for nanofabrication. Electron beam lithography directs a beam of electrons to create a pattern on a material sensitive to electron irradiation, which is later developed or etched to form features on the irradiated material or an underlying substrate.[93] Similarly, ion beam lithography utilizes a focused beam of ions to either remove a substrate material or deposit a dissociated precursor material onto the substrate.[94] Dip-pen lithography adapts a scanning atomic force microscopy probe to direct inorganic or biological ink molecules across a substrate where they subsequently adsorb.[95] Because maskless techniques require low throughput *de novo* pattern creation, they are often used to create a master mold, which is then used to transfer the inverse pattern to other materials through nanoimprinting.[96-99] In addition, templating of polymeric material with nanoporous membranes provides high-throughput fabrication of nanowire arrays.[100, 101] In template synthesis, a polymer is exposed to a nanoporous membrane at a temperature greater than the polymer's glass transition temperature. The polymer is incorporated into the membrane, and the membrane is then selectively dissolved, leaving the polymer with the inverse nanowire array. Membrane selection provides control over the nanowire diameter and spacing, and templating time and temperature are adjusted to control nanowire length.

1.7. Strategies to increase micro/nanofabricated oral drug delivery device adhesion

The GI tract presents unique barriers and micro/nanoscale features that can be addressed by oral drug delivery systems. Micro- and nanofabrication approaches provide precise control over device geometry, surface modification, material composition, symmetry, and size, all of which can be used to design drug delivery systems for specific interactions with GI tract tissue. One particular interaction that is advantageous for oral drug delivery is bioadhesion, as adhesion to GI tract enhances drug uptake by 1) prolonging device residence time and drug exposure and 2) allowing for release of drug in high concentrations proximally to epithelial tissue for enhanced permeation effects.[20, 21] Drug delivery platforms can be fabricated to adhere to the lining of the GI tract via geometric, mechanical, biochemical, nanotopographical and/or motion-based approaches.[102, 103] To promote adhesion to specific regions of the GI tract, these approaches may utilize bioresponsive "smart" materials or be used in combination with other targeting technologies such as enteric coating.

Microscale drug delivery systems are capable of enhanced adhesion over macroscale drug delivery systems as a result of their high surface-area-to-mass ratio and ability to become entrapped within the microscale villi [6]. Geometry-based approaches can further promote device adhesion by utilizing a flat or planar device shape that is typical of microdevices for oral drug delivery.[21, 39, 45, 46, 60, 62, 104] As shown in Figure 1.2, a planar geometry promotes adhesion by 1) increasing the contact area available for interaction with the epithelial lining of the GI tract and 2) decreasing the force exerted on the devices from the fluid flow in the GI tract.[20, 21] Furthermore, microdevices can be fabricated asymmetrically with a drug reservoir on only one side of the device, providing unidirectional drug release to create a steep concentration gradient to increase drug permeation. Tao et al. investigated the effect of device geometry on adhesion by incubating

planar, asymmetric devices with dimensions of 150 × 150 × 5 μm over a monolayer of Caco-2 intestinal epithelial cells and exposing the devices to multiple washing steps.[46] After washing, 68% of the planar microdevices remained adhered while 17% of poly(methyl methacrylate) (PMMA) microspheres of similar surface area remained adhered. When loaded with the model drug fluorescein and added to a Caco-2 monolayer under flow conditions, these devices increased permeation of drug 10-fold over that of a bolus dose.[39] Furthermore, Chirra et al. demonstrated the effect of planar device geometry on adhesion *in vivo*.[104] When PMMA microdevices 200 μm in diameter and 8 μm in thickness were administered to mice, they showed 27% retention in the proximal small intestine after 2 hours while PMMA microspheres of similar surface area demonstrated 12% retention.[104] When loaded with drug, the planar PMMA microdevices provided a four-fold increase in oral bioavailability of acyclovir, a Biopharmaceutics Classification System (BCS) class III poorly permeable drug, relative to that of a bolus dose.

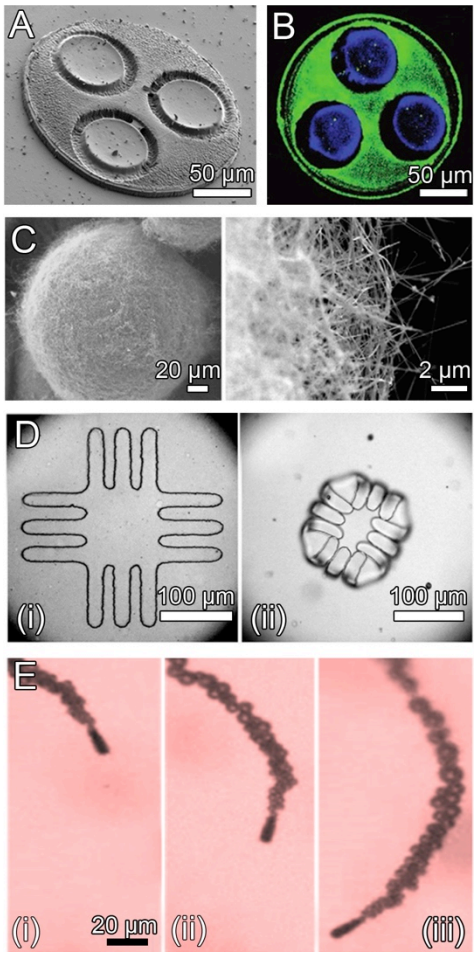

Figure 1.5. Micro- and nanofabrication-based approaches to enhance bioadhesion. A. A planar device geometry for increased surface area available for interaction with epithelial tissue and decreased force from intestinal fluid flow.[104] **B.** Lectin (green) surface modification to promote bioadhesion of the side of devices with drug reservoirs (blue) for unidirectional drug release.[45] **C.** Silica nanowires coating silicon microparticles provide increased surface area, promoting muco- and cytoadhesion.[85] **D.** Bilayered microdevices before (i) and after (ii) exposure to water. Microdevice folding is designed for mechanical attachment to intestinal mucosa.[66] **E.** Micromotors consisting of a zinc core encased within a polymeric microtube react with gastric acid, propelling the micromotors for entrapment within the stomach lining (1 s intervals, i-iii).[103] Images reproduced with permission.

In addition to providing geometry-mediated enhancement in bioadhesion, micro and nanofabricated oral drug delivery platforms can be surface modified with bioadhesive compounds to promote adhesion. Microdevices are typically fabricated on a silicon wafer or other substrates, facilitating asymmetric functionalization of exposed device regions.[22] This asymmetric surface modification can be used to promote binding of the drug-releasing side of the device, providing unidirectional drug release toward epithelial tissue.[20, 21] Lectins, carbohydrate-binding proteins capable of binding to glycosylated proteins and cell membrane components to provide muco- and cytoadhesion,[14] have been functionalized onto drug delivery systems to promote adhesion to the lining of the GI tract.[6, 46, 60, 104-107] PMMA microdevices modified with tomato lectin (Figure 1.5 B), which binds selectively to the epithelium of the small intestine,[108] demonstrated 92 ± 4% retention in an *in vitro* Caco-2 adhesion assay, whereas devices lacking modification showed 29 ± 9% retention.[60] *In vivo,* lectin-conjugated PMMA microdevices showed 41% retention in the proximal small intestine of mice two hours following oral administration as opposed to 27% for bare devices.[104] Biochemical adhesion utilizing high-affinity interactions between a targeting ligand and specific moieties can provide highly specific binding to the small intestine or diseased tissue. However, one drawback to the use of biomolecules and other surface modifications to promote adhesion is degradation as a result of the low pH of the stomach and proteolytic and metabolic enzymes throughout the GI tract.[109] Therefore, molecular stability must be considered for surface modification of oral drug delivery platforms.

Topography-mediated adhesion presents an alternative approach to promote bioadhesion that is dependent upon geometry rather than degradable surface modifications. By increasing surface area, micro- and nanofeatures increase the interfacial surface adhesion.[110-113] Cylindrical

pills coated with microneedles designed for physical penetration of epithelial tissue to increase drug permeation are also likely to provide the additional benefit of increased adhesion to the GI tract.[114] As with asymmetric surface functionalization, asymmetric topographical modifications have potential to promote unidirectional drug release toward epithelial tissue. In an example of hierarchical microdevice structure, multi-layer fabrication was employed to modify one surface of 150 × 150 μm microdevices with microposts 10 μm in diameter.[67] In an alternate approach, bottom-up nanofabrication approaches have been employed to create nanoengineered microparticles (NEMPs) consisting of silicon oxide nanowire-coated silicon microparticles for oral drug delivery (Figure 1.5 C).[85-87, 100, 115] Following contact with an epithelial layer, the nanowire coating of these microparticles interdigitated with the microvilli on the surface of the epithelial cells.[100] The NEMPs showed a 100-fold increase in required lift-off force from an *in vitro* epithelial monolayer relative to unmodified microparticles.[100] *In vivo,* the retention time of the NEMPs in the GI tract following oral administration was 10-fold that of bare microparticles.[85] While NEMPs can be fabricated with a relatively planar shape for enhanced adhesion,[86] the fabrication approaches used for NEMP fabrication do not allow for asymmetric nanowire functionalization for unidirectional drug release or use of highly biocompatible polymers. However, the techniques of photolithography and nanotemplating were recently combined to asymmetrically coat PMMA microstructures with polycaprolactone (PCL) nanowires.[116] While not yet applied to oral drug delivery, this approach has potential to combine the benefits of asymmetric, planar microdevices with nanowire-mediated adhesion while utilizing polymers with FDA approval for medical applications.[117, 118]

As an alternative to surface modification, a number of mucoadhesive materials including alginate,[119, 120] chitosan and chitosan derivatives,[121-123] hyaluronic acid,[124, 125] gelatin,[126, 127] cellulose

derivatives,[128, 129] and a number of synthetic polymers[130] are available for use as a bulk material in fabrication of oral drug delivery systems. Among these materials, chitosan has been highly utilized in a number of oral drug delivery systems, including chitosan-based micro- and nanoparticulate drug delivery systems,[131-136] chitosan-drug conjugates,[137, 138] and chitosan macroscale patches.[139, 140] Chitosan is an attractive material for micro/nanofabricated platforms as it is compatible with a number of microfabrication approaches,[141, 142] is stable through pH values relevant to GI physiology,[143] and has been utilized in microfabricated oral drug delivery systems.[66, 70]

While device surface modifications including biochemical and nanotopographical cues are capable of interacting with epithelial tissue to enhance cytoadhesion and drug permeability, the mucus layer may prevent direct interaction between nanofeatures and epithelial cells. Mechanical and motion-based adhesion approaches may provide a mechanism for microscale devices to penetrate through the mucus layer and directly contact epithelial tissue.

Microscale drug delivery systems can be designed to mechanically respond to the environment of the GI tract to promote adhesion. Self-folding devices have been developed to respond to solvent exposure,[66, 70] temperature,[144, 145] pH,[70] and ionic strength.[146] Self-folding properties have been incorporated into microscale oral drug delivery systems to promote mechanical attachment to the lining of the GI tract. For example, Guan et al. fabricated bilayered devices consisting of chitosan and a copolymer of poly(ethylene glycol) methacrylate (PEGMA) and poly(ethylene glycol) dimethacrylate (PEGDMA) which used differential swelling to fold upon exposure to water (Figure 1.5 D)[70] Similar bilayered devices composed of crosslinked poly(methacrylic acid) (PMAA) and poly(hydroxyethyl methacrylate) (PHEMA) were capable of mechanical attachment to excised pig intestinal mucosa,[66] and demonstrated enhanced

mucoadhesion, lower drug leakage into luminal space, and improved unidirectional delivery, resulting in improved drug transport across excised porcine mucosal epithelium.[102] While these self-folding devices have not demonstrated specificity in binding to the small intestine or other regions of the GI tract, alternative bioresponsive materials could be utilized to respond to pH or other cues for more specific targeting. Alternatively, these self-folding devices could be combined with other targeting technologies such as enteric capsules to release these devices at the desired region of the GI tract.

In an alternate approach involving motion-based adhesion, a number of technologies for chemically induced locomotion have been developed.[147-152] Gao et al. applied this technology to oral drug delivery systems by developing a pH-responsive micromotor approach to enhance device adhesion and payload delivery to the lining of the mouse stomach (Figure 1.5 E).[103] Their design of micromotors consisting of a zinc core encased within a poly(3,4-ethylenedioxythiophene) (PEDOT) microtube was then tested in mice by oral administration. Upon exposure to the low pH of the stomach, the zinc core reacted to form hydrogen gas, propelling the micromotors into the lining of the stomach, enhancing binding and retention of the devices and delivery of gold nanoparticles to the stomach wall. The reaction of these micromotors to low pH environments makes them ideal for promotion of stomach-specific adhesion. However, different compounds will need to be incorporated into the micromotor core to improve adhesion in other regions of the GI tract with higher pH values.

1.8. Efficacy of microdevices *in vitro* and *in vivo*

Within the last few years, the utilization of semi-conductor industry principles to fabricate oral microdevices has advanced leaps and bounds. Yet, the testing of these devices in

improving the overall efficacy of most therapeutics is still at its relative infancy. Recent studies related to *in vitro* drug release and permeation have been done over monolayers of Caco-2 epithelial cells using Transwell® inserts. Ainslie et al. showed that the localized high concentration of drug at the device-cell interface resulted in an enhancement of drug permeation across the Caco-2 monolayer under physiological fluid flow, with a ten-fold increase in fluorescein permeation when released from microdevices relative to fluorescein free in solution.[39] Also, a sequential release of different sized drugs, insulin and camptothecin, was achieved with the use of a dual layered hydrogel system that was present in microdevices made up of a single reservoir.[20] While sequential release can be harnessed to improve drug bioavailability by first releasing a permeation enhancer followed by the drug of interest, the release kinetics of the drug are co-dependent on the release kinetics of the permeation enhancer from its respective top hydrogel layer. To overcome this co-dependence issue, Chirra et al. used multiple reservoirs that can be filled with different drugs using different hydrogel/biodegradable polymeric systems.[45] Figure 1.6B shows the independent release of multiple model fluorophore-tagged BSAs from respective reservoirs as shown in Figure 1.6A. Such a device system can be used to release permeation enhancers, proteolytic enzyme inhibitors, and drugs of interest at independent rates and release times, thereby making oral microdevices effective for increasing drug efficacy as well as for combinatorial therapy. The Desai Lab also used Caco-2 monolayer coated parallel plate flow chambers to study the extent of oral microdevice retention under GI flow conditions. They have shown that 93% of tomato lectin microdevices remain attached to the cell surface under one hour of physiological shear conditions after initial binding, indicating that microdevices are capable of remaining attached to GI tissue for extended periods of time under physiological conditions.[20]

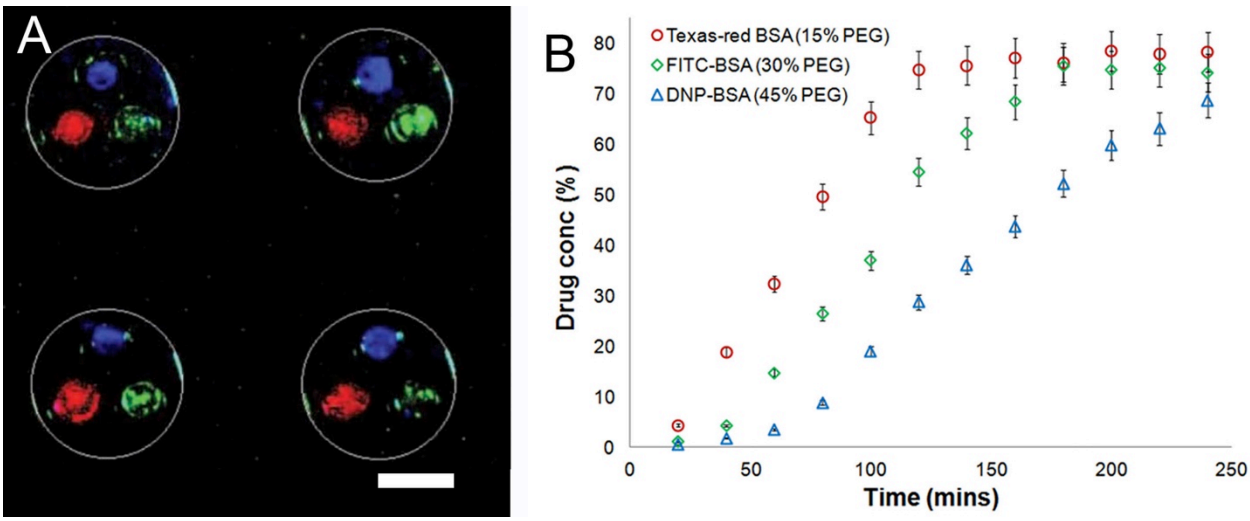

Figure 1.6. Microdevices loaded with multiple drugs with separate release profiles. **A**. Fluorescent image demonstrating separate drug loading of each microdevice reservoir with device shape outlined in white. Scale bar is 100 μm. **B.** Custom release profiles for each drug controlled by hydrogel crosslinking density. Reproduced with permission. [45]

The several advantages of using asymmetric planar oral microdevices including unidirectional release to avoid luminal drug loss, increased contact surface area and reduced shear stress with a planar design, and selective modification of reservoir side of device to introduce muco- or cytoadhesive properties were recently tested *in vivo*. Our lab observed that upon oral administration to mice, PMMA microdevices having the same contact surface area as that of symmetric PMMA microparticles have a 27% retention in the proximal small intestine after 2 hours due to the relatively low shear stress experienced by the thin device side walls, as compared to a retention of 12% for the curvilinear microparticles.[76] Also, a further enhancement of microdevice retention to 41% was observed after conjugation of the bioadhesive protein lectin, which targeted the intestinal epithelial cell wall. We have shown that with the help of

microdevices, even the poorly permeable drug Acyclovir had a five-fold increase in oral bioavailability in mice as compared to that of a conventional solution of Acyclovir of same dosage.[76] This enhancement of oral bioavailability drastically reduces the overall dosage needed for effective therapy. Such a reduction in dosage with improved bioavailability proves vital in significantly alleviating issues of systemic side effects, thereby opening up oral administration to an array of toxic and expensive therapeutics. While most of the recent *in vivo* work was done using small molecule drugs, microdevices can be applied to the oral delivery of macromolecules and high-efficacy low-dosage drugs (e.g. Leuprolide, human growth hormone, etc.). Detailed studies on improving drug loading, dosage optimization, improved protection against GI environment, sustained release for systemic delivery, targeted attachment, and GI pathology oriented localized delivery are currently underway and are of much interest for future work. Therefore, the use of microfabricated planar oral devices holds promise in augmenting the range of oral therapeutics used, while solving pharmacokinetic issues associated with low permeability and avoiding systemic side effects.

1.9. Conclusion

The GI tract presents a complex set of physiological barriers that limit drug uptake. Micro- and nanotechnology provide flexibility in microdevice design, allowing for fabrication of drug delivery platforms that specifically address these barriers. The efficacy of micro/nanofabricated oral drug delivery systems may be enhanced by incorporating 1) tunable and/or responsive drug reservoir polymers for targeted release of intact drug, 2) adhesive polymers, surface modifications, and topographies to enhance adhesion, and 3) chemical and topographical permeation enhancers to increase drug permeability. With recent success *in vivo*,

these technologies show promise for clinical trials. However, many of the top-down approaches used to fabricate these platforms for proof of concept are low-throughput and expensive relative to bottom-up fabrication techniques. To scale these technologies to the clinic, efficient, low-cost fabrication and drug loading approaches are being developed. Furthermore, to maximize cost-efficiency, these platforms may be used with highly potent drugs to minimize the number of devices required per dosage. As micro- and nanofabrication approaches continue to incorporate new technologies, future micro/nanofabricated oral drug delivery systems may combine smart materials, bioadhesive functionalization, nanotopography, planar shape, asymmetric design, and/or motion-based responses to address the many barriers to oral drug uptake in a manner not possible with conventional technologies. While a relatively unexplored concept, the incorporation of nanotopography is particularly promising as it has potential to enhance device adhesion, drug loading, and epithelial permeability.

Chapter 2 – Fabrication of Micropatterned Polymeric Nanowire Arrays for High-Resolution Reagent Localization and Topographical Cellular Control

2.1. Abstract

Coating the surface of microdevices with nanotopography has a number of possible advantages for oral drug delivery, including enhance device bioadhesion, efficient drug loading, and enhanced drug permeability via disruption of cell-cell junctions. However, techniques for scalable incorporation of nanoscale features onto microstructures are not available. Herein, we present a novel approach for the fabrication of micropatterned polymeric nanowire arrays that addresses the current need for scalable and customizable polymer nanofabrication. We describe two variations of this approach for the patterning of nanowire arrays on either flat polymeric films or discrete polymeric microstructures and go on to investigate biological applications for the resulting polymeric features. We demonstrate that the micropatterned arrays of densely packed nanowires facilitate rapid, low-waste drug and reagent localization with micron-scale resolution as a result of their high wettability. We also show that micropatterned nanowire arrays provide hierarchical cellular control by simultaneously directing cell shape on the micron scale and influencing focal adhesion formation on the nanoscale. This nanofabrication approach has potential applications in scaffold-based cellular control, biological assay miniaturization, and biomedical microdevices for oral drug delivery. We go on to fabricate nanowire-coated microdevices and demonstrate that the nanowires provide efficient drug loading and enhance device bioadhesion, indicating that nanowires may enhance the properties of oral drug delivery devices.

2.2. Introduction

While nanofabricated microdevices are a promising technology for oral drug delivery, there is a need to develop new fabrication approaches to create such devices in a scalable manner. Furthermore, substrates that contain micro- and nanoscale features are important for a number of additional biological applications. For example, topographical cues at the micro- and nanoscale can direct cellular behavior,[153, 154] micro- and nanoarrays provide high-throughput biological analysis,[155-157] and micro- and nanoscale devices can enhance drug uptake and localization.[87, 158-160] However, nanofabrication techniques are restricted in either pattern customization or throughput, limiting their application and/or scalability in biotechnology.[154] While direct-write fabrication approaches, including electron beam, focused ion beam, and dip pen lithography, provide custom polymer patterning on the nanoscale[161, 162] with electron beam lithography capable of sub-10 nm resolution under ideal conditions,[163] these techniques require sequential formation of individual nanoscale features, limiting throughput and scalability and increasing cost.[154] These drawbacks are mitigated in the technique of nanoimprint lithography (NIL), in which multiple resists or substrates can be mechanically deformed by a nanopatterned mold, thereby increasing throughput.[164] However, molds for NIL are typically fabricated with low-throughput direct-write techniques and have limited lifetimes.[165, 166] Conversely, bottom-up nanofabrication approaches, including block copolymer self-assembly, nanosphere lithography, and nanoporous membrane-based templating, provide high-throughput, scalable fabrication of polymeric nanofeatures with tunable dimensions but do not typically allow for custom patterning.[167-169] Therefore, there is an unmet need for scalable, customizable fabrication techniques for cost-effective application of nanofabrication to biotechnology.

Efficient approaches to polymer nanofabrication may be particularly advantageous in the scale-up of nanotopographical tissue scaffolds. Because micro- and nanotopography influence cellular adhesion, alignment, shape, proliferation, and differentiation,[153, 154, 170] topographical cues incorporated into cellular scaffolds are capable of controlling a wide range of cellular behaviors. Many studies have found that anisotropic and/or hierarchical patterning is essential in achieving the intended cellular effects.[170-177] The enhanced control provided by hierarchical structures is not surprising, as cells are influenced both on the microscale by contact guidance and on the nanoscale through direct interaction of cellular receptors with external physical cues.[178-180]

Hierarchical substrates may also have utility for micron-scale reagent and drug loading of miniaturized biological assays and biomedical microdevices. A number of techniques have been utilized to load micron-scale reservoirs, including photolithography, inkjet printing, and supercritical polymer impregnation,[45, 181-183] but no approach is capable of both highly scalable and low-waste drug loading.[184] As a result of dramatically increased surface area, densely packed nanowires are capable of providing super-hydrophilic surfaces with extreme wettability.[185, 186] Super-wettable nanowire arrays have been used to enhance drug loading capacity[87, 187-189] but have not been applied for custom, spatially controlled drug localization. We hypothesize that micropatterned nanowire arrays can provide rapid, low-waste reagent and drug localization with micron-scale resolution.

To address the need for customizable, scalable nanofabrication, we developed a non-sequential approach to fabricate polymeric nanowire arrays with custom micropatterns and tunable nanowire dimensions. We utilized two variations of this approach to pattern nanowire arrays over either flat polymeric films, for applications in tissue engineering and microarray technology, or on discrete polymeric microstructures, for applications in biomedical microdevice

technology. We went on to investigate the ability of these micropatterned nanowire arrays to 1) provide efficient drug/reagent localization with micron-scale resolution, 2) influence cellular behavior through both micro- and nanoscale interactions, and 3) increase device bioadhesion.

2.3. Methods

2.3.1. Micropatterned nanowire array fabrication

Unless otherwise noted, all materials were purchased from Sigma-Aldrich (St. Louis, MO.) Micropatterned PCL nanowire arrays on PMMA films were fabricated by spin-coating a nanoporous AAO membrane (GE Healthcare, Piscataway, NJ) with Microposit S1818 positive photoresist (MicroChem, Westborough, MA) at 2500 rpm for 30 s with a ramp speed of 1000 rpm/s. The photoresist was baked at 110 °C for 1 min. and allowed to cool. The photoresist was then exposed to 225 mJ/cm^2 of 405 nm UV light through a computer-designed photomask with grooves with 10, 20, 40, or 80 μm widths and equal spacing or other various micropatterns. The micropatterned AAO membrane was then submerged in 351 Developer (MicroChem) for 1 min. with gentle shaking, rinsed with dH_2O, and allowed to dry. Separately, a silicon wafer was coated with a 110 mg/mL solution of 950 kDa PMMA in anisole (MicroChem) at 350 rpm for 15 s followed by 1400 rpm for 30 s and baked at 110 °C for 1 min. The resulting 5 μm PMMA base layer was coated with an overlying layer of PCL (Mn = 80 kDa, Sigma-Aldrich) 5, 10, or 15 μm in thickness. The 5, 10, and 15 μm PCL layers were obtained by spin-coating 50 to 150 mg/mL PCL in 2,2,2-trifluoroethanol (TFE) at 1000 to 2000 rpm for 30 s following a pre-spin at 500 rpm for 10 s. The PCL was then brought into contact with the micropatterned side of the AAO

membrane and heated to 80 °C for 5 min. After uptake of melted PCL into pores of the AAO membrane in regions not coated with photoresist, the AAO membrane and photoresist were selectively dissolved in 0.5 M NaOH for 1 h to expose the PCL nanowires. Finally, the features were rinsed 5 times with dH_2O. For cell culture experiments, the film was peeled from the silicon wafer prior to sterilization.

To fabricate nanowire arrays on discrete PMMA microstructures, a 110 mg/mL solution of 950 kDa PMMA in anisole (MicroChem) was spin-coated onto a silicon wafer at 350 rpm for 15 s followed by 1400 rpm for 30 s and baked at 110 °C for 1 min. The PMMA layer was coated with Microposit S1818 positive photoresist at 500 rpm for 10 s followed by 2500 rpm for 30 s and baked at 110 °C for 1 min. The photoresist was then exposed to 225 mJ/cm^2 of 405 nm UV light through a computer-designed photomask with arrays of opaque squares with 10, 20, 40, or 80 μm edge lengths and equal spacing or other various micropatterns. The wafers were then submerged in 351 Developer for 1 min. with gentle shaking, rinsed with IPA, and dried with nitrogen. The photoresist pattern was then transferred to the PMMA layer by reactive ion etching with oxygen plasma (450 W, 200 mTorr, 6.5 min.) to form PMMA microstructures. The remaining photoresist was stripped with Microposit Remover 1112A (MicroChem) for 1 min. under gentle shaking. The PMMA features were then heated to 80 °C and brought into contact with PCL spun-cast onto a separate wafer at thicknesses of 5, 10, or 15 μm, and the wafers were separated. The PCL-coated features were templated with an AAO membrane at 80 °C for 5 min., and the membrane was subsequently etched in 0.5 M NaOH for 1 h. Finally, the features were washed 5 times with dH_2O.

2.3.2. Non-templated, micropatterned PCL film fabrication

SU-8 2005 (MicroChem) was spun-cast onto a silicon wafer at 500 rpm for 10 s followed by 5000 rpm for 30 s and baked at 95 °C for 1 min. The SU-8 was then exposed to 365 nm UV light at 100 mJ/cm^2 through a photomask with 10 μm grooves with equal spacing and baked at 95 °C for 2 min. The wafer was developed in SU-8 Developer (MicroChem) for 1 min under gentle shaking, rinsed with IPA, and dried with nitrogen. Sylgard 184 (Sigma-Aldrich) polydimethylsiloxane (PDMS) was mixed and de-gassed according to the manufacture's instructions and poured over the SU-8 mold. After de-gassing under vacuum for an additional 30 min, the PDMS was cured at 100 °C for 1 h, allowed to cool, and peeled from the SU-8 mold. A 100 mg/mL solution of 80 kDa PCL in TFE was then poured over the PDMS mold and allowed to cure overnight at room temperature. The PCL film was submerged in 200-proof ethanol, peeled from the PDMS mold, and treated with 0.5 M NaOH for 1 h prior to sterilization for cell culture.

2.3.3. Measurement of AAO membrane pore diameter and density and PCL nanowire diameter

Cross sections of Whatman Anodisc® AAO membranes with nominal pore diameters of 0.02, 0.1, and 0.2 μm and nanowires resulting from templating PCL with these membranes were imaged with SEM, and the images were analyzed with ImageJ software to measure the average diameters of the AAO pores and PCL nanowires. Fifty measurements were made for each sample. Pore density of AAO membranes with 200 nm nominal pore sizes were determined by imaging five 2 μm × 2 μm regions of the AAO surface and counting the number of pores in each region, including overlapping pores on the bottom and left edges of the region and excluding

overlapping pores on the right and top edges of the region. Mean values were reported with standard deviation.

2.3.4. Contact angle measurements

Contact angle measurements were performed with a Rame-Hart Standard Goniometer (Model 200-F4). Water (5 μL) was dispensed onto films with surfaces consisting of untemplated PCL, untemplated PCL treated with 0.5 M NaOH for 1 h (to match NaOH treatment for AAO membrane etching), and PCL nanowires with and without pre-wetting. Pre-wetting consisted of submerging the membanes in water for 1 min, spinning the films at 2000 rpm for 5 s to remove excess water, and imaging droplets within 1 min after spinning. Contact angles were measured on both sides of each droplet for 3 droplets per sample with DROPimage Standard software, and mean contact angles were reported with standard deviation.

2.3.5. Drug and reagent localization

PMMA microstructures coated with either non-templated PCL or PCL nanowires were wetted with FITC-BSA and FITC-dextran (average MW = 10 kDa) in dH_2O and Oregon Green – paclitaxel and Nile red in ethanol at 5 $\mu g/cm^2$. The microstructures were then inverted and allowed to dry at room temperature. Arrays coated with non-templated PCL were fabricated in an identical manner to arrays coated with nanowires, except the templating step was omitted. PCL nanowire arrays on PMMA films were loaded in an identical manner to PMMA microstructures. All arrays used for drug localization were fabricated using PCL thicknesses of 10 μm. Z-stacks of drug/reagent-loaded features were captured at 1 μm intervals, capturing the

entire microarray structures and wafer base layer, with a spectral confocal microscope. Drug/reagent localization was also observed with a conventional fluorescence microscope. Three-dimensional reconstruction of confocal images was performed with ImageJ software. Localization efficiency was calculated by merging Z-stacks into a single image according to average intensity and quantifying fluorescence intensity with ImageJ. Specifically, localization efficiency was calculated as the ratio of fluorescence intensity integrated over microstructured regions to the total fluorescence intensity integrated over the entire region analyzed. Localization efficiencies were reported with standard deviation.

2.3.6. Cell culture, staining, and imaging

PMMA-PCL films with PCL layers 5 μm in thickness were templated with AAO membranes patterned with grooves 10 μm in width and spacing. These films had nanowires approximately 5 μm in length as calculated from SEM images, accounting for the 45° imaging angle. Non-templated PCL, non-patterned nanowire array (fabricated without lithography steps), and micropatterned non-templated PCL (grooves 10 μm in width and 5 μm in height) films were used as controls, with all films incubated in 0.5 M NaOH for 1 h to avoid differences in PCL surface treatment. Prior to cell seeding, the films were rinsed with dH_2O 5 - 10 times and then incubated in a 70% ethanol solution for 5 min. The films were then rinsed in dH_2O and allowed to dry under sterile conditions. The films were seeded with NIH/3T3 cells (ATCC, Manassas, VA) in DMEM (ATCC) medium supplemented with 10% fetal bovine serum and 1× Penicillin-Streptomycin at a density of 5000 cells/cm^2. Following two days of cell culture, cells were fixed with 4% paraformaldehyde, permeabilized in 1% Triton X, and blocked in 1% BSA in PBS. The cells were then stained for vinculin with polyclonal anti-vinculin antibodies produced in rabbit

(Sigma-Aldrich) diluted 100-fold in 1% BSA in PBS followed by Alexa Fluor® 647 anti-rabbit IgG antibodies produced in goat (Invitrogen) diluted 200-fold in 1% BSA in PBS. The cells were also stained with Alexa Fluor® 488 Phalloidin (Life Technologies) and DAPI (Invitrogen) and mounted for fluorescence imaging. To quantify cellular elongation, at least three separate regions of cells were selected for each sample, and the distance between the two furthest points of each fully visible cell as determined from actin staining was quantified using ImageJ. To quantify cellular alignment, the angle of the line formed by these points relative to the horizontal axis of the images (which was aligned to microgrooves, if present), was determined using ImageJ, and results were plotted in polar histograms with bins of 30° ranges.

2.3.7. Caco-2 flow cell adhesion assay

An epithelial flow cell adhesion assay was performed as previously outlined[85, 100, 190, 191] with minor modifications. Briefly, approximately 400 microdevices, either with PCL nanowires or flat, sodium hydroxide-treated flat PCL as a control, were scraped from the silicon wafer with a razor, suspended in 1 mL PBS, and added to a monolayer of Caco-2 epithelial cells (ATCC) in a petri dish. The microdevices were incubated over the cellular monolayer for 5 min under gentle shaking. A flow cell was then assembled over the microdevices, and a solution of PBS was passed through the flow cell at increasing flow rates in a stepwise fashion, achieving fluid shear stress values of 0.1, 0.5, 1, 5, 10 dyn/cm^2. After 5 min at each flow rate, the number of completely adhered microdevices (i.e., the number of microdevices lying flat on the Caco-2 monolayer) was determined by counting under a dissecting microscope, and the ratio of microdevices adhered to the original number of microdevices was determined.

2.4. Results

2.4.1. Micropatterned nanowire array fabrication and characterization

Our fabrication approach employed polymer templating, a rapid and inexpensive nanofabrication technique that involves extruding a polymer into a nanoporous membrane and subsequently etching the membrane to expose polymeric nanowires.[168, 192, 193] Previous studies have micropatterned templated nanowire arrays by scraping with a microstructured tool to remove nanowires in regions of contact and create grooved arrays 400 μm in width separated by 60 μm gaps,[194] but no techniques are currently available for custom two-dimensional patterning of nanotemplated arrays. For custom nanowire array micropatterning and enhanced resolution, we combined templating and photolithographic techniques. As shown in Figure 2.1, two approaches were used to fabricate polycaprolactone (PCL) nanowire arrays on either a flat polymethyl methacrylate (PMMA) film or on discrete PMMA microstructures. PMMA is a common material in FDA-approved orthopedic implants,[195] and PCL is a polymer used in FDA-approved sutures and drug delivery devices and has been shown to facilitate cellular adhesion and growth.[101, 196]

To form micropatterned PCL nanowire arrays on PMMA films (Figure 2.1A), a nanoporous anodized aluminum oxide (AAO) membrane (GE Healthcare, Piscataway, NJ) was spun-cast with Microposit S1818 positive photoresist (MicroChem, Westborough, MA) and patterned via photolithography with grooves of 10, 20, 40, or 80 μm widths and equal spacing or other various micropatterns. The patterned side of the AAO membrane was then brought into contact with a silicon wafer spun-cast with a PMMA base layer and an overlying layer of PCL 5, 10, or 15 μm in thickness and heated to 80 °C, above the melting temperature of PCL but below

that of PMMA. After uptake of melted PCL into pores of the AAO membrane in regions not coated with photoresist, the AAO membrane and photoresist were selectively dissolved in a 0.5 M sodium hydroxide solution for 1 h to expose the PCL nanowires.

To form nanowire arrays on discrete PMMA microstructures (Figure 2.1B), PMMA and an overlying photoresist layer were spun-cast onto a silicon wafer, and the photoresist was patterned with arrays of squares with 10, 20, 40, or 80 μm edge lengths and equal spacing or other various micropatterns via photolithography. The photoresist pattern was then transferred to the PMMA layer by reactive ion etching with oxygen plasma to form PMMA microstructures. After chemically stripping the remaining photoresist, the PMMA features were heated to 80 °C and brought into contact with PCL spun-cast onto a separate wafer at thicknesses of 5, 10, or 15 μm. Upon separation of the wafers, the PCL lifted off onto the PMMA features. Finally, the PCL-coated features were templated with an AAO membrane at 80 °C, and the membrane was etched in 0.5 M sodium hydroxide for 1 h.

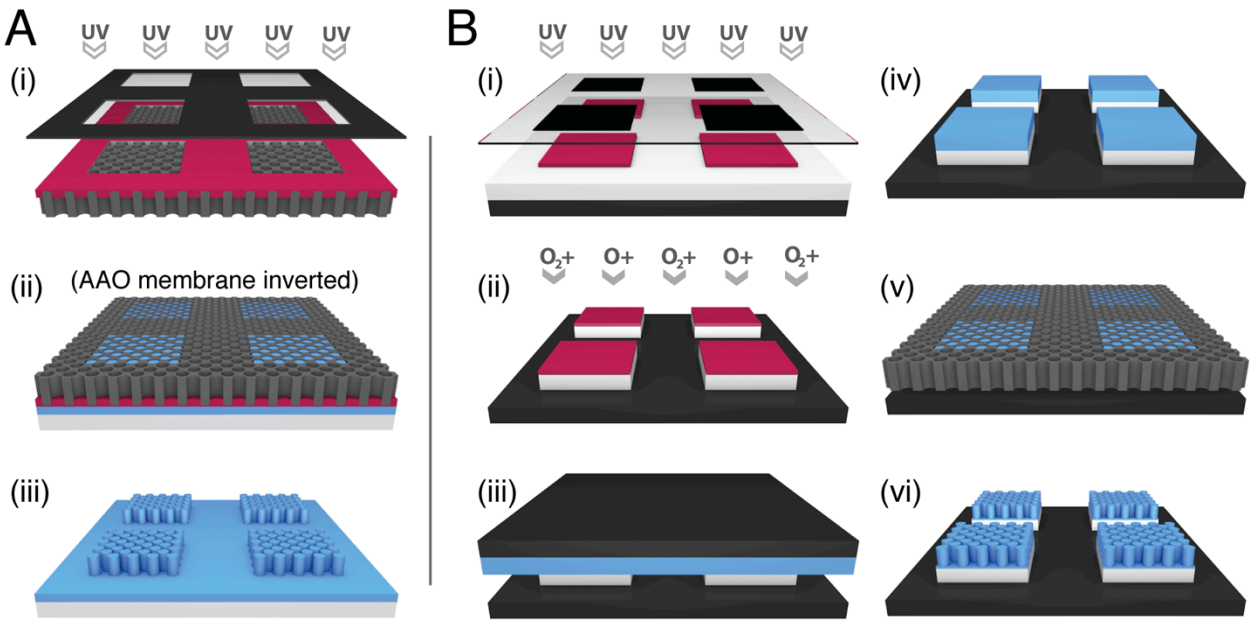

Figure 2.1. Fabrication approaches to create micropatterned PCL nanowire arrays. A. Fabrication of micropatterned PCL nanowire arrays on PMMA films. **(i)** A nanoporous AAO membrane (gray) is spun-cast with positive photoresist (red) and patterned by exposure to UV light through a computer-designed photomask. Photoresist is cleaved in regions exposed to UV light, and these regions are selectively dissolved upon chemical development. **(ii)** The AAO membrane is inverted, and its micropatterned side is brought into contact with a layer of PCL (blue) deposited over a PMMA base layer (white) under heat, allowing PCL to melt and extrude into membrane pores in regions not coated with photoresist. **(iii)** The AAO and resist are selectively dissolved in an alkaline solution to expose the PCL nanowires. **B.** Fabrication of PCL nanowire arrays on PMMA microstructures. **(i)** A layer of PMMA (white) spun-cast onto a silicon wafer (black) is spun-cast with positive photoresist (red), which is exposed to UV light through a computer-designed photomask. Photoresist is cleaved in regions exposed to UV light, and these regions are selectively dissolved upon chemical development. **(ii)** The photoresist pattern is transferred to the PMMA layer by anisotropic reactive ion etching with oxygen plasma. **(iii)** After stripping the photoresist, the PMMA microstructures are heated and brought into contact with PCL (blue) spun-cast onto a separate silicon wafer, bonding PCL in regions of contact. **(iv)** Upon separation of the wafers, the PCL lifts off onto the PMMA microstructures. **(v)** The PCL is melted and templated with an AAO membrane (gray). **(vi)** The AAO membrane is selectively dissolved in an alkaline solution to expose the PCL nanowires.

These fabrication approaches resulted in micropatterned arrays of densely packed PCL nanowires on either flat PMMA films or discrete PMMA microstructures (Figure 2.2). Both fabrication approaches had adequate resolution for all feature sizes tested (10 to 80 μm). Nanowires formed clusters approximately 1 to 10 μm in width, possibly as a result of capillary force during drying in preparation for SEM. The micropatterned nanowire arrays on PMMA films had well-defined borders, but the nanowire arrays on PMMA microstructures had rounded corners and edges overhanging the PMMA base layer (Figures 2.2 and 2.3A), likely due to beading of molten PCL during the lift-off step and/or compression during templating.

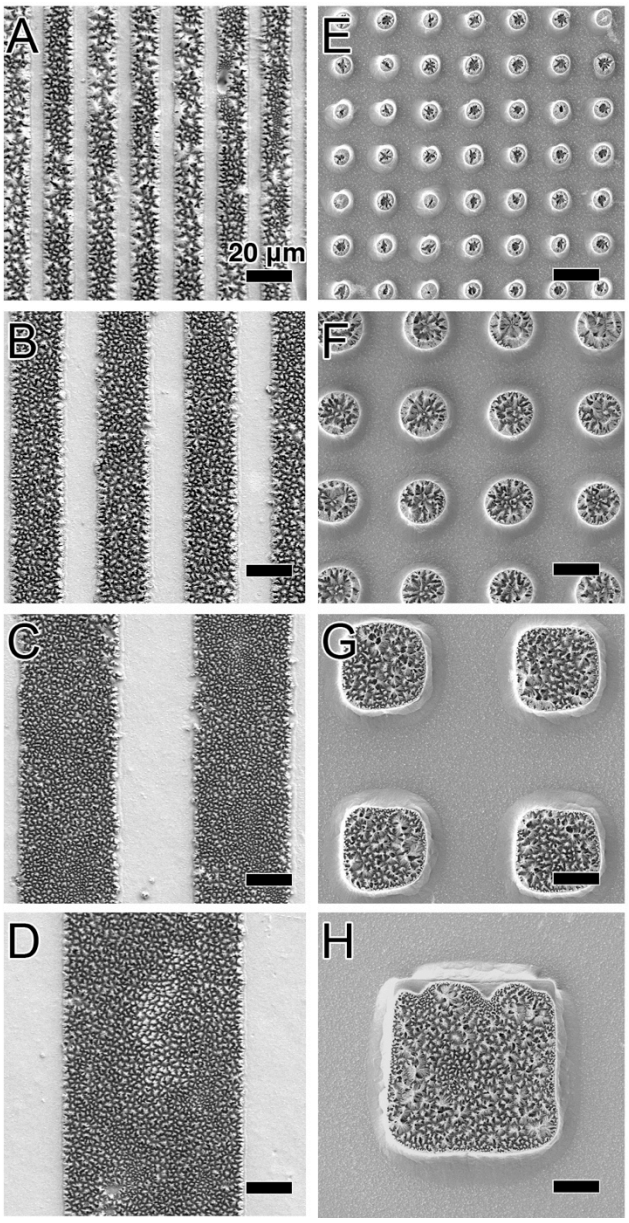

Figure 2.2. Nanowire array fabrication approaches demonstrate sufficient resolution to pattern features as small as 10 µm. SEM micrographs of PCL nanowire arrays on PMMA films (**A-D**) and PMMA microstructures (**E-H**) with 10 µm (**A, E**), 20 µm (**B, F**), 40 µm (**C, G**), and 80 µm (**D, H**) feature sizes. Scale bars are 20 µm.

2.4.2. Nanowire dimensions are tunable

After demonstrating custom patterning of nanowire arrays, we proceeded to investigate approaches to tune nanowire dimensions. We first examined an approach to adjust nanowire length. In previous studies, PCL templating was performed without a PMMA base layer, and templating time and temperature were adjusted to control nanowire length.[101, 168, 197] For the approach used in this study, we hypothesized that templating would occur until the AAO membrane contacted the PMMA base layer, allowing for control of nanowire length by adjusting PCL thickness. For film-based nanowire arrays, nanowire lengths roughly matched respective PCL thicknesses for PCL layers 5, 10, and 15 μm thick (Figure 2.3A). Nanowires coating PMMA microstructures also scaled in length with PCL thickness but were shorter than nanowires of film-based arrays fabricated with identical PCL thicknesses, indicating only partial adhesion of the PCL layer during the lift-off step. We also investigated control over nanowire diameter through selection of AAO membranes of varying pore sizes. As shown in Figure 2.3B, templating PCL-coated microstructures with AAO membranes with mean pore diameters of 120 ± 40, 200 ± 60, and 290 ± 50 nm (Figure 2.4) resulted in mean nanowire diameters of 140 ± 30, 190 ± 30, and 320 ± 50 nm, respectively. Thus, in addition to customizable nanowire array patterning, nanowire dimensions can also be tuned for length and diameter by adjusting PCL thickness and AAO pore size, respectively.

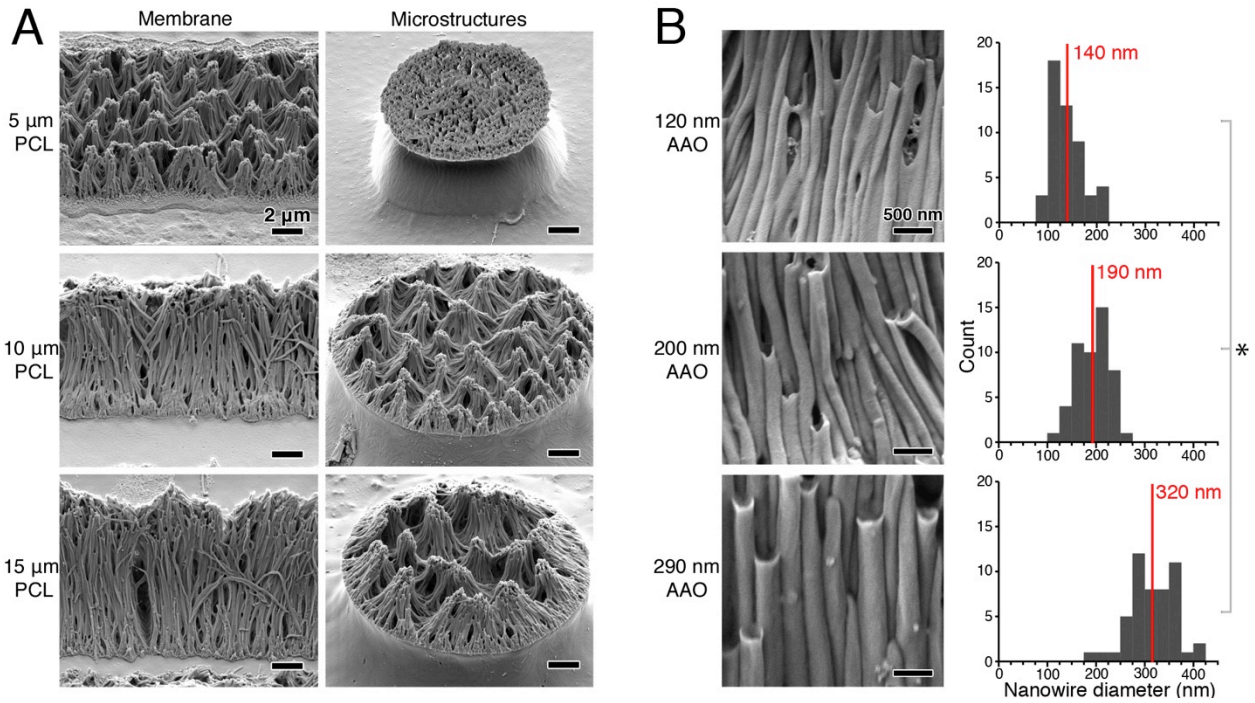

Figure 2.3. Templating parameters can be adjusted to tune nanowire dimensions. A. PCL thickness controls nanowire length. 45° SEM micrographs of nanowire-coated films and microstructures fabricated with PCL thicknesses of 5, 10, and 15 µm demonstrate that nanowire length increases with PCL thickness. Scale bars are 2 µm. **B.** AAO membrane pore size controls nanowire diameter. As shown in SEM micrographs and histograms, diameters of PCL nanowires fabricated on PMMA microstructures correlated with AAO membrane diameter. Templating with mean membrane pore diameters of 120 ± 40, 200 ± 60, and 290 ± 50 nm yielded mean nanowire diameters of 140 ± 30, 190 ± 30, and 320 ± 50 nm, respectively. Scale bars are 500 nm. *Indicates statistically significant difference between average nanowire diameter with $p < 0.001$.

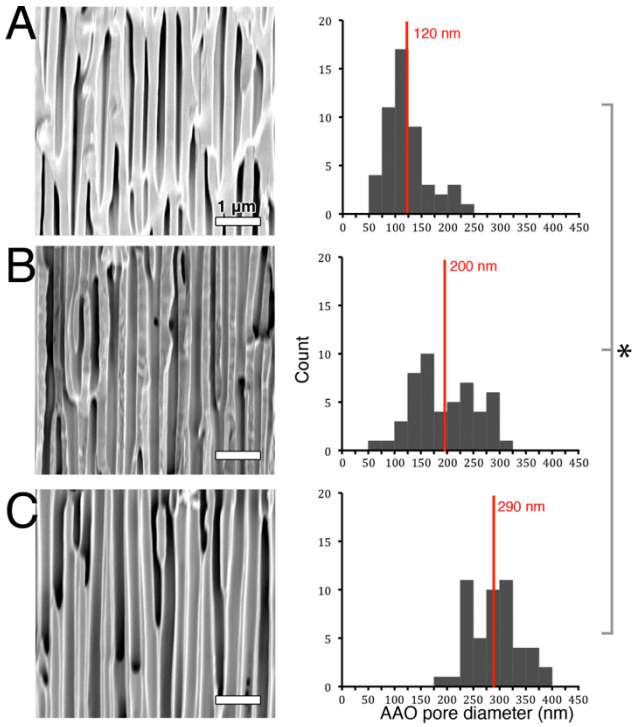

Figure 2.4. SEM images and histograms of AAO pore diameters. Cross sections of Whatman Anodisc® AAO membranes with nominal pore diameters of 0.02 μm (**A**), 0.1 μm (**B**), and 0.2 μm (**C**) were imaged with SEM, and diameters were measured to determine average pore diameters of 120 ± 40, 200 ± 60, and 290 ± 50 nm, respectively. Scale bars are 1 μm. *Indicates statistically significant difference between average nanowire diameter with $p < 0.001$.

2.4.3. Nanowire wettability enhances drug localization

We hypothesized that, once wetted with drug/reagent solution, micropatterned nanowire arrays would facilitate high-resolution drug/reagent localization as solvent evaporated. The wettability of a nano-rough surface is highly dependent upon the entrapment of air within the nanofeatures, with entrapped air reducing liquid-solid contact and thereby reducing surface wettability.[198, 199] To compare the wettability of PCL nanowire arrays to non-templated PCL films under conditions relevant to the localization approach proposed in this study, contact angles were

measured for non-templated PCL, non-templated NaOH-treated PCL (to investigate the effects of NaOH exposure during AAO etching), and PCL nanowire arrays under pre-wetted conditions. Films were pre-wetted by submerging in water and then spinning at 2000 rpm for 5 s to remove excess water. Droplets added to PCL nanowires were taken into the nanowire arrays and could not be measured for contact angle while the contact angles of non-templated PCL and non-templated NaOH-treated PCL were 78 ± 2° and 73 ± 4°, respectively (Figure 2.5). The dramatically enhanced wettability of PCL nanowires over non-templated PCL under pre-wetted conditions suggested that micropatterned nanowire arrays could potentially draw in drug/reagent solution as solvent evaporated, providing high-resolution drug/reagent localization.

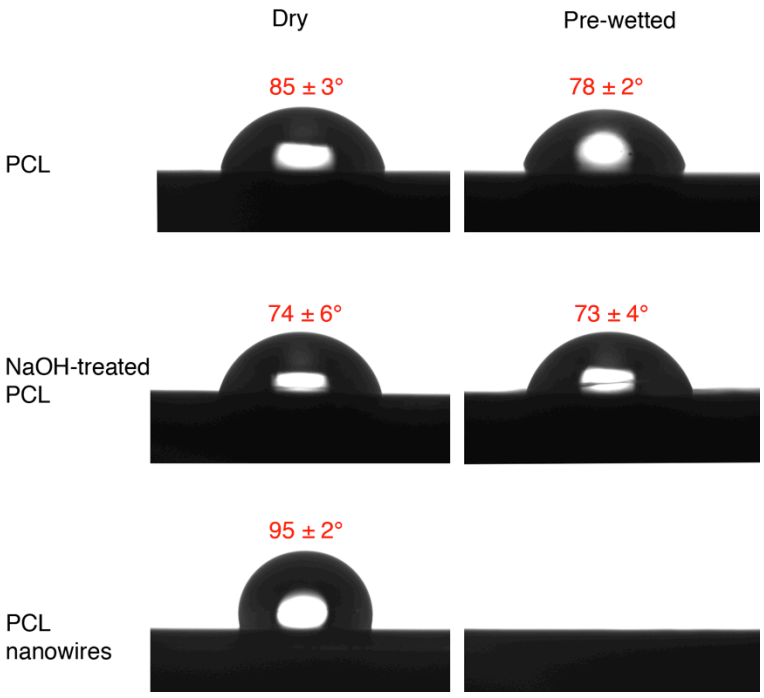

Figure 2.5. Nanowire films are highly wettable following initial contact with water. Water (5 μL) water was dispensed onto PCL films composed of PCL, PCL treated with 0.5 M NaOH for 1 h (to match NaOH treatment for AAO membrane etching), and PCL nanowires with and without pre-wetting. Pre-wetting consisted of submerging the films in water, spinning the films at 2000 rpm for 5 s to remove excess water, and imaging droplets within 1 min. Under dry conditions, the nanowire coating resulted in a higher contact angle than both non-templated PCL and NaOH-treated non-templated PCL, possibly as a result of air entrapment within the nanowire arrays. However, when nanowire films were pre-wetted, water droplets were taken up by the nanowire arrays, preventing measurement of contact angle and demonstrating that nanowires arrays are highly wettable following initial exposure to water.

To investigate this approach, 40 μm PMMA microstructures coated with either PCL nanowires or non-templated PCL lacking nanowires as a control were wetted with solutions of the hydrophilic reagents FITC-BSA and FITC-dextran (average MW = 10 kDa) in water or the hydrophobic reagents Oregon Green 488 - paclitaxel and Nile red in ethanol at 5 μg/cm^2, inverted, and allowed to dry. The thin film of water or ethanol dried within 10 min (Figure 2.6).

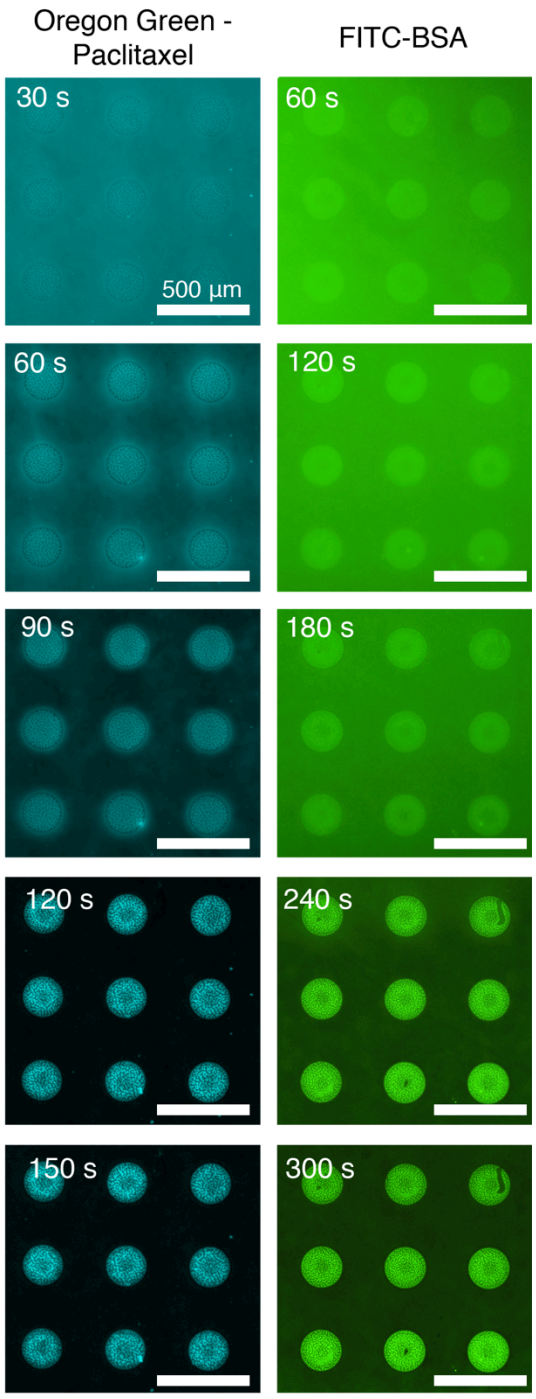

Figure 2.6. Time-lapse fluorescence imaging of Oregon Green – Paclitaxel and FITC-BSA localization over micropatterned PCL nanowire array films. Each image is labeled with the time after the addition of drug/reagent. Scale bars are 500 µm.

The features were then imaged with confocal microscopy to determine the localization of the fluorescently labeled drug/reagent. While features coated with non-templated PCL demonstrated drug/reagent localization to regions between the PMMA microstructures (Figure 2.7 A,D), features coated with PCL nanowires facilitated localization to the surface of the microstructures (Figure 2.7 B,E) indicating that the nanowire arrays mediated drug/reagent localization. Within the nanowire arrays, drug/reagent fluorescence intensity patterns showed clustered regions approximately 1 to 10 μm in width (Figure 2.7 C,F), similar to the PCL nanowire folding/clustering pattern observed in nanowire arrays (Figures 2.2 and 2.3).

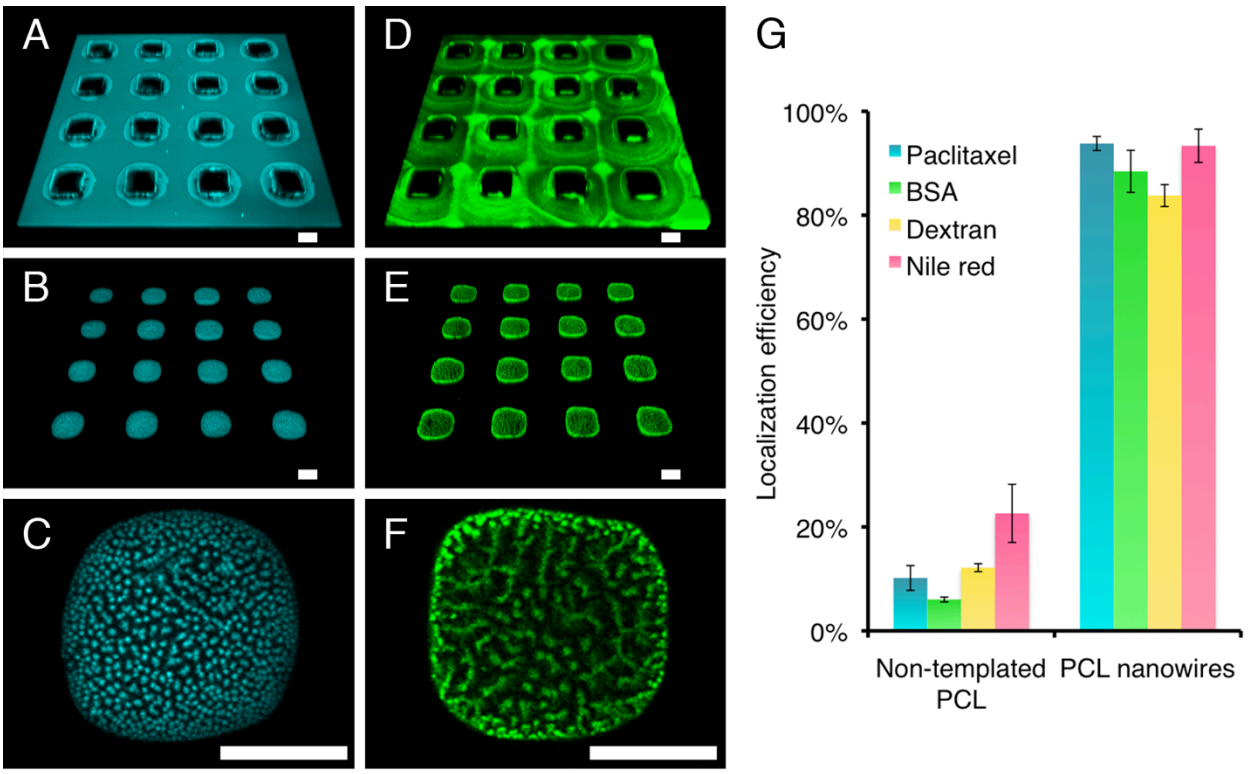

Figure 2.7. Nanowires mediate drug/reagent localization. Three-dimensional confocal imaging reconstructions of 5 μg/cm^2 Oregon Green 488 - paclitaxel (**A-B**) and FITC-BSA (**D-E**) loaded onto features with either non-templated PCL (**A, D**) or PCL nanowires (**B, E**) demonstrate that nanowires dramatically enhance drug/reagent localization to array features. Two-dimensional confocal imaging slices of loaded nanowire arrays (**C, F**) show clustered localization patterns, suggesting that drug/reagent collects between nanowires as a result of capillary action. **G.** Localization efficiencies of drugs/reagents were quantified as the ratio of fluorescence intensity integrated over the microstructures to the fluorescence intensity integrated over the entire analyzed region. All scale bars are 20 μm.

This intensity pattern indicated that drug/reagent localized to clustered nanowires, suggesting that localization was mediated by capillary action between nanowires as solvent evaporated. Furthermore, time-lapse fluorescence imaging demonstrated that drug/reagent solutions collected over nanowire-coated features over time as solvent dried (Figure 2.6), further

suggesting that nanowires enhanced drug/reagent localization by drawing in drug solution. While many drug loading techniques are only compatible with water-soluble drugs,[181, 182] micropatterned nanowire arrays provided efficient localization of both hydrophilic, water-soluble and hydrophobic, water-insoluble reagents through selection of solvents to maximize solubility. To quantify drug/reagent localization to microfeatures, the confocal imaging Z-stacks were merged by mean intensity values, and localization efficiency was calculated as the ratio of fluorescence intensity integrated over the microstructures to fluorescence intensity integrated over the entire analyzed region. The presence of nanowires dramatically increased localization efficiencies for all reagents tested (Figure 2.7G). Further investigation of FITC-BSA localization demonstrated efficient localization onto nanowire arrays coating both PMMA films and PMMA microstructures for all feature sizes tested (Figure 2.8). Together, these results demonstrated a rapid, low-waste drug/reagent localization approach. Furthermore, because this drug localization is non-sequential, this approach could be easily scaled for a larger number of features.

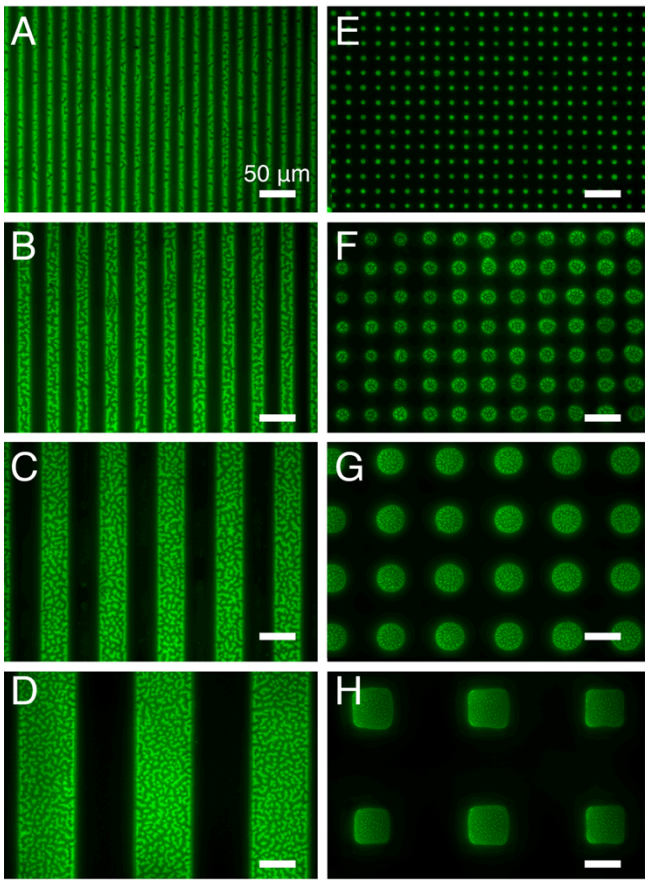

Figure 2.8. Nanowires provide efficient, high-resolution localization of BSA-FITC onto micropatterned PCL nanowire arrays coating PMMA films and microstructures. Fluorescent images of nanowire-coated films (**A-D**) and microstructures (**E-H**) with 10 µm (**A, E**), 20 µm (**B, F**), 40 µm (**C, G**), and 80 µm (**D, H**) feature sizes loaded with FITC-BSA at 5 µg/cm^2 show efficient localization for all feature sizes tested. Scale bars are 50 µm.

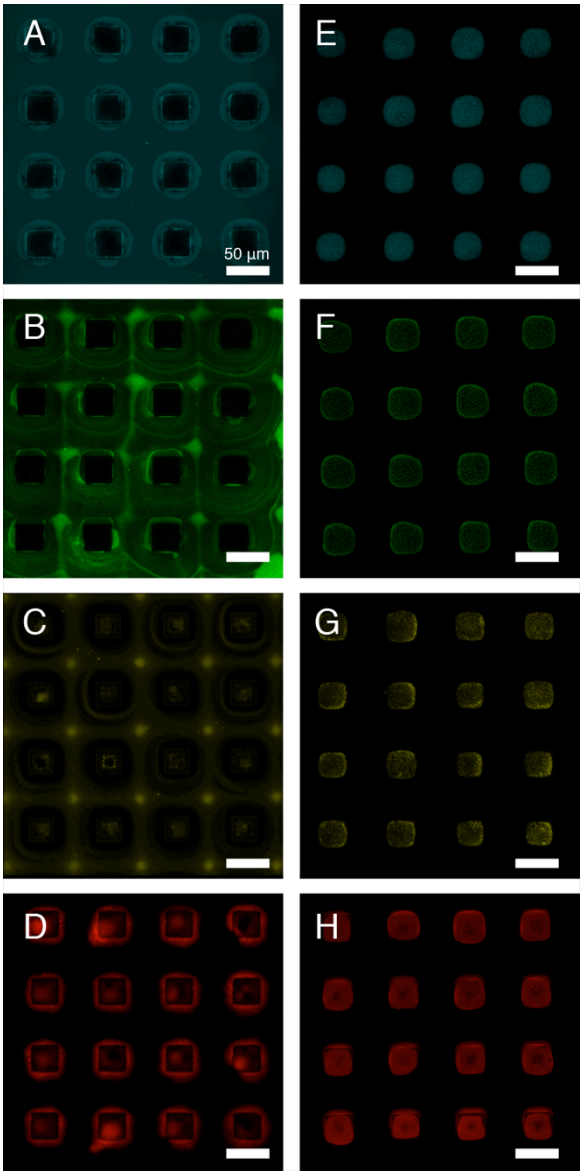

Figure 2.9. Nanowires provide efficient localization for hydrophobic and hydrophilic model drugs. Z-stacks of confocal fluorescent images of non-templated (**A-D**) and nanowire-coated (**E-H**) microstructures loaded with Oregon Green - paclitaxel (**A, E**), FITC-BSA (**B, F**), FITC-dextran (**C, G**), and Nile red (**D, H**) merged according to mean intensity values prior to quantification of fluorescence intensity to calculate localization efficiency. Scale bars are 50 µm.

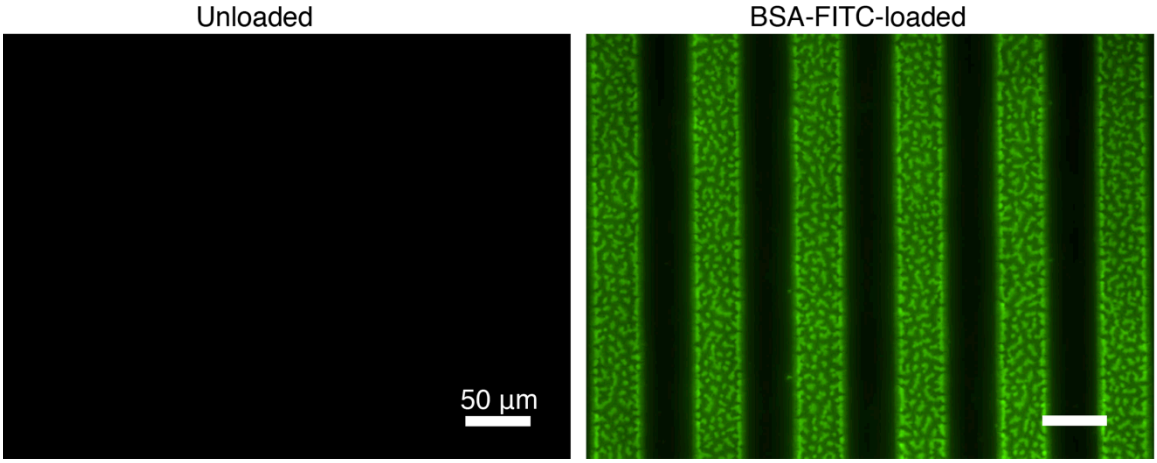

Figure 2.10. Drug localization signal is not a result of polymer autofluorescence. Micro-grooved nanowire arrays on PMMA films show no detectable signal before loading but show localized signal under identical fluorescence imaging conditions after loading FITC-BSA at 5 $\mu g/cm^2$, indicating that observed signal is a result of FITC-BSA fluorescence rather than polymer autofluorescence. Scale bars are 50 µm.

The ability to concentrate reagents onto high-resolution patterns could be employed to enhance biological analysis. For example, micropatterned nanowire arrays could be utilized to miniaturize biological assays into a microarray format while providing rapid, low-waste localization of reagents or samples. In addition to efficient localization, the concentration of luminescent samples to microscale regions may also increase local signal intensity, thereby enhancing sensitivity. Furthermore, based on a pore density of 13 ± 1 pores/μm^2 for the 290 nm pore size AAO membranes (Figure 2.11), nanowires fabricated from these membranes to 15 µm in length and 320 nm in diameter will provide greater than a 1000-fold increase in surface area available for conjugation of biomolecules or reagents, also potentially enhancing signal intensity.

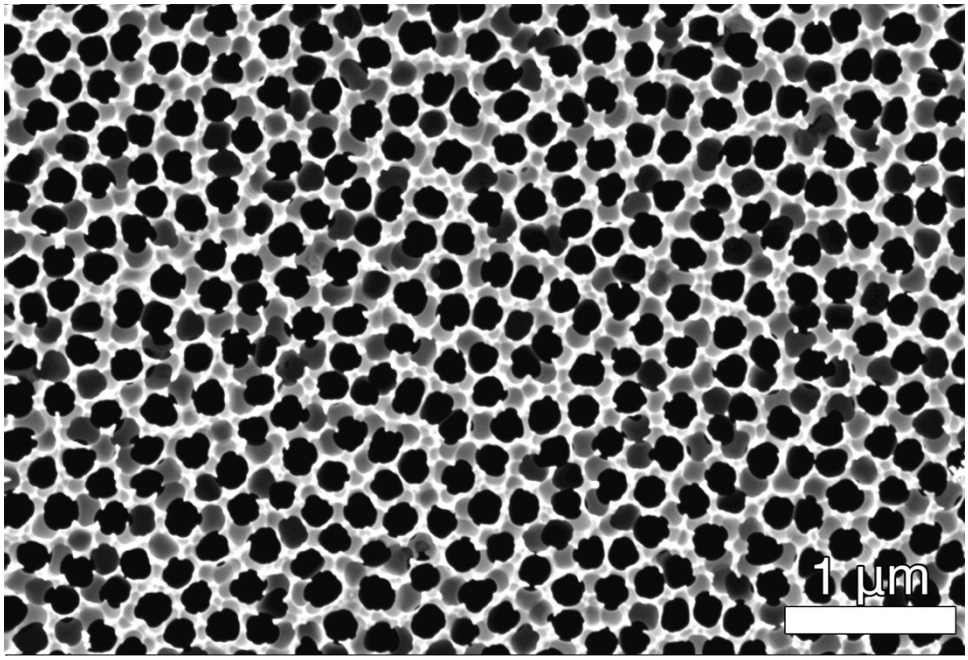

Figure 2.11. SEM imaging and quantification of AAO membrane pore density. Five regions of 200 nm nominal pore size AAO membranes were analyzed to determine a density of 13 ± 1 pores / μm^2.

This localization approach may also have applications to biomedical microdevice technology. Microfabricated devices loaded with drug can significantly increase the uptake of drug *in vitro* and *in vivo*.[39, 183, 200, 201] However, the task of loading drug into the micron-scale reservoirs of these devices is a major challenge to the scale-up of this technology. For example, relatively high-throughput loading approaches such as photolithography suffer from wasted materials as a result of the spin-casting and development steps,[45, 182, 183] which is a major drawback when loading expensive drugs. Conversely, low-waste approaches such as ink-jet printing allow for quasi-zero-waste loading but require sequential loading of individual drug reservoirs, limiting throughput and scalability.[181, 182,184] Here, we present the first example of polymeric, nanowire-coated microparticles and demonstrate an inherent mechanism for rapid,

low-waste drug localization. Such structures may be used in the development of more cost-effective and scalable biomedical microdevices and drug delivery systems.

2.4.4. Micropatterned nanowire arrays control cellular morphology through both microscale and nanoscale interactions

We also investigated the application of micropatterned nanowire arrays to provide hierarchical topographical control over cellular behavior. Microscale topography influences cell growth through the alignment of cells with topographical features, a cellular behavior known as contact guidance.[179] This influence over cellular shape and elongation can alter cytoskeletal tension, resulting in altered signal transduction.[202] Nanoscale features, which approach the macro-molecular scale, interact more directly with integrins, transmembrane receptors that allow cells to recognize and bind to their external environment, leading to the formation of focal adhesion complexes.[154, 203] Both the nanoscale distribution of integrin receptors and the micron-scale size and shape of focal adhesions influence cellular behavior through downstream signaling pathways.[178, 180] *In vivo*, cells reside in niche environments with tissue-specific micro- and nanotopography. Skin, bone, tendon, neural tissues, skeletal muscle, and blood vessels all present hierarchical micro/nanostructures of specific dimensions.[154, 204] Scaffolds designed to mimic the micro- and nanotopography of cellular niche environments have been used to decrease fibrosis and enhance regeneration for wound healing,[174, 176, 205, 206] maintain stem cell pluripotency *in vitro*,[180, 207-209] and direct stem cell growth and differentiation for therapeutic applications.[171, 172, 177, 210, 211]

To investigate the ability of micropatterned nanowire arrays to simultaneously influence cells on both the microscale and nanoscale, 3T3 fibroblast cells were grown on films consisting

of non-templated PCL, PCL nanowires, micropatterned non-templated PCL (with grooves 10 μm in width and 5 μm in height), and micropatterned nanowire arrays (with grooves 10 μm in width and nanowires 5 μm in length) (Figure 2.12 A-D). After two days of culture, fibroblasts were fixed, permeabilized, and stained to visualize nuclei, actin, and vinculin, a focal adhesion protein (Figure 2.12 E-L). While fibroblasts cultured on films without micropatterns showed isotropic morphology as indicated by actin staining (Figure 2.12 E-F), fibroblasts cultured on micropatterned films extended along the microgrooves (Figure 2.12 G-H). However, fibroblasts cultured on micropatterned nanowires showed a significantly higher degree of elongation than cells cultured on non-templated PCL microgrooves lacking nanotopography. Vinculin staining, which visualized the effects of scaffold topography on cellular focal adhesion formation, provided a possible explanation for this enhanced cellular elongation. The extensions of cells grown on nanowire arrays (Figure 2.12 J,L) showed increased vinculin localization relative to cells grown on films lacking nanotopography (Figure 2.12 I,K). This observation suggested that nanowires enhanced focal adhesion formation, which agrees with previous studies demonstrating that polymeric nanowire arrays promote cellular adhesion.[197, 212] It is possible that, when micropatterned to direct cellular alignment and the direction of cellular growth, the enhanced focal adhesion provided by nanowires in turn increases cellular elongation.

Taken together, these results demonstrate that the micropatterned nanowire arrays influenced cells through both microgroove-mediated contact guidance and nanowire-mediated focal adhesion formation to provide a unique cellular morphology not achievable through micro- or nanotopographies alone. With customizable micropatterning and tunable nanowire length and diameter, this fabrication approach could be used to create scaffolds designed to mimic different cellular niche environments with specific nanoscale topographies and microscale patterns. As

PCL can be functionalized and matrix-loaded with chemical factors,[213, 214] future studies may also incorporate signaling molecules into these scaffolds to further recapitulate cellular niche environments.

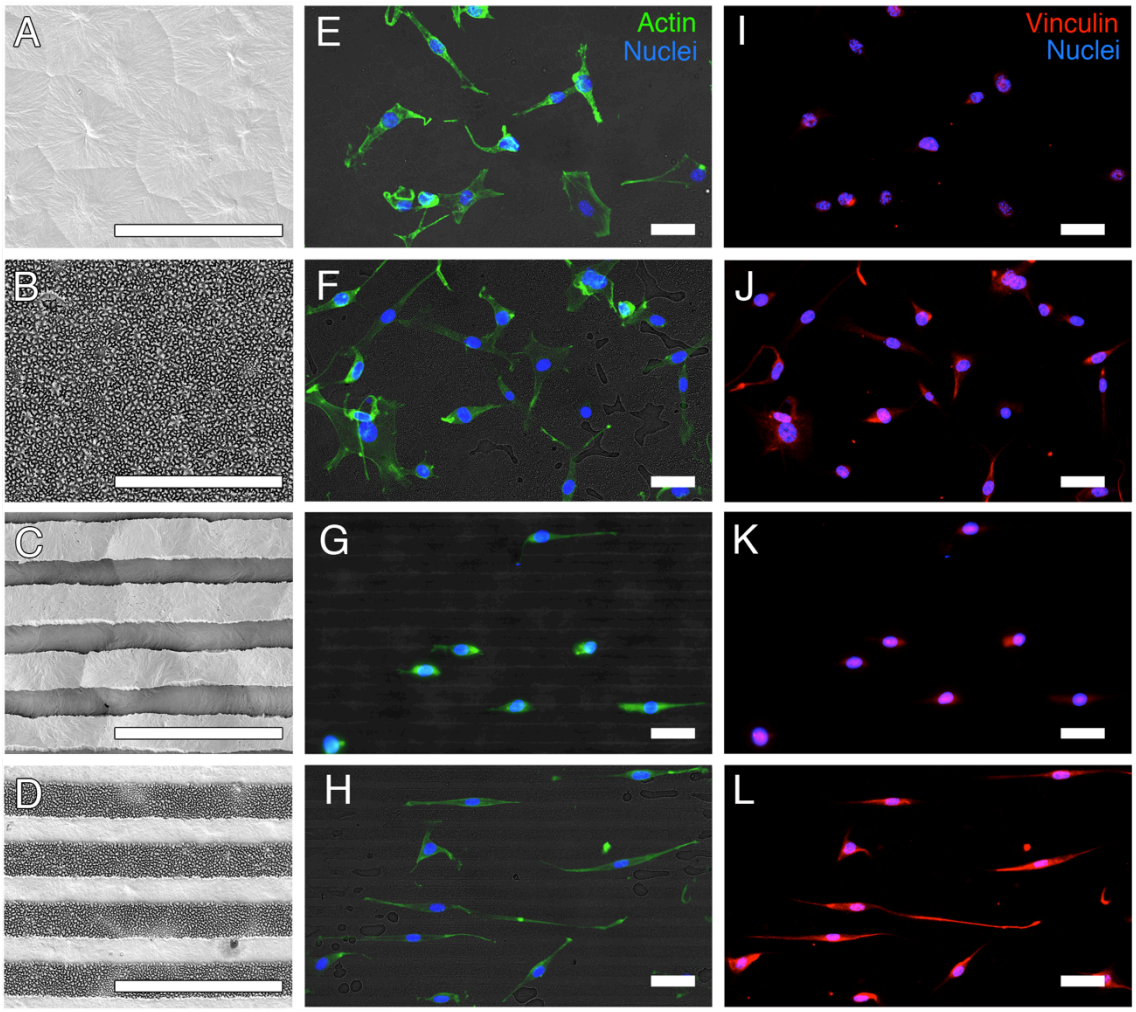

Figure 2.12. Micropatterned nanowire arrays simultaneously influence cellular behavior on both the micro- and nanoscales. Fibroblasts were cultured on non-templated PCL (**A**), PCL nanowire (**B**), micropatterned non-templated PCL (**C**), and micropatterned PCL nanowire (**D**) films (imaged with SEM). Staining of actin (green) and nuclei (blue) merged with brightfield images (**E-H**) demonstrates that micropatterned films (**G-H**) promote cellular alignment to microgrooves, with micropatterned nanowires (**H**) providing enhanced cellular elongation relative to micropatterned PCL lacking nanotopography (**G**). Vinculin (red) and nuclei (blue) staining (**I-L**) demonstrates that nanowires increase vinculin localization to cellular extensions (**J, L**) relative to cells cultured on non-templated PCL (**I, K**), indicating that nanowires enhance focal adhesion formation. Scale bars are 50 μm.

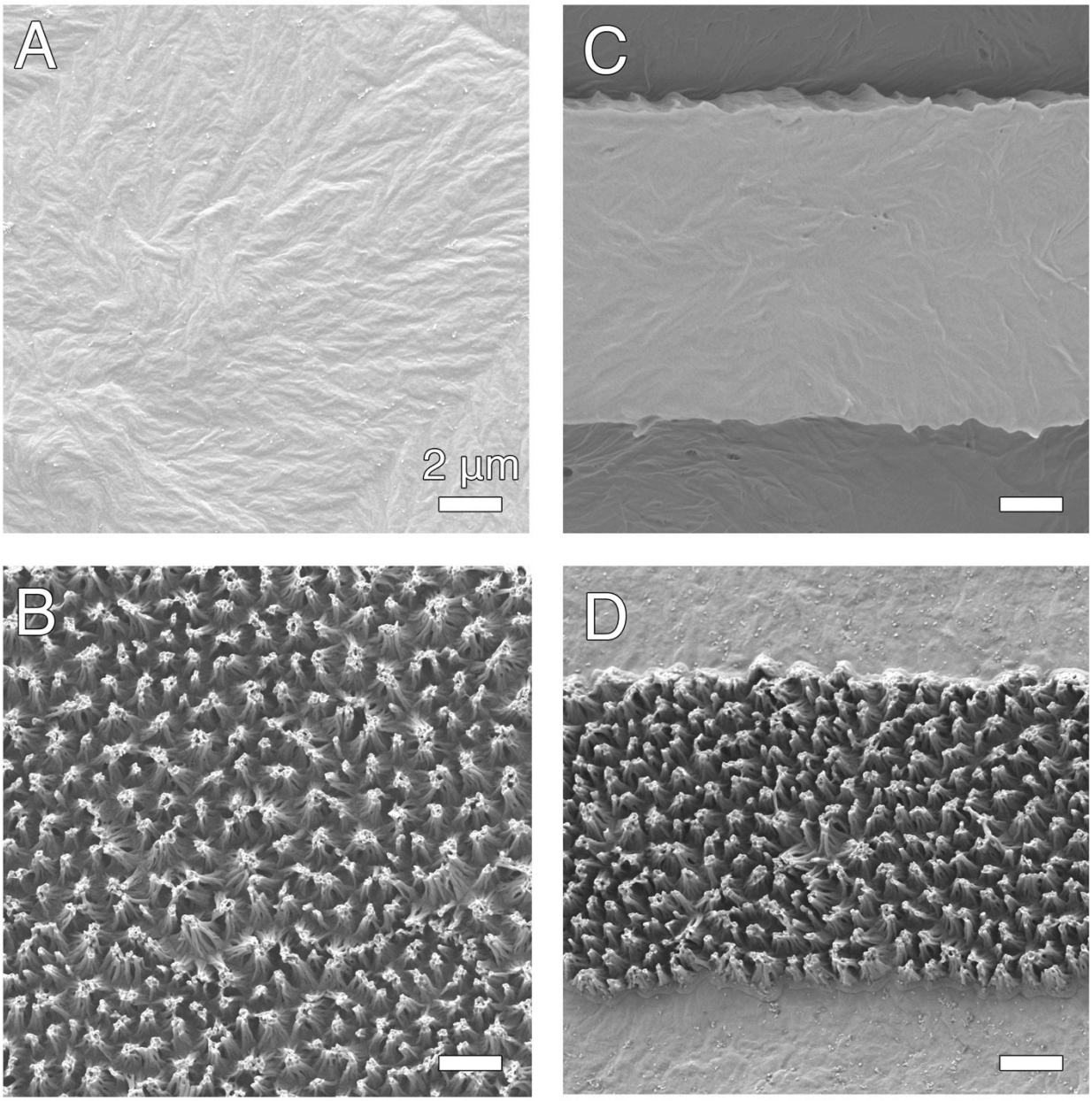

Figure 2.13. High-resolution SEM micrographs of cellular scaffolds. Non-templated PCL (**A**), PCL nanowire (**B**), micropatterned non-templated PCL (**C**), and micropatterned nanowire (**D**) films were used for fibroblast cell culture. Scale bars are 2 µm.

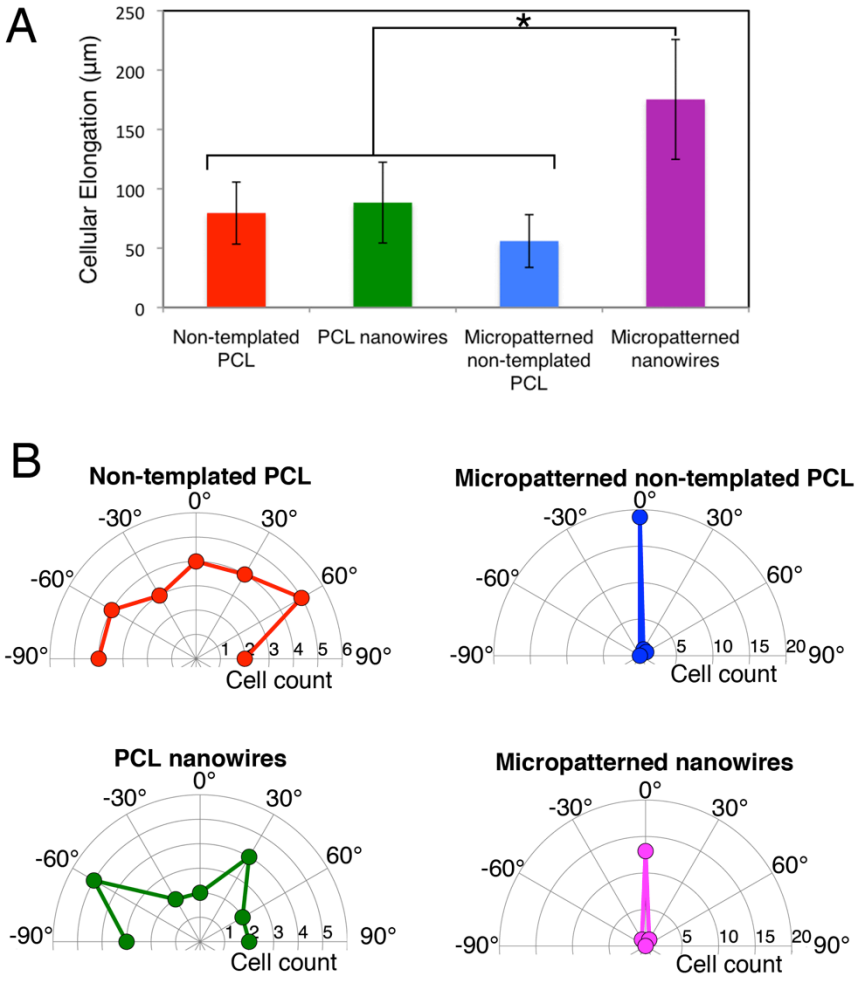

Figure 2.14. Quantification of cellular elongation and alignment of cells grown on PCL films. A. Quantification of cellular elongation, as determined by the distance between the two furthest points of each cell, demonstrated that cells grown on micropatterned nanowires were significantly more elongated than cells grown on films lacking micro- and/or nanotopography. *Indicates statistically significant difference between average cellular elongation with $p < 0.01$. **B.** Quantification of cellular alignment, plotted as histograms of the angles formed by the lines between two furthest points of each cell relative to the orientation of the microscale grooves, if present, demonstrated that micropatterned films enhanced cellular alignment in the direction of microgrooves.

2.4.5. Incorporating PCL nanowires onto the surface of microdevices for oral drug delivery

The fabrication approach reported here has potential to modify microdevices to enhance their properties for oral drug delivery. While microfabricated devices loaded with drug can significantly increase the uptake of drug *in vitro* and *in vivo*,[6, 39, 76, 215] the task of loading drug into the micron-scale reservoirs of these devices is a major challenge to the scale-up of this technology. For example, relatively high-throughput loading approaches such as photolithography suffer from wasted materials as a result of the spin-casting and development steps,[6, 45, 216] which is a major drawback when loading expensive drugs. Conversely, low-waste approaches such as ink-jet printing allow for quasi-zero-waste loading but require sequential loading of individual drug reservoirs, limiting throughput.[216, 217,218] Coating microdevices with nanowires could provide an inherent mechanism for high-throughput, low-waste drug loading. Furthermore, we hypothesized that the dramatic increase in surface area provided by nanowires would enhance device bioadhesion.

In order to test these hypotheses, we first used the fabrication approach presented here to create nanowire-coated microdevices (Figure 2.15). These devices were approximately 200 μm in diameter and 20 μm in thickness (Figure 2.16). These devices are detachable from the silicon wafer (Figure 2.17) and are similar in geometry to previously developed microfabricated devices for enhanced drug uptake. Specifically, they are planar in shape with a drug reservoir on only one side of the device, features shown to facilitate adhesion to monolayers of epithelial cells and unidirectional drug release toward epithelial tissue.[6, 39, 76, 215]

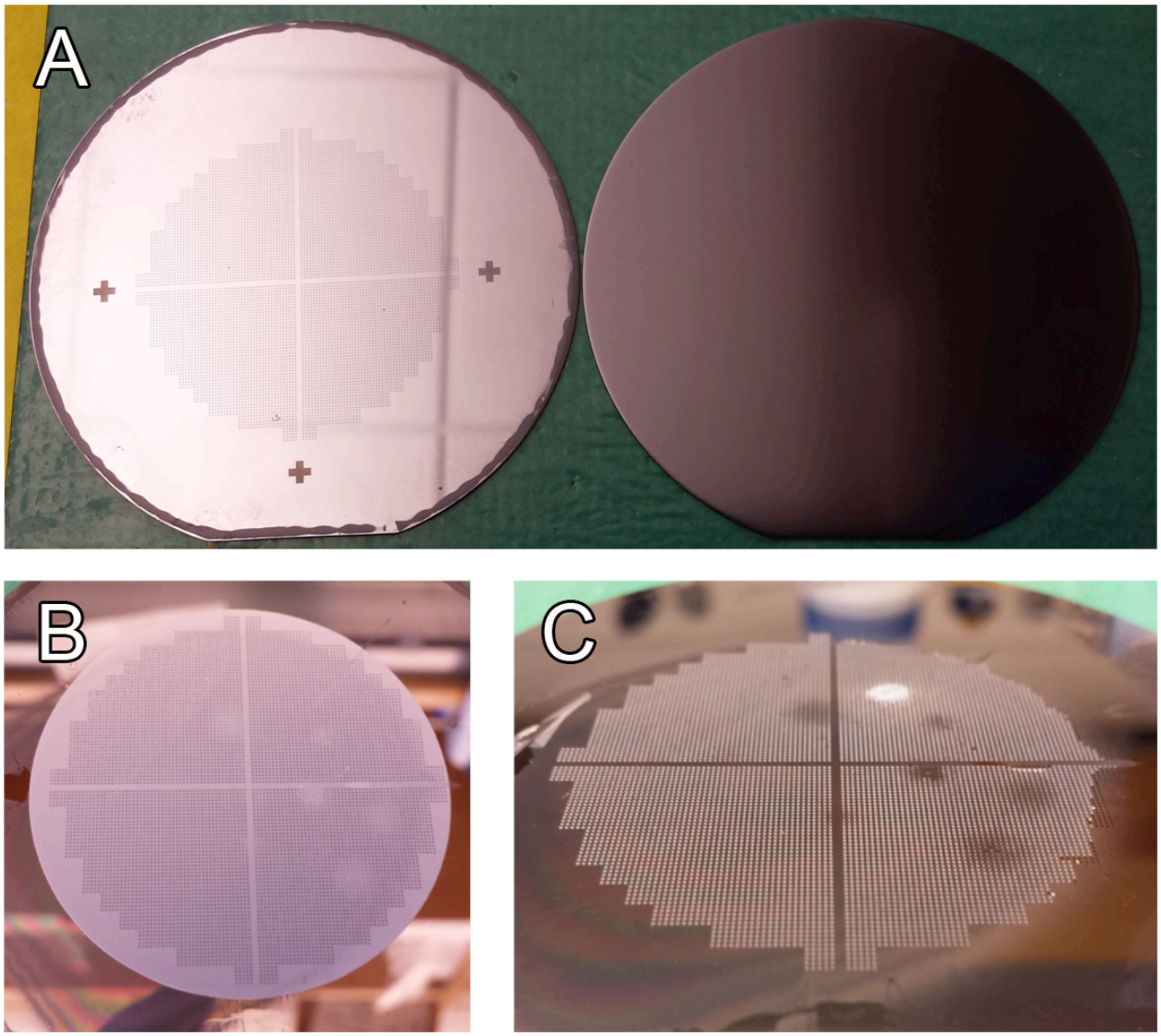

Figure 2.15. Images of microdevice fabrication process. A. PMMA microdevices (left wafer) and PCL layer (right wafer) prior to contact of both wafers under heat to coat microdevices with PCL. **B.** Image of PCL-coated microdevices templated with a nanoporous AAO membrane. **C.** Nanowire-coated microdevices after etching of AAO membrane in sodium hydroxide.

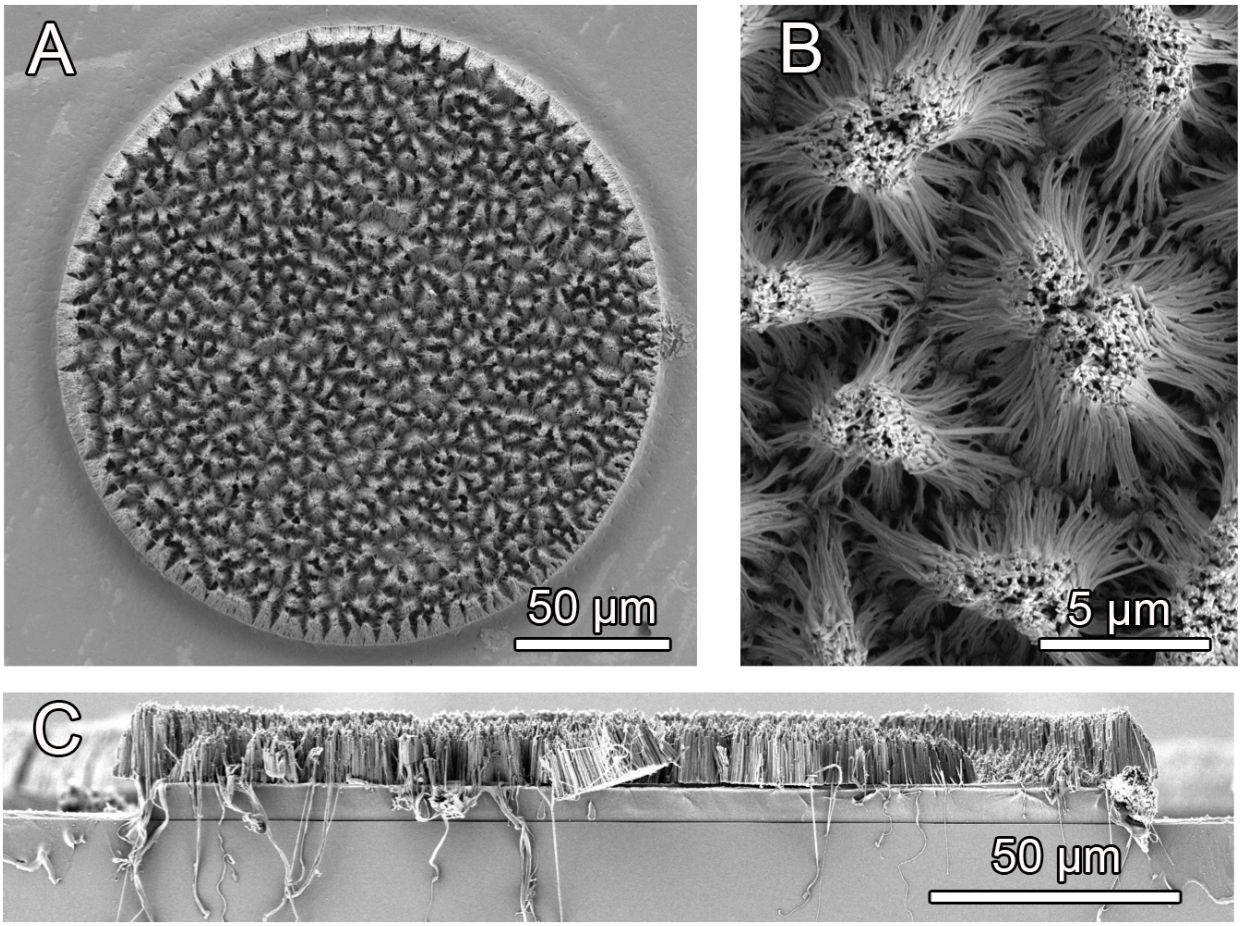

Figure 2.16. SEM images of nanowire-coated microdevices. Images show complete device structure (**A**), nanowires coating device (**B**), and a cross section showing the PCL nanowires coating the PMMA base structure (**C**).

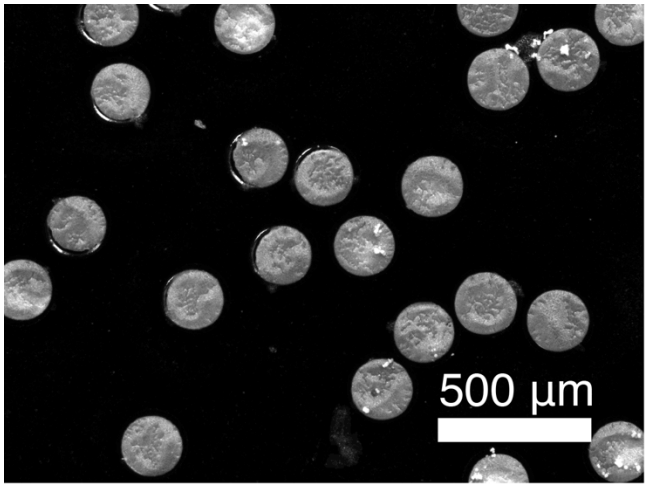

Figure 2.17. Nanowire-coated microdevices are detachable. A brightfield image of nanowire-coated microstructures following detachment by scraping the silicon wafer with a razor.

As demonstrated for nanowire-coated microstructures with smaller microstructure dimensions, the nanowires provided rapid and efficient drug loading onto the microdevices (Figure 2.18). Drug loading by capillary action is rapid, passive, and non-sequential, making it a scalable approach to drug loading of microdevices.

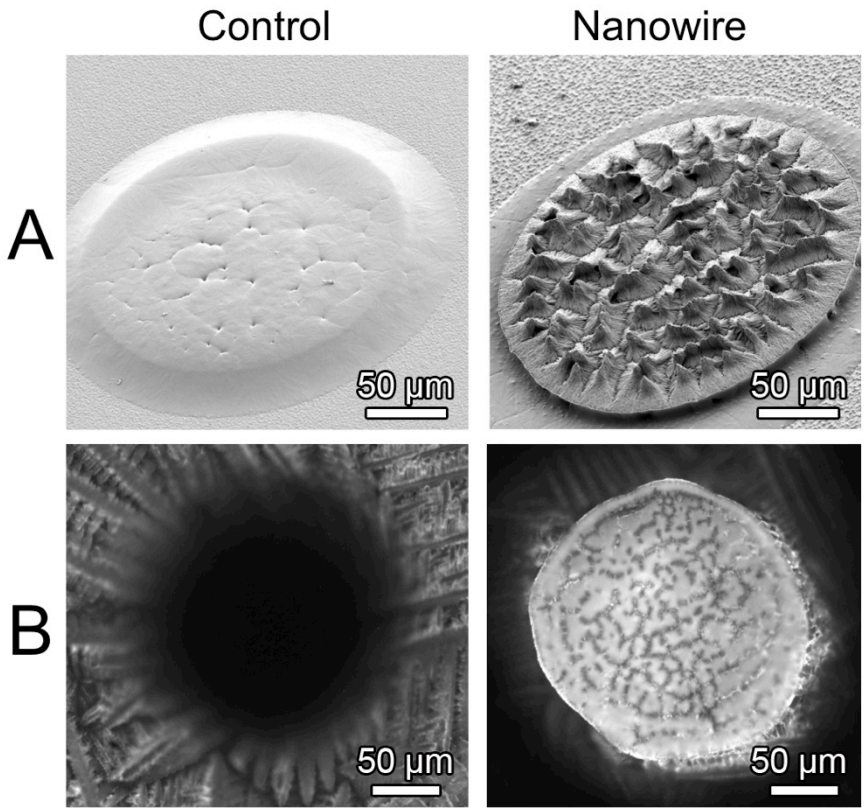

Figure 2.18. Nanowires enhance microdevice drug loading. A. SEM images of microdevices fabricated with nanowires or flat PCL as a control. **B.** Microdevices were loaded by solvent evaporation of FITC-BSA at 5 µg/cm^2, and drug localization was determined by fluorescence microscopy.

To determine the effect of the nanowire coating on device bioadhesion, we performed a flow cell adhesion assay in which we incubated the devices on Caco-2 intestinal epithelial cells and exposed the devices to increasing flow rates (Figure 2.19). Devices coated with PCL nanowires demonstrated consistently higher retention to the Caco-2 monolayer relative to devices coated with flat PCL, demonstrating that nanowires enhance device bioadhesion. This finding indicates that nanowires may be incorporated onto the surface of devices to enhance their adhesion to the GI tract, thereby prolonging drug exposure.

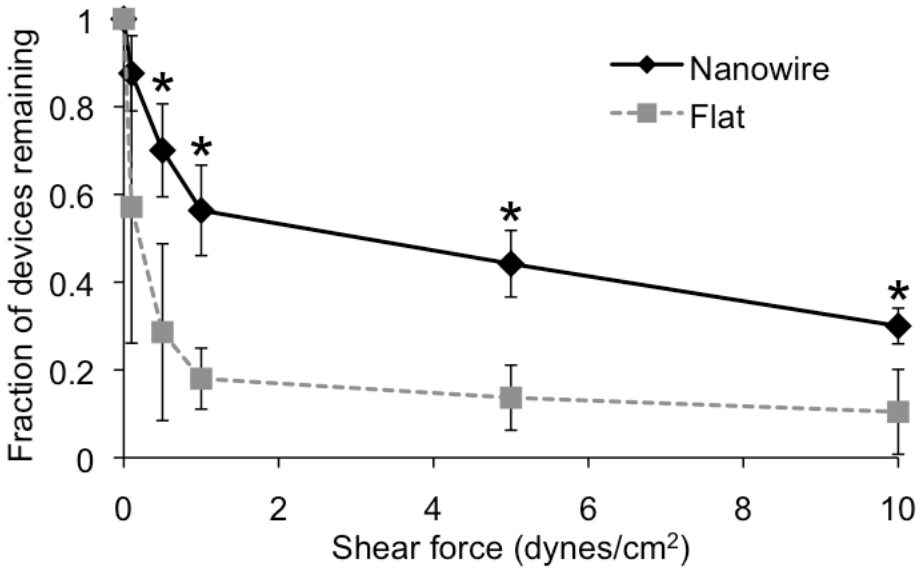

Figure 2.19. Nanowires enhance microdevice adhesion to a monolayer of Caco-2 epithelial cells. Nanowire-coated microdevices or control devices coated with flat PCL were incubated on Caco-2 cells and then exposed to increasing flow rates corresponding to physiological fluid shear stress values. The fraction of devices remaining adhered to the Caco-2 monolayer was determined at each time point. *Indicates statistically significance ($p < 0.05$).

The nanowire coating may provide additional advantages, as nanowires are capable of interacting with epithelial layers to increase cytoadhesion[85-87] and interrupting cell-cell junctions to enhance epithelial permeability.[87, 88, 219] Future studies will determine the efficacy of the nanowire-coated microdevices in enhancing drug uptake through these mechanisms.

2.5. Conclusion

Hierarchical micro/nanostructures have a number of biological applications, but the lack of nanofabrication approaches that are scalable while also allowing for custom patterning is a limiting factor in the application of these technologies. We have presented an approach to fabricate micropatterned arrays of polymeric nanowires without the need for sequential-write nanofabrication approaches. Furthermore, the techniques utilized in this approach have been shown to be highly scalable; roll-to-roll anodization approaches allow for high-throughput, relatively inexpensive fabrication of AAO membranes for templating,[220] and many automated photolithography approaches are capable of processing more than 60 wafers per hour.[221] Therefore, this approach could be easily scaled up in a cost-effective manner. In addition, the templating utilized in this approach creates nanowires with dimensions not easily achievable through other nanofabrication techniques. Specifically, the high pore density of AAO membranes and the ability to etch away the membrane after templating allow for creation of densely packed nanowires with aspect ratios >100,[168] features likely to increase the number of contact regions with cellular receptors and enhance drug/reagent loading capacity. Two variations of this approach provide fabrication of micropatterned nanowire arrays on either flat films or discrete microstructures, both with tunable nanowire dimensions and an inherent drug/reagent localization mechanism. This scalable nanofabrication approach has a number of possible biological applications in tissue scaffold fabrication, bioassay miniaturization, and biomedical microdevice technology. Notably, this fabrication approach could be used to incorporate nanotopography into microdevices for oral drug delivery. Given that nanoscale features have been shown to 1) significantly enhance microparticle adhesion,[85, 115] 2) disrupt epithelial tight junctions to increase drug permeability,[88] and 3) provide rapid capillary-action-

mediated drug loading as outlined here, this approach has potential to enhance microdevices through numerous mechanisms.

2.6. Acknowledgments

This work was partially funded by the National Institutes of Health. CBF was supported by NIH Training Grant 5T32GM007175-37 and an ARCS Fellowship. JK and EBS were supported by NIH Training Grant T32GM008155-29. We gratefully acknowledge use of the Carl Zeiss Ultra FE-SEM at San Francisco State University for all SEM imaging. The FE-SEM and supporting facilities were obtained under NSF-MRI award #0821619 and NSF-EAR award #0949176. Fluorescence imaging was conducted at the Nikon Imaging Center, UCSF. Reactive ion etching was performed at the UC Berkeley Biomolecular Nanotechnology Center. The authors would like to thank Drs. Kevin Healy and Peter Loskill for generously providing use of and training for the contact angle goniometer.

Chapter 3 – Sealed Nanostraw Microdevices to Enhance Oral Drug Bioavailability

3.1. Abstract

Coating microdevices with nanowires enhanced device bioadhesion and provide a rapid, efficient mechanism for drug loading. However, because the drug is surface-loaded onto the devices, release rates are difficult to tune. Additionally, fragile biological therapeutics may be damaged by the drying that occurs during the loading process. Here we seal microdevices with nanostraw membranes – porous nanostructured biomolecule delivery substrates – to mitigate issues with drug release rates and drying. We demonstrate that the nanostraws facilitate facile drug loading and tunable drug release, limit the influx of external molecules into the sealed drug reservoir, and increase the adhesion of devices to epithelial tissue. These findings highlight the potential of nanostraw microdevices to enhance the oral absorption of a wide range of therapeutics by binding to the lining of the GI tract, providing prolonged and proximal drug release, and reducing the exposure of their payload to drug-degrading biomolecules.

3.2. Introduction

The oral route of drug administration is preferred due to its ease of use and low cost, but the physiological barriers of the GI tract prevent the absorption of intact biological therapeutics and many small molecule drugs. Specifically, metabolic and proteolytic enzymes present throughout the GI tract and the low pH of the stomach degrade drugs, and the intestinal

epithelium and its adherent mucus layer limit permeation of drugs with high molecular weight or high polarity.[6, 222, 223] Additionally, many drugs exhibit low solubility and dissolve poorly within the small intestine, the primary site of systemic drug absorption.[6, 222, 224] Of such drugs with limited oral bioavailability, biological therapeutics are particularly challenging given their fragile nature and high molecular weights. However, some biological therapeutics currently require daily injections for periods of years to life (*e.g.* insulin to treat diabetes, human growth hormone to treat growth hormone insufficiency, calcitonin and parathyroid hormone to treat osteoporosis)[225] and are thus highly desired candidates for oral drug delivery.

Micron-scale devices with planar, asymmetric geometries, termed microdevices, have been designed to address the barriers to oral drug absorption. Microdevices readily adhere to the lining of the GI tract for prolonged durations while releasing drug at high concentrations, thereby increasing drug permeation.[226] Microdevice bioadhesion is facilitated by the micron scale of the devices, which increases their surface-area-to-volume ratio, and the planar device geometry, which increases their interfacial surface area and decreases the force from fluid flow exerted on devices.[39, 104] Furthermore, the asymmetric device design with the drug reservoir on only one side of the device can further enhance drug permeation; if the drug-releasing side of the device is selectively modified to have increased bioadhesion, then the devices can provide unidirectional release of drugs directly toward GI tissue.[46]

Microdevices are capable of significantly enhancing drug absorption both *in vitro* and *in vivo*.[39, 45, 104] However, loading drugs into the micron-scale reservoirs of these devices in a facile manner while also minimizing drug damage and achieving tunable and sustained drug release remains a challenge.[226] Additionally, incorporating nanotopography onto the surface of microdevices is likely to further enhance device bioadhesion by dramatically increasing their

interfacial surface area, but developing fabrication approaches to coat microdevices with nanoscale features remains technically challenging.[226, 227]

In this study, we enhance microdevice properties for oral drug delivery by incorporating nanostraw membrane caps. Nanostraws have been developed to facilitate the transport of nucleic acids, proteins, and drugs into cells for *in vitro* applications.[228-231] By piercing through membranes of seeded cells, nanostraws provide a pipeline for the diffusion of biomolecules directly into the cytosol.[228, 231] Here, we develop an approach to fabricate planar microdevices with drug reservoirs sealed by nanostraw membranes and validate the structure and integrity of these devices. We go on to demonstrate that the nanostraws facilitate tunable and sustained drug release, limit the influx of outside biomolecules, and increase device bioadhesion. These findings indicate the potential of these devices to increase the oral absorption of a wide range of drugs with poor bioavailabilities. Furthermore, the fabrication approach presented here may be adapted to create other diagnostic and therapeutic devices where sealed microchambers with sustained release of biomolecules, protection of loaded reagents, and/or enhanced bioadhesion are required.

3.3. Methods

3.3.1. Fabrication of nanostraw microdevices

Unless otherwise noted, all materials were purchased from Sigma-Aldrich (St. Louis, MO). First, two layers of 110 mg/mL 950 kDa PMMA (MicroChem) in anisole were deposited onto a 3-inch-diameter <111> silicon wafer (Addison Engineering) by spin casting at 1350 rpm

and curing at 110 °C for 1 min. Microposit S1818 photoresist (MicroChem) was spun cast over the PMMA at 2500 rpm and cured at 110 °C for 1 min. The photoresist was exposed to 225 mJ/cm^2 of UV light through a computer-designed photomask with arrays of opaque annuli (200 μm outer diameters, 100 μm inner diameters, 400 μm pitch). The photoresist was submerged in 351 Developer (MicroChem) diluted 1:3 in dH_2O for 2 min under gentle shaking. The 8 μm PMMA layer was anisotropically etched with oxygen plasma (450 W, 250 mTorr, 6.5 min) by 5.5 μm in regions not protected by photoresist. The remaining photoresist was removed by submerging in Microposit Remover 1112A (MicroChem) for 2 min and then rinsing with dH_2O. A wafer previously spun cast with 75 mg/mL 80 kDa PCL in trifluoroethanol at 1750 rpm was brought into contact with the microdevices on a hot plate at 80 °C, and the wafers were quickly separated. Nanostraw membranes were fabricated as previously described,[231] with minor modifications. Briefly, track-etch polycarbonate membranes with densities of either 10^7 cm^{-2} (AR Brown Global) or 3×10^7 cm^{-2} (GVS, Sanford, ME) and varying pore diameters were coated with aluminum oxide by atomic layer deposition, and the aluminum oxide layer was anisotropically etched by reactive ion etching with BCl_3 and Cl_2 in Argon (300 W, 40 sccm BCl_3, 30 sccm Cl_2, 5 mTorr, 5 min) on both sides of the membrane, waiting until the final fabrication step to expose the nanostraws by etching PC with oxygen plasma. The membrane was then brought into contact with the microdevices at 80 °C, melting the PCL and bonding the membrane to the devices. The membrane was spun cast with two layers of 75 mg/mL PVA at 2500 rpm, curing at 95 °C for 1 min after each deposition. SU-8 2015 (MicroChem) was then spun cast at 1250 rpm and cured at 95 °C for 5 min. The SU-8 was exposed to 250 mJ/cm^2 of UV light through an opaque photomask with 200 μm transparent circles aligned to the microdevices and then baked at 95 °C for 5 min. The devices were submerged in SU-8 Developer (MicroChem) for

5 min under gentle shaking and dried with a nitrogen gun. The membrane overhang and remaining PMMA between microdevices were removed by etching with oxygen plasma (450 W, 250 mTorr, 40 min). The devices were rinsed in dH_2O, dissolving the PVA and allowing the SU-8 caps to detach. The nanostraws were then exposed by partially etching the surrounding polycarbonate with oxygen plasma at a lower energy (100 W, 250 mTorr, 20 min).

3.3.2. Scanning electron microscopy

Non-biological samples were prepared for SEM by sputter coating with 8 nm of gold or iridium. Biological samples were prepared for SEM by fixing regions of tissue in 4% (w/v) paraformaldehyde in PBS followed by dehydration in a graded series of 20, 40, 60, 80, and 100% ethanol with 30 min of incubation at room temperature for each solution. Samples were stored in anhydrous ethanol at 4 °C overnight and then underwent critical point drying followed by sputter coating with 20 nm gold and iridium. Samples were imaged with a Carl Zeiss Ultra 55 Field Emission Scanning Electron Microscope. Nanostraw diameters were measured to be 62 ± 3, 94 ± 5, 165 ± 9, (membranes fabricated with nanostraw densities of 10^7 cm^{-2}) and 86 ± 17 nm (membrane fabricated with a nanostraw density of 3×10^7 cm^{-2}) by analyzing SEM images with Fiji software.[232, 233] Nanostraw lengths were measured with the same approach, accounting for the 45° imaging angle. All values in this study are reported with standard deviation.

3.3.3. Confocal imaging of internal microdevice structure

Microdevices were incubated overnight at 4 °C in a PBS solution (pH 7.4) with 10 mg/mL FITC-BSA (Sigma-Aldrich) to load device reservoirs with FITC-BSA and allow for

adsorption of FITC-BSA to device surfaces. The devices were then incubated at 37 °C in PBS for approximately 8 hours to allow for partial release of FITC-BSA from device reservoirs for reduced fluorescence intensity during imaging. The devices were then imaged while submerged in PBS with a spectral confocal microscope with a 488 nm laser for excitation and a 525 nm emission filter. Z-stacks were captured at 1 μm intervals over the entire device structure. Fiji software was used to restack confocal images along the z-axis.

3.3.4. Reservoir seal integrity assay

Microdevices fabricated using a nanostraw membrane (inner nanostraw diameter: 60 nm, nanostraw density: 10^7 cm^{-2}) or with a non-porous PC membrane were incubated in 10 mg/mL FITC-insulin (Sigma-Aldrich) in PBS overnight and rinsed with PBS. Microdevices were then submerged in PBS and imaged with brightfield microscopy to show device structure and fluorescence microscopy to observe FITC-insulin diffusion into device reservoirs.

3.3.5. Drug release assay

Silicon wafers with nanostraw microdevices were scored and broken into pieces approximately 1 – 2 cm^2 in area, and the microdevices on each piece were counted. The microdevices were then incubated in a PBS solution of 10 mg/mL FITC-insulin at 4 °C for 36 – 48 hours, rinsed in PBS for 1 min, and placed in PBS at 37 °C. The PBS solution was sampled with complete buffer exchange at 0.25, 0.5, 1, 2, and 4 hours. Drug concentrations were determined with fluorescence spectroscopy using a standard curve of serially diluted FITC-insulin, and the cumulative mass of released drug was normalized to device count.

3.3.6. Quantification of FITC-dextran permeation into device reservoirs

Nanostraw microdevices were incubated in a PBS solution of 1 mg/mL 10 kDa FITC-dextran (Sigma-Aldrich) at 37 °C. At 0.5, 1, 2, 4, and 48 hours, microdevices were quickly rinsed in PBS and imaged with confocal fluorescence microscopy, collecting images with 2 μm z-steps over the entire device reservoirs. All samples were imaged under identical conditions while avoiding saturation of fluorescence signal. To allow for comparison between rates of influx of outside biomolecules and release of loaded drug, the fluorescence intensity of FITC-insulin loaded into microdevices at 10 mg/mL was also monitored at 0, 0.5, 1, 2, and 4 h through identical methods. The fluorescence intensity within device reservoirs was integrated for each time point with Fiji software. FITC-dextran fluorescence intensity was normalized to devices equilibrated with the outside FITC-dextran concentration (t = 48 h), and FITC-insulin fluorescence intensity was normalized to devices imaged immediately after FITC-insulin loading (t = 0 h).

3.3.7. Caco-2 flow cell adhesion assay

An epithelial flow cell adhesion assay was performed as previously outlined[85, 100, 190, 191] with minor modifications. Briefly, approximately 400 microdevices, with or without oxygen plasma etching to expose nanostraws (inner diameter: 60 nm, density: 10^7 cm^{-2}), were scraped from the silicon wafer with a razor, suspended in 1 mL PBS, and added to a monolayer of Caco-2 epithelial cells (ATCC) in a petri dish. The microdevices were incubated over the cellular monolayer for 5 min under gentle shaking. A flow cell was then assembled over the microdevices, and a solution of 20 g/L porcine mucin (Sigma-Aldrich) in PBS was passed through the flow cell at increasing flow rates in a stepwise fashion, achieving fluid shear stress

values of 0.5, 1, 5, 10, 20, and 40 dyn/cm^2. After 5 min at each flow rate, the number of completely adhered microdevices (i.e., the number of microdevices lying flat on the Caco-2 monolayer) was determined by counting under a dissecting microscope, and the ratio of microdevices adhered to the original number of microdevices was determined.

3.3.8. *Ex vivo* adhesion assay

An *ex vivo* nanostraw microdevice adhesion assay was adapted from previous protocols.[234-237] Six C57BL/6 mice (Jackson Labs, maintained in specific-pathogen-free conditions) were sacrificed at 4 – 6 weeks of age, and the jejunum was excised. The intestinal segments were flushed with oxygenated Tyrode's solution (pH 6.8) to clear intestinal contents and confirm the absence of punctures, and the tissue was stored in oxygenated Tyrode's solution on ice until use within 4 h. For each sample, a jejunum segment was placed in a 37 °C bath of oxygenated Tyrode's solution. A 1 – 2 cm^2 piece of silicon wafer with approximately 400 – 800 nanostraw microdevices or control devices without exposed nanostraws (all loaded with 10 mg/mL FITC-insulin and washed in PBS for 1 min as previously described) was coated with 100 μL oxygenated Tyrode's solution, and devices were scraped from the surface of the silicon wafer with a razor. The suspended devices were slowly pipetted into the oral side of the jejunum and then flowed through the jejunum in oxygenated Tyrode's solution at 0.2 mL/min via a peristaltic pump. The buffer flowing out of the jejunum was passed through a metal grid with 70 μm spacing to collect detached devices. After 1 h of flow, the jejunum was cut longitudinally and placed between glass slides. The number of devices remaining within the jejunum and the number of devices collected in the metal grid were counted *via* fluorescence microscopy, and the percentage of devices remaining attached to the jejunum was calculated for each sample.

3.3.9. Device profilometry

Device height profiles were measured with an Ambios XP2 profilometer at various fabrication steps to determine nanostraw microdevice dimensions. Specifically, the height profiles of microdevices with etched PMMA after removal of photoresist, etched PMMA coated with PCL, and complete nanostraw microdevices were measured over the center of the devices. The thicknesses of the nanostraw membrane (following etching to expose nanostraws) and the PMMA base layer were also measured via profilometry. The PMMA base layer was scratched to expose the underlying silicon wafer prior to measurement. To account for the thickness of PMMA yet to be etched in remaining fabrication steps, the thickness of the PMMA base layer was added to the height profiles of the etched PMMA devices and the etched PMMA devices coated with PCL. The profile of the base of the nanostraw membrane was determined by subtracting the thickness of the nanostraw membrane from the profile of complete devices.

3.3.10. Quantification of nanostraw density heterogeneity at the cellular scale

Caco-2 cells were cultured as previously described to facilitate formation of a cellular monolayer.[88] SEM imaging indicated that the Caco-2 cells could be approximated as having edge lengths on the order of 10 μm. A nanostraw membrane (inner nanostraw diameter: 60 nm, nanostraw density: 10^7 cm^{-2}) was imaged with SEM. The SEM images were divided into 10 μm × 10 μm regions, an approximation of the dimensions of intestinal epithelial cells. The number of nanostraws contained within each of 100 analyzed regions was determined and plotted as a histogram showing the number of regions containing a given number of nanostraws.

3.3.11. Confocal fluorescence imaging to compare the amount of adsorbed FITC-insulin to the amount of in-solution FITC-insulin in device reservoirs

Nanostraw microdevices (inner nanostraw diameter: 60 nm, nanostraw density: 10^7 cm^{-2}) were incubated in 10 mg/mL FITC-insulin at 4 °C for 48 h and then washed in PBS for 1 min. The devices were imaged with confocal fluorescence microscopy, collecting images with 2 μm z-steps over the entire device reservoirs. The devices were incubated in 37 °C PBS for 24 h to facilitate drug release and imaged again under identical conditions.

3.3.12. Testing nanostraw microdevice retention of drug following detachment of microdevices from the silicon wafer

Microdevices were incubated in a PBS solution of 10 mg/mL FITC-insulin overnight, rinsed with PBS, and scraped from the wafer with a razor. Microdevices were then loaded into a channel formed by placing a 1.5 × 24 × 0.12 mm adhesive spacer (Grace Bio-labs) between a glass slide and coverslip. The microdevices were incubated at room temperature for approximately 30 min and then imaged with brightfield and fluorescence microscopy.

3.3.13. Determining if device reservoirs become saturated with FITC-dextran after incubation for 48 h

Nanostraw microdevices were incubated in 1 mg/mL FITC-dextran and analyzed with confocal microscopy as performed for the FITC-dextran influx assay, except the timepoints used were 48 and 72 h.

3.3.14. Determining total nanostraw microdevice drug capacity

Devices were loaded with 10 mg/mL FITC-insulin and monitored for drug release as described previously except the mass of drug released was determined at 48 h, after which time no significant drug release was detected.

3.4. Results

3.4.1. Device fabrication and characterization

To retain the planar, asymmetric microdevice design shown to enhance oral drug absorption, we designed the nanostraw microdevices to have circular bodies 200 μm in diameter with 100 μm diameter drug reservoirs sealed by nanostraw membrane caps, with a total device thickness less than 20 μm. The devices were fabricated through a series of deposition, photolithography, and anisotropic etching steps as shown in Figure 3.1. First, an 8 μm thick layer of poly(methyl methacrylate) (PMMA) followed by a layer of positive photoresist were spun cast onto a silicon wafer. The device body was then defined by exposing with UV light through a computer-designed photomask with arrays of opaque annuli (200 μm outer diameter, 100 μm inner diameter, 400 μm pitch) and subsequently developing the patterned photoresist (Figure 3.1 A). The PMMA was anisotropically etched by approximately 5.5 μm with oxygen plasma (Figure 3.2) in regions not protected by the photoresist (Figure 3.1 B). The remaining photoresist was chemically stripped, and the devices were briefly brought into contact with a polycaprolactone

(PCL) film under heat, coating the topmost surface of the PMMA device bodies with a layer of PCL (Figure 3.1 C).

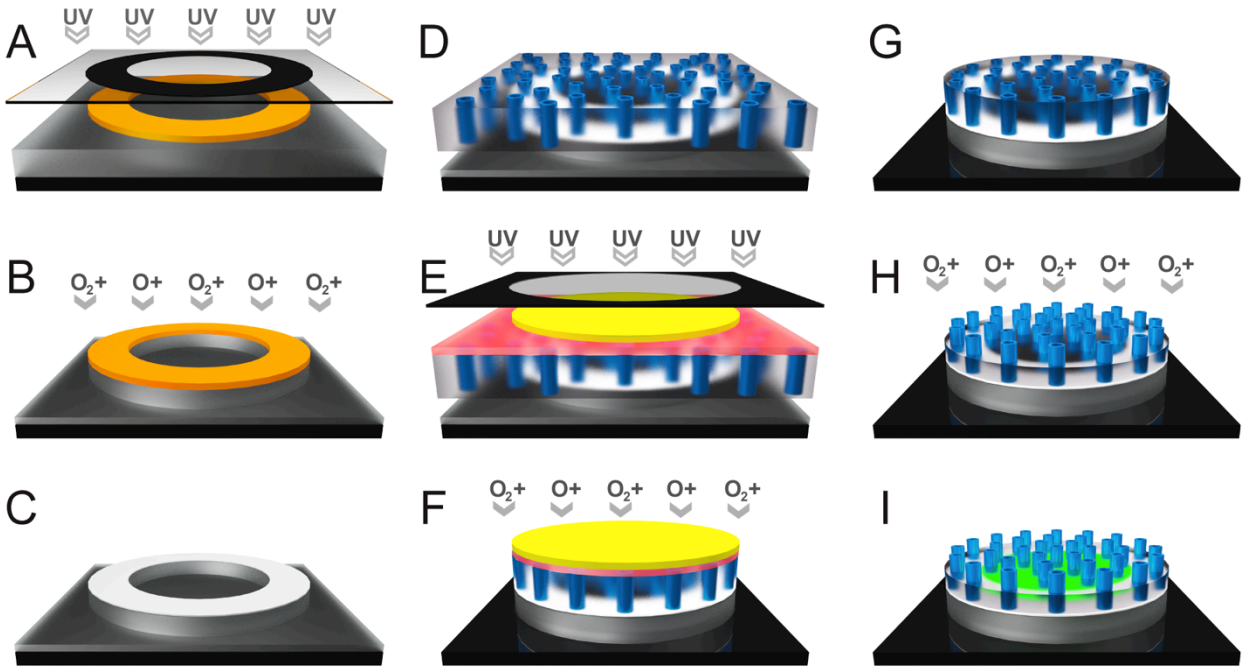

Figure 3.1. Nanostraw microdevice fabrication schematic. A. A silicon wafer (black) is spun cast with 1) PMMA (gray) and 2) positive photoresist (orange), and the photoresist is patterned *via* UV exposure through a computer-designed photomask with subsequent development. **B.** The PMMA layer is partially etched with oxygen plasma to form the device body. **C.** Following chemical removal of remaining photoresist, PCL (white) is transferred onto the surface of the devices by contact under heat. **D.** The devices are heat-bonded to a nanostraw membrane composed of PC (semi-transparent) interspersed with aluminum oxide nanostraws (blue), sealing the devices. **E.** The nanostraw membrane is spun cast with 1) PVA (red) and 2) negative photoresist (yellow), which is patterned over the devices *via* UV exposure through a photomask with subsequent development. **F.** The nanostraw membrane and PMMA are removed in regions not protected by the patterned photoresist by etching with oxygen plasma. **G.** The photoresist caps are detached by dissolving the underlying PVA layer in water. **H.** The polycarbonate is partially etched with oxygen plasma to expose the alumina nanostraws. **I.** Following incubation in a drug solution to facilitate drug loading *via* diffusion through nanostraws, the device reservoirs contain high concentrations of drug (green).

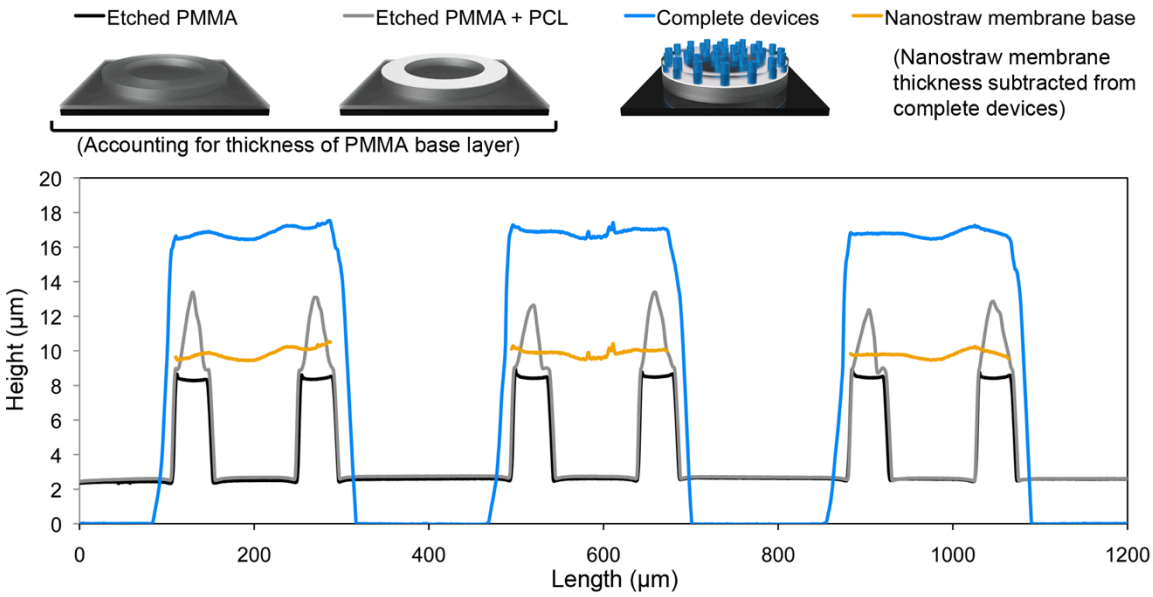

Figure 3.2. Height profiles of microdevices at various stages of fabrication. Height profiles show thicknesses of approximately 2.5 µm for the PMMA base layer, 7.5 µm for drug reservoirs, 7 µm for nanostraw membranes (following etching to expose nanostraws), and 17 µm for total device thickness (not accounting for nanostraw length). PCL thickness was 5 µm before nanostraw membrane bonding and 1 – 2 µm following compression during bonding.

To seal the device reservoirs, a nanostraw membrane composed of track-etched polycarbonate (PC) interspersed with vertically oriented aluminum oxide nanostraws was fabricated as previously described[231] and heat-bonded to the PCL (Figure 3.1 D). The track etch membranes used to fabricate nanostraw membranes can be tuned for precise control over pore diameter and density, with pore diameters ranging from 8 nm to the millimeter scale and densities as high as 10^{10} cm^{-2}.[228, 229, 231, 238-240] In this study, microdevices were sealed with nanostraw membranes ranging from 60 to 160 nm in inner nanostraw diameter and from 10^7 to 3 × 10^7 cm^{-2} in nanostraw density (drug release assays). For all other assays, devices were sealed with membranes with 60 nm inner nanostraw diameter and 10^7 cm^{-2} nanostraw density. To protect the nanostraw membrane during subsequent lithography steps, a sacrificial poly(vinyl

alcohol) (PVA) layer was spun cast over the nanostraw membrane. A negative photoresist was spun cast over the PVA and exposed to UV light through an opaque photomask with 200 μm transparent circles aligned to the devices. The photoresist was then placed in developer, dissolving the photoresist in regions not crosslinked by UV exposure (Figure 3.1 E). The regions of the nanostraw membrane and PMMA not covered by the crosslinked photoresist were etched with oxygen plasma (Figure 3.1 F), and the devices were rinsed in water to dissolve the PVA and release the photoresist caps (Figure 3.1 G). The devices were then exposed to low-energy oxygen plasma to partially etch the PC, exposing the nanostraws (Figure 3.1 H). Finally, the devices were incubated in concentrated drug solutions to load the device reservoirs *via* diffusion through nanostraws (Figure 3.1 I). The final nanostraw microdevices were composed of PMMA, PCL, PC, and aluminum oxide, which are FDA-approved materials in various implanted biomedical devices.[117, 241-243]

Scanning electron microscopy (SEM) demonstrated that nanostraw membrane caps were bound to the underlying PMMA device bodies (Figure 3.3A). The membranes had intact nanostraws measuring 2.2 ± 0.1 μm in length. While the distribution of nanostraws of membranes used in this study was stochastic on the nanometer scale, this distribution became more uniform on the cellular scale (Figure 3.4). This indicated that the nanostraw membranes would be capable of homogenous transfer of drugs at the cellular and tissue scales.

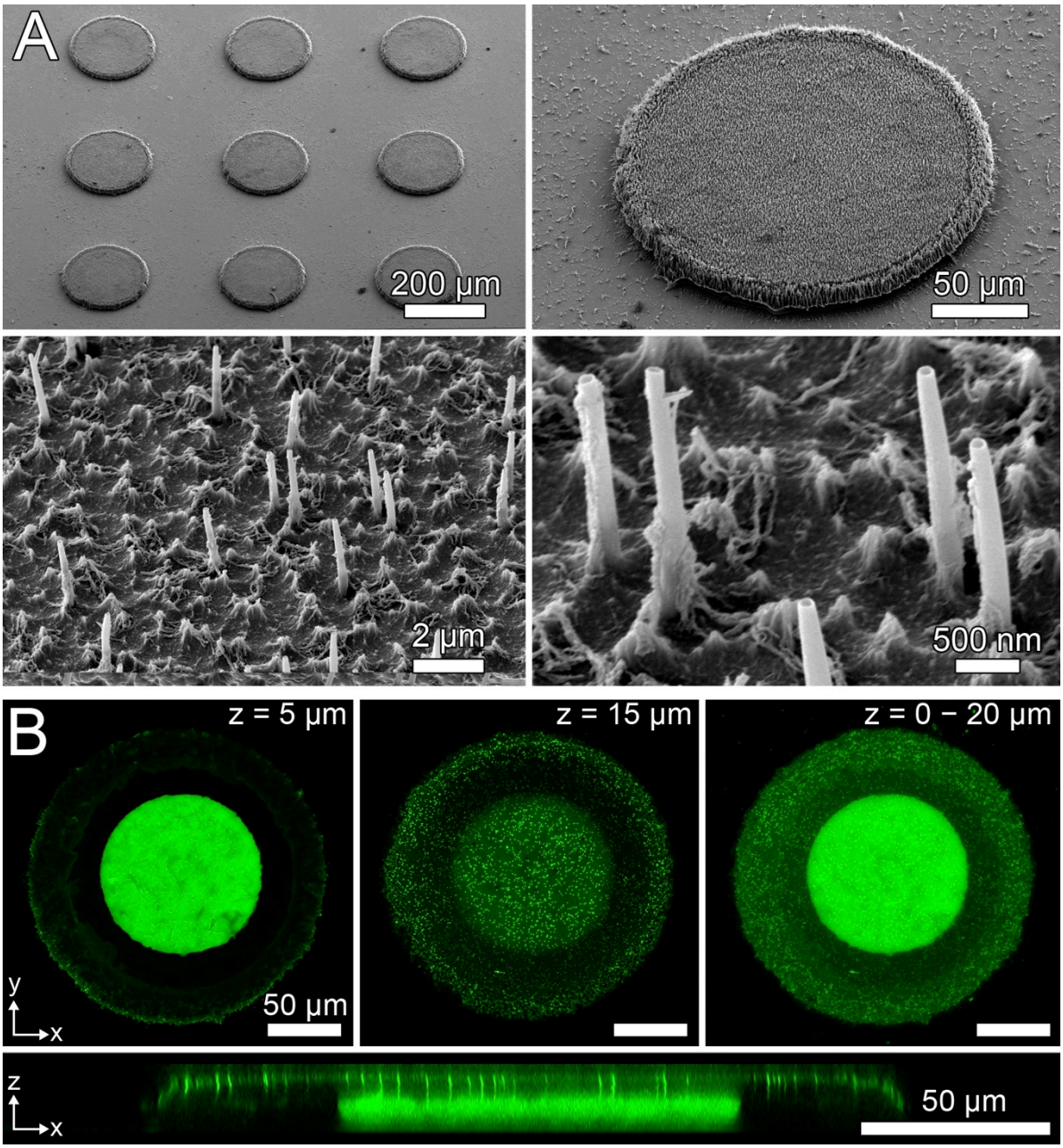

Figure 3.3. Characterization of nanostraw microdevice structure. A. SEM images demonstrate that microdevices were fabricated with intact nanostraw membranes. **B.** Confocal fluorescence microscopy of nanostraw devices incubated in a FITC-BSA solution and imaged while submerged in PBS provides visualization of the drug reservoir (z = 5 µm), the overlying nanostraw membrane (z = 15 µm), and overall device structure (z = 0 – 20 µm). An x-z cross section shows that nanostraws provide a fluidic conduit for drug diffusion between device reservoirs and the external environment.

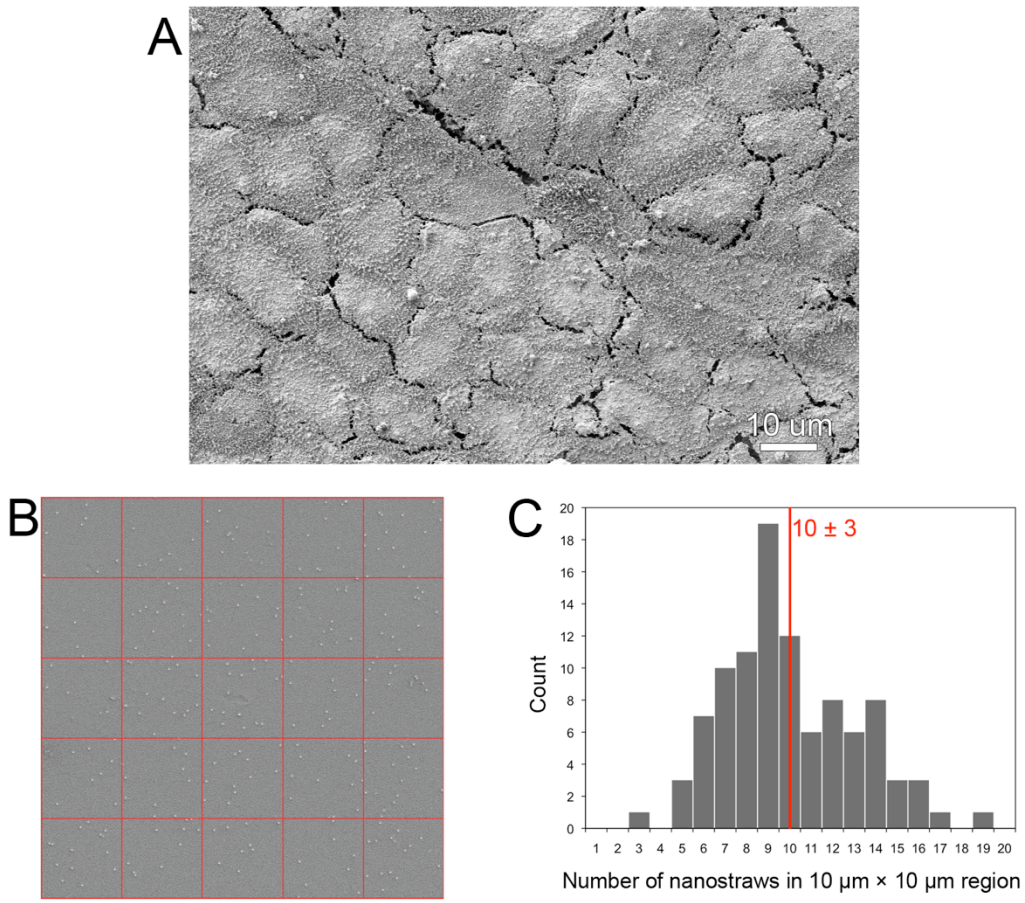

Figure 3.4. Quantification of heterogeneity in nanostraw density at the cellular scale. A. SEM imaging demonstrated that the cuboidal Caco-2 intestinal epithelial cells can be approximated as having edge lengths on the order of 10 µm. **B.** To determine the heterogeneity in nanostraw distribution at the cellular scale, SEM images of a nanostraw membrane (inner nanostraw diameter: 60 nm, nanostraw density: 10^7 cm^{-2}) were analyzed by quantifying the number of nanostraws within 10 µm × 10 µm regions (outlined in red). **C.** A histogram showing the number of regions containing a given number of nanostraws. There was a mean of 10 ± 3 nanostraws per 10 µm × 10 µm region (n = 100).

To characterize the internal structure of the devices, we incubated the microdevices overnight in FITC-tagged bovine serum albumin (FITC-BSA), a protein known to have high adsorption to a variety of surfaces.[191] This step allowed the fluorescently labeled BSA to both diffuse into device reservoirs and adsorb onto the surfaces of the microdevices. The microdevices were then incubated in phosphate buffered saline (PBS) for 8 h to allow for partial FITC-BSA release, thereby reducing fluorescence intensity of FITC-BSA dissolved within the drug reservoirs and allowing both the drug reservoirs and the device surfaces to be visualized. Adhered and loaded FITC-BSA was then imaged with confocal fluorescence microscopy. While biomolecular adsorption was found to be minimal relative to the amount of dissolved drug within the device reservoir (Figure 3.5), the adsorption of FITC-BSA to the surfaces of the devices (Figure 3.3 B) indicated that the devices could be incubated in concentrated BSA in order to block adsorption of drugs loaded in later steps. This treatment could block adsorption of drugs found to adhere to device surfaces to increase the efficiency of drug release from device reservoirs.[244]

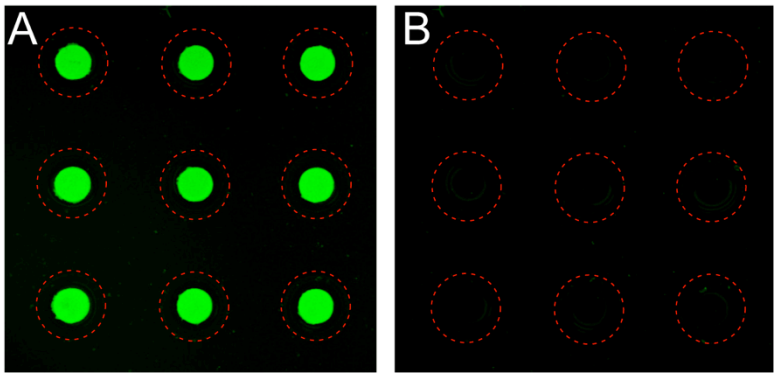

Figure 3.5. FITC-insulin adsorption to devices is minimal relative to the amount of FITC-insulin loaded within device reservoirs. A. Images of nanostraw microdevices loaded with FITC-insulin and washed in PBS for 1 min show that the fluorescence intensity of FITC-insulin adsorbed onto the surfaces of the devices (outlined in dotted red lines) is much lower than that of drug in solution within the device reservoirs, demonstrating that the 1 min wash in PBS was effective in removing non-loaded insulin from the external surfaces of the devices. **B.** The devices were imaged under identical conditions after the drug had been released in PBS at 37 °C for 24 hours, and the fluorescence intensity of FITC-insulin remaining adsorbed onto the surfaces of the devices was much lower than the amount of FITC-insulin that was previously loaded into device reservoirs, demonstrating that FITC-insulin adsorption to internal device surfaces is also minimal relative to the amount of loaded drug.

Z-slices of different depths showed the presence of drug reservoirs 100 μm in diameter with a surrounding device body and an overlying nanostraw membrane, both 200 μm in diameter (Figure 3.3 B). Cross sections along the z-axis showed that nanostraws spanned through the membrane cap, connecting the device reservoirs to the external environment. Together, these findings suggested that loading of the microdevice reservoirs was mediated by diffusion of drug through the nanostraws.

Minimizing drug stress while loading microdevice reservoirs has proven challenging in previous studies. Current methods of microreservoir drug loading such as surface loading by

capillary action,[85, 100, 115, 116] photolithography,[39, 45, 62] and inkjet printing[216, 245] require exposure of drug to UV light, crosslinking agents, organic solvents, and/or dehydration. These damaging conditions can potentially cause loss of drug structure and bioactivity, especially for biological therapeutics.[226] The nanostraw microdevices in this study were designed to facilitate in-solution drug loading, allowing drug to be loaded under mild conditions.

To confirm nanostraws as the route of drug diffusion into the device reservoirs and validate the integrity of device sealing, we fabricated devices with either nanostraw membrane caps or non-porous PC film caps as a control. Devices were then incubated overnight in a PBS solution of 10 mg/mL FITC-insulin, rinsed with PBS for 1 min, and imaged with fluorescence microscopy. FITC-insulin diffused into the reservoirs of devices with nanostraw membranes but not into the reservoirs of microdevices sealed with non-porous PC (Figure 3.6), demonstrating functional device reservoir sealing with drug diffusion occurring primarily through nanostraws. Additionally, drug-loaded microdevices retained FITC-insulin upon being scraped from the silicon wafer (Figure 3.7), indicating that the microdevices remained sealed upon device detachment.

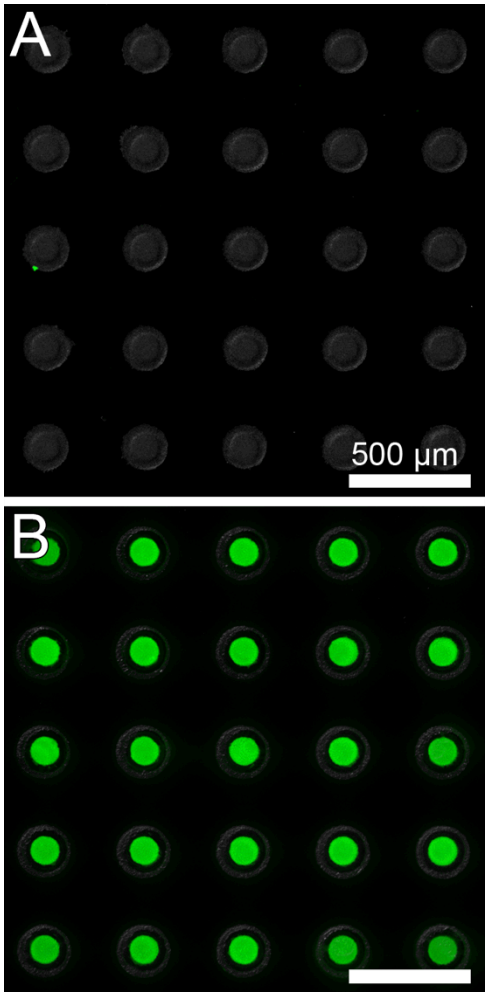

Figure 3.6. Nanostraw microdevice reservoirs are sealed, with nanostraws facilitating in-solution drug loading. Microdevices fabricated using a non-porous PC membrane (**A**) or a nanostraw membrane (**B**) were incubated in 10 mg/mL FITC-insulin overnight, rinsed with PBS, and imaged for device structure (brightfield signal, shown in grayscale) and FITC-insulin localization (fluorescence signal, shown in green). Only microdevices with nanostraws showed significant loading of insulin into reservoirs, indicating proper sealing of microdevices with drug diffusion occurring primarily through nanostraws.

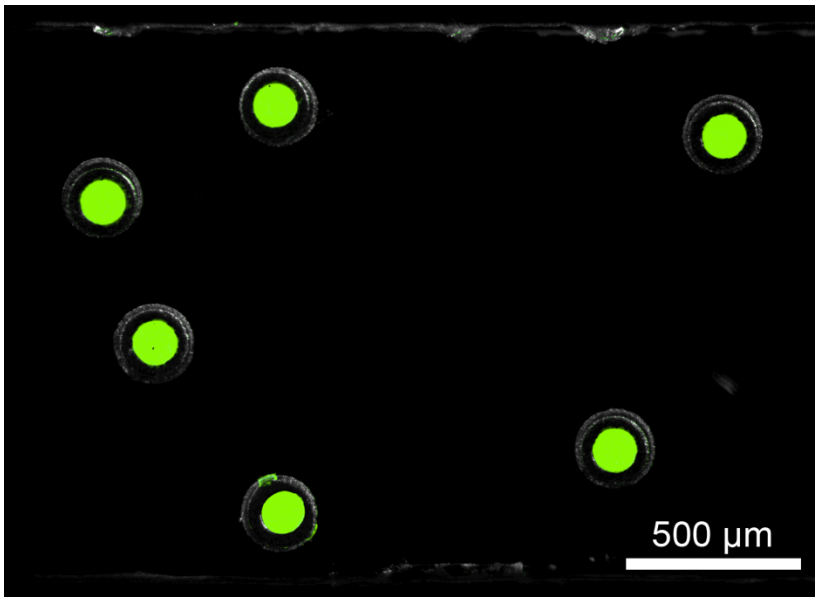

Figure 3.7. Loaded nanostraw microdevices retain drug after detachment from the silicon wafer. Nanostraw microdevices were incubated in a PBS solution of 10 mg/mL FITC-insulin overnight, rinsed with and submerged in PBS, and scraped from the silicon wafer with a razor. The PBS-suspended microdevices were added to a chamber formed by placing an adhesive spacer between a glass slide and a coverslip and incubated at room temperature for 30 min. The microdevices were then imaged for structure (brightfield signal, shown in grayscale) and FITC-insulin localization (fluorescence signal, shown in green). FITC-insulin remained within the device reservoirs, indicating that the devices remained sealed following detachment from the silicon wafer.

3.4.2. Nanostraws provide sustained and tunable drug release

In order to take full advantage of the prolonged residence time in the GI tract, bioadhesive microdevices should provide sustained drug release. Furthermore, an ability to tune the rate of drug release allows for targeting of specific regions of the GI tract and adjustment for more favorable pharmacokinetic profiles.[6] For example, rapid drug release could facilitate delivery of the majority of loaded drug to the buccal cavity, while slow release could maximize delivery of drug to the colon. We hypothesized that the hollow nanostraws, which can be

fabricated with varying diameters and densities,[228-231] would provide the additional advantage of tunable and sustained drug release.

To test this hypothesis, we monitored the release rates of the model drug FITC-insulin from microdevices sealed by nanostraw caps of varying nanostraw inner diameters and densities (Figure 3.8 A). For each type of nanostraw membrane, 400 – 800 microdevices were loaded by incubation in a PBS solution of 10 mg/mL FITC-insulin at 4 °C for 36 – 48 hours. The microdevices were then rinsed in PBS for 1 min to remove non-loaded FITC-insulin and placed in PBS at 37 °C for measurement of drug release. The GI tract environment varies dramatically in composition, enzyme concentrations, and pH by region.[226] While drug release was performed in the absence of digestive enzymes to allow for the accurate measurement of drug concentrations, the pH at which drug release was tested (pH 7.4) falls within the pH ranges of the buccal cavity and esophagus (pH 5.3 – 7.8),[246] small intestine (pH 6 – 7.4),[247] and colon (pH 6.8 – 7.4)[248] but is significantly higher than the pH of the stomach (pH 1.0 – 3.5).[249] However, nanostraw microdevices could be encapsulated within pH-sensitive enteric capsules in order to allow them to bypass the stomach before dissolution of the capsule and release of devices within the higher-pH environments of the intestine or colon.[44, 226] Drug release was monitored by fluorescence spectroscopy, normalizing to device count (Figure 3.8 B). Drug release rates scaled with both nanostraw diameter and density, demonstrating that drug release kinetics could be tuned by adjusting nanostraw membrane properties.

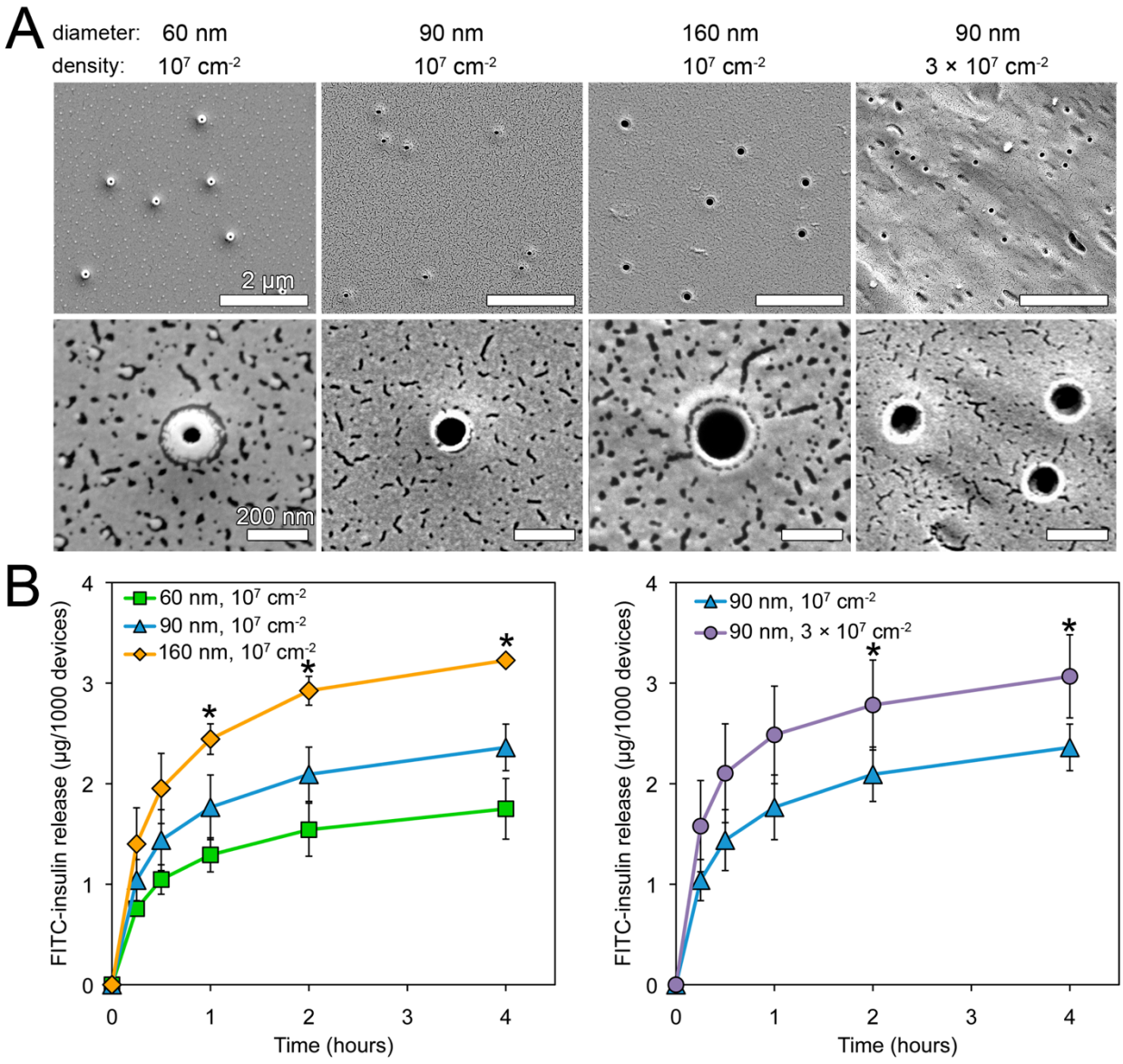

Figure 3.8. Drug release rates scale with nanostraw diameter and density, allowing for tunable release. A. SEM images of nanostraw membranes fabricated with varying nanostraw inner diameters (60, 90, 160 nm) and densities (10^7, 3×10^7 cm^{-2}). **B.** FITC-insulin release from microdevices sealed with these membranes was monitored over time. Release rates scaled with both nanostraw diameter and density. *Indicates statistically different values between all samples at a given time point ($p < 0.05$).

3.4.3. Nanostraw membranes limit exposure of loaded drug to outside biomolecules

To mitigate drug degradation, microdevices can be designed to protect loaded drug from exposure to damaging biomolecules such as metabolic and proteolytic enzymes that are present throughout the GI tract.[226] We hypothesized that, in addition to limiting diffusion of loaded drugs out of the reservoir, the nanostraw membrane would also limit the influx of outside biomolecules, thereby providing a mechanism to protect the drug payload. To model the diffusion of biomolecules into drug reservoirs, we incubated nanostraw microdevices (inner nanostraw diameter: 60 nm, nanostraw density: 10^7 cm^{-2}) in 1 mg/mL 10 kDa FITC-dextran, a biological molecule with a hydrodynamic radius (2.3 nm)[250] similar to drug-degrading enzymes such as trypsin (1.9 nm),[251] chymotrypsin (2.5 nm),[252] and DNase I, (2.5 nm).[253]

We monitored FITC-dextran diffusion into the device reservoirs at 0.5, 1, 2, and 4 h with confocal fluorescence microscopy (Figure 3.9). We then quantified the fluorescence intensity values within the device reservoirs. As a control for the concentration of FITC-dextran outside of the device reservoirs, fluorescence intensity was also measured at 48 h, by which time internal FITC-dextran concentration had equilibrated to that of the external environment (Figure 3.10).

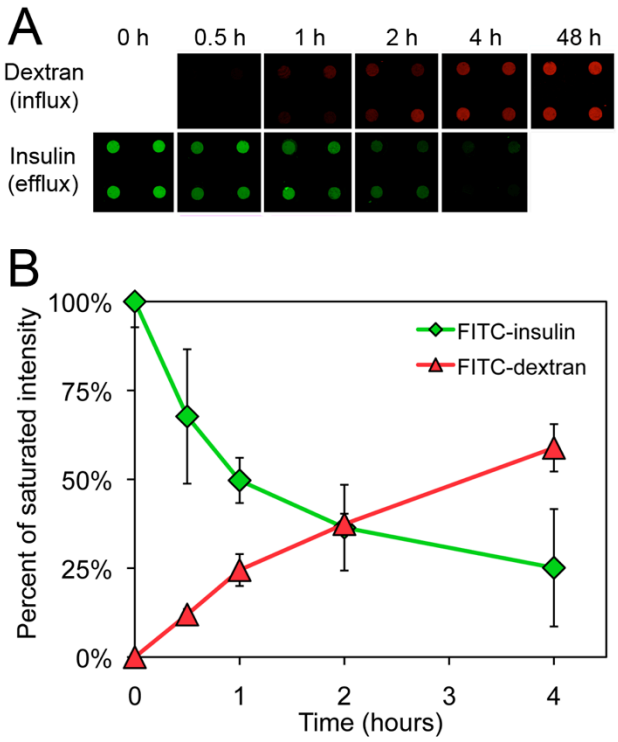

Figure 3.9. Nanostraw membranes limit the influx of biomolecules into device reservoirs. A. To determine the ability of nanostraw microdevices to limit the influx of outside biomolecules, nanostraw microdevices were incubated in 1 mg/mL 10 kDa FITC-dextran at 37 °C and imaged with confocal fluorescence microscopy over time. As a reference for the rate of drug release from the reservoirs, the release of FITC-insulin loaded into microdevices at 10 mg/mL was also monitored through identical detection methods. **B.** FITC-dextran influx and FITC-insulin efflux were quantified by integrating fluorescence intensity values in the device reservoirs at each time point and normalizing to the respective saturated intensity values. Specifically, FITC-dextran fluorescence intensity was normalized to devices equilibrated with the outside FITC-dextran concentration (t = 48 h), and FITC-insulin fluorescence intensity was normalized to loaded devices (t = 0 h).

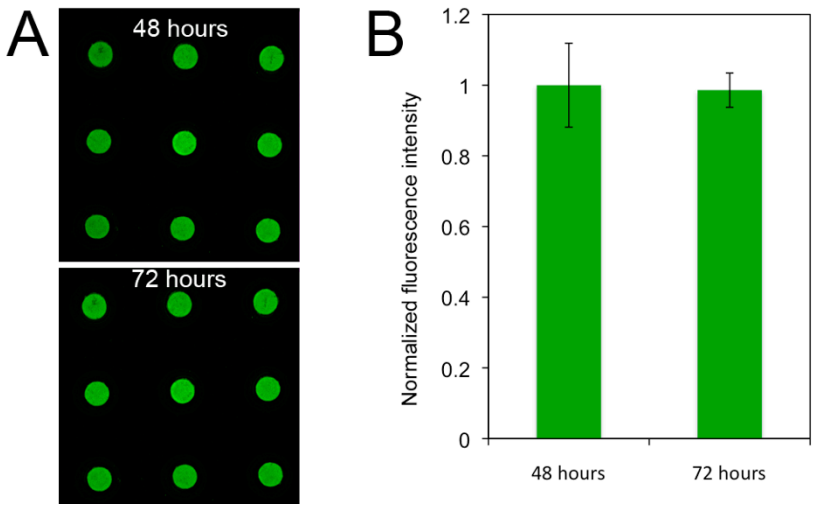

Figure 3.10. Device reservoirs become saturated with FITC-dextran after incubation for 48 h. A. Nanostraw microdevices used for the influx assay were incubated at 37 °C in 1 mg/mL FITC-dextran (10 kDa) for 48 or 72 h and then imaged with confocal microscopy. **B.** The fluorescence intensity values at 48 and 72 h were statistically similar, indicating that the device reservoirs had equilibrated with the external 1 mg/mL FITC-dextran solution by 48 h.

All earlier timepoints were normalized to the fluorescence intensity at this later time point, allowing for comparison between the concentration within the devices to the external concentration. During incubation in FITC-dextran, the normalized fluorescence intensity in device reservoirs remained below 50% of the 48-hour control for over 2 hours, suggesting that the nanostraw membrane will reduce the exposure of loaded drug to external biomolecules relative to the outside concentration, especially within the first few hours of administration. As a reference for the rate of drug release from the reservoirs, we also monitored the release of FITC-insulin from nanostraw microdevices through identical methods, normalizing to initial FITC-insulin fluorescence intensity. We observed significant FITC-insulin release during the same time frame, demonstrating that nanostraw microdevices can decrease the exposure of loaded drug to outside biomolecules prior to release.

3.4.4. Nanostraws enhance device bioadhesion *in vitro* and *ex vivo*

We hypothesized that the adhesive properties of microdevices would be enhanced by the presence of nanostraws. To determine the effect of nanostraws on bioadhesion, microdevices sealed with nanostraw membrane caps that had either been etched with oxygen plasma to expose nanostraws (depicted in Figure 3.1 H) or not treated with the final etching step, resulting in control devices without exposed nanostraws (depicted in Figure 3.1 G) were analyzed with a flow cell adhesion assay. Approximately 400 microdevices were detached from the silicon wafer and incubated in PBS over a monolayer of Caco-2 epithelial cells for 5 min with gentle shaking, facilitating contact between the nanostraw microdevices and the epithelial monolayer. A flow cell was then assembled over the microdevices, and a solution of porcine mucin was passed through the flow cell at increasing rates to achieve stepwise increments of fluid shear stress as previously outlined.[85, 100, 190, 191]

We determined the fraction of microdevices remaining completely adhered to the Caco-2 monolayer following 5 min of flow at each shear stress value. Microdevices with exposed nanostraws demonstrated significantly higher adhesion than control microdevices (Figure 3.11 A). Following exposure to fluid shear stress values increasing to 40 dyn/cm^2, 77 ± 7% of microdevices with exposed nanostraws and 33 ± 23% of microdevices without exposed nanostraws remained adhered, demonstrating that nanostraws dramatically enhance device bioadhesion. The high fraction of nanostraw microdevices remaining adhered also indicated that bound nanostraw microdevices are likely to remain attached to the intestinal epithelium while under physiological shear stress, which can range from 0.02 to 35 dyn/cm^2 during peristalsis.[254]

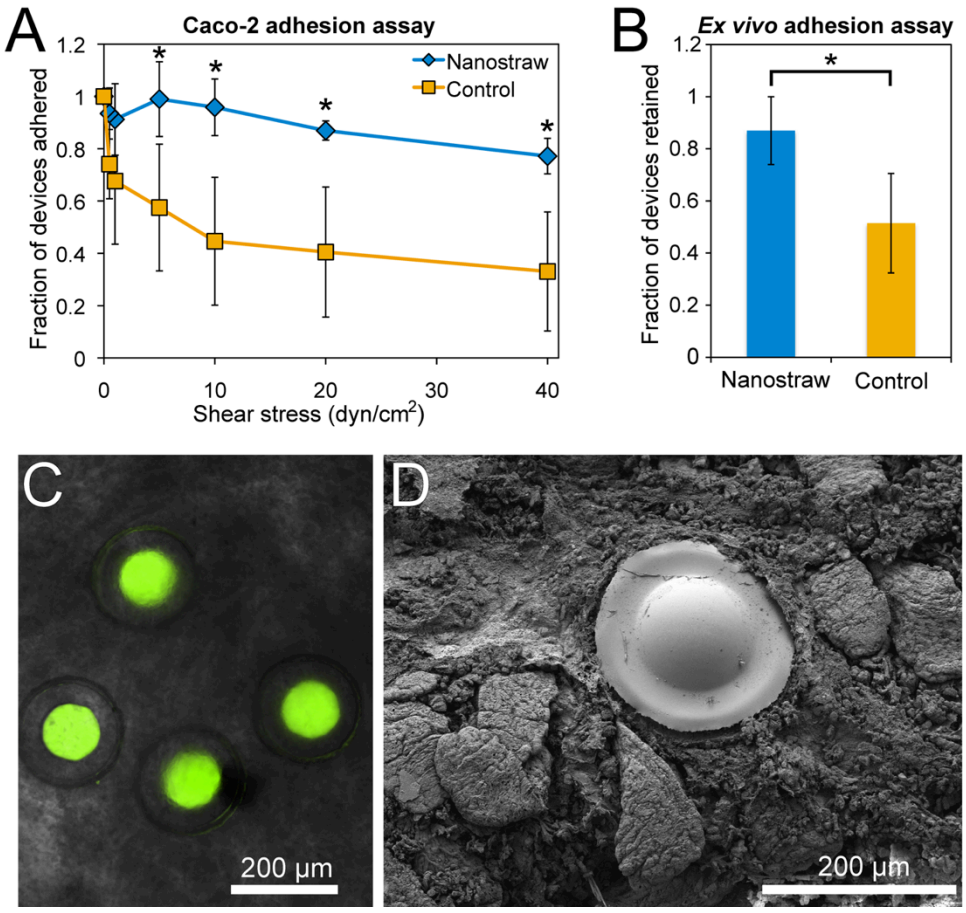

Figure 3.11. Nanostraws enhance microdevice bioadhesion. A. *In vitro* flow cell assay in which nanostraw microdevices or control devices sealed with membranes lacking exposed nanostraws were incubated on Caco-2 cells and then exposed to increasing flow rates corresponding to physiological fluid shear stress values. The fraction of devices remaining adhered to the Caco-2 monolayer was determined at each time point. **B.** *Ex vivo* murine intestinal adhesion assay in which nanostraw microdevices or control devices were flowed through excised murine intestinal tissue at 0.2 mL/min for 1 hour. The fraction of devices remaining within the intestinal tissue was then determined with fluorescence microscopy. **C.** Fluorescence microscopy following the *ex vivo* adhesion assay showed that intact nanostraw microdevices loaded with FITC-insulin (green) had adhered to intestinal tissue. **D.** An SEM image showing a microdevice adhered to the intestine as a result of the nanostraw membrane becoming entrapped within the mucus layer. A majority of devices (76%) observed by SEM were adhered with the nanostraw membrane in contact with the intestinal mucosa (n = 21), indicating that devices selectively bound in this orientation ($p < 0.05$). *Indicates statistically different values ($p < 0.05$).

To characterize device interaction with the mucus layer coating intestinal epithelium, we performed an *ex vivo* adhesion assay with excised murine intestinal tissue. In an assay adapted from previous studies,[234-237] we excised the jejunum from sacrificed mice and flowed devices suspended in oxygenated Tyrode's solution through the intestinal segment at 0.2 mL/min, a flow rate previously proposed for mice.[234, 235, 237] After 1 h of flow, we cut the jejunum longitudinally and used fluorescence microscopy to determine the number of devices remaining within the intestinal tissue and the number of devices that had flowed through the jejunum. Of the total devices counted, 87 ± 13% of the nanostraw devices remained within the intestinal segment after 1 h of flow while only 51 ± 19% of the control device remained (Figure 3.11 B). Fluorescence microscopy showed adhesion of intact insulin-loaded devices to the intestinal mucosa (Figure 3.11 C).

SEM analysis of *ex vivo* tissue showed that 76% of 21 nanostraw microdevices observed were adhered in the orientation with the nanostraw membrane coming into contact with the intestinal tissue as shown in Figure 3.11 D, indicating that this binary event was non-random and selectively favored adhesion of the nanostraw membrane surface of the devices ($p < 0.05$). SEM imaging also demonstrated that the nanostraw membranes of the devices adhered to and became entrapped by the mucus layer. The enhanced mucoadhesion observed in the presence of nanostraws is likely due to penetration of nanostraws into the mucus, which could prevent device detachment by providing increased interfacial surface area and impeding lateral device movement. Therefore, an upper limitation of the residence time of these devices in the GI tract may be the turnover rate of the motile mucus in the small intestine, which is on the order of hours, unless the devices penetrate through this motile mucus layer to interact with the underlying epithelium, which has a turnover time on the order of days.[255-257] Thus, these devices

are not likely to degrade before excretion from the GI tract as they are composed of materials that degrade on the order of months or longer.[258-261] Together, the *in vitro* and *ex vivo* adhesion assays demonstrated that the nanostraws enhanced adhesion of the drug-releasing device surface to the intestinal epithelium while exposed to fluid flow, indicating that the nanostraws will facilitate prolonged and unidirectional drug release directly toward GI tissue.

3.5. Conclusion

To address the barriers to oral drug absorption, we present a novel approach to fabricate microdevices sealed with nanostraw membranes. These devices retain the planar, asymmetric geometry previously shown to enhance device adhesion and drug absorption. We demonstrate that nanostraw membranes incorporated into the microdevices provide the additional advantages of 1) facile, in-solution drug loading with sustained, tunable drug release, 2) limited influx of outside molecules into device reservoirs, and 3) nanotopography-mediated bioadhesion. Nanostraw microdevices have potential to increase oral drug absorption by binding to GI tissue, releasing drug at high local concentrations over a prolonged period of time, and reducing the exposure of their payload to drug-degrading biomolecules. Given their facile, in-solution drug loading mechanism and ability to limit the exposure of loaded drug to outside biomolecules, nanostraw microdevices may prove particularly advantageous for fragile biological therapeutics. Thus, future *in vivo* studies will determine the ability of these microdevices to enhance the delivery of a wide range of hormones, nucleic acids, peptides, and proteins for either enhanced systemic absorption or local uptake into diseased GI tissue.

Even for drugs with high bioavailability, there is a strong motivation to develop devices capable of releasing drugs in the GI tract for prolonged periods of time to decrease dosing

frequency, allowing for simplified dosing regimens and better patient adherence to therapies.[262] With high bioadhesion under physiological shear stress and tunable drug release rates, nanostraw microdevices have potential to significantly extend durations of systemic drug exposure. The fabrication approach presented here may also be applied outside the field of oral drug delivery to miniaturize implantable drug release systems, biosensors, and other biomedical devices where bioadhesion, tunable release, and/or protection of a payload from outside biomolecules are advantageous.

3.6. Acknowledgments

CBF was supported by NIH Training Grant 5T32GM007175-37 and an ARCS Fellowship. YC was supported by Grant 70NANB15H192 from the U.S. Department of Commerce, National Institute of Standards and Technology. CLN was supported by NSF Graduate Research Fellowship DGE-1106400. RWC was supported by NIH Training Grant 5T32DK007762-38. AMX was supported by NSF Graduate Fellowship DGE-114747 and an NDSEG Fellowship. We gratefully acknowledge use of the Carl Zeiss Ultra FE-SEM at San Francisco State University for all SEM imaging. The FE-SEM and supporting facilities were obtained under NSF-MRI award #0821619 and NSF-EAR award #0949176. Confocal fluorescence imaging was conducted at the Nikon Imaging Center, UCSF. Nanostraw membrane fabrication was performed the Stanford Nano Shared Facilities. Remaining fabrication was performed at the UCSF Biomedical Micro & Nanotechnology Core and UC Berkeley Biomolecular Nanotechnology Center. The authors would like to thank Colin Zamecnik, Margaret Lowe, and Jessie Lee for providing mouse tissue for the *ex vivo* experiments.

Chapter 4 – Picoliter-Volume Printing of Drug into Device Reservoirs for Zero-Waste, High Capacity Loading

4.1. Abstract

The geometry of microdevices facilitates prolonged drug exposure with unidirectional release of drug toward gastrointestinal epithelium. While these devices have significantly enhanced drug bioavailability *in vitro* and *in vivo*, loading drug into the micron-scale reservoirs of the devices in a low-waste, high-capacity manner remains challenging. Here, we use picoliter-volume inkjet printing to load topotecan and insulin into planar microdevices efficiently. Following a simple surface functionalization step, drug solution can be spotted into the microdevice reservoir. We show that relatively high capacities of both topotecan and insulin can be loaded into microdevices in a high-throughput, automated process with quasi-zero drug waste.

4.2. Introduction

Drug loading remains a great challenge in the application of microdevices to oral drug delivery. Traditional oral dosage requires large amounts of drug, which can be cost prohibitive. Previously, microdevices have been loaded by spin-casting a drug-hydrogel solution over the microdevices and then selectively crosslinking the solution within device reservoirs by ultraviolet light (UV) exposure.[104] However, drug-loading efficiency is decreased due to losses during the spin-casting step, and the extra hydrogel volume reduces the drug capacity of the devices. Furthermore, UV light can damage photosensitive molecules and lead to degradation of the active compound. More recently, we demonstrated the use of nanostraw membranes to passively take up drug into the microdevice via diffusion.[263] Unfortunately, this method requires

the use of concentrated drug solution that is usually discarded after loading thus leading to waste, and drug-loading capacity is limited to the product of the drug solubility and microdevice reservoir volume. Therefore, alternative loading methods need to be considered.

Inkjet printing is a technique that has been previously used for microarray spotting, surface functionalization, cell culturing, and drug formulation.[264-267] A major advantage of inkjet printing is its drop-on-demand mode, which allows for spotting of precise volumes of liquid onto a surface. Previously, it has been shown that small-volume dispensing systems can be used to print polymer solutions into micro-scale containers.[216, 268] When printing drugs, the solutions ideally would not contain polymer, thus maximizing the free volume available for drug. These previous methods were used for tall micro-containers measuring over 250 μm in height with aspect ratios typically >1.[216] However, planar microdevices for oral drug delivery are typically designed with heights < 10 μm and aspect ratios > 0.1.[6] To our knowledge, this method has not been used with thin (<10 μm thickness) microdevices, which typically have reservoir volumes in the tens of pL range rather than the > 500 pL volume reservoirs previously utilized for inkjet printing.[45, 268]

In this study, we demonstrate the use of inkjet printing to efficiently load planar microdevices with topotecan, a small molecule chemotherapeutic agent, and insulin, a peptide hormone. Both drug solutions were prepared in acidic solutions and were directly spotted into the reservoirs of each microdevice with high precision and accuracy in an automated fashion. We also introduce a simple surface modification step to improve the surface hydrophobicity of the microdevices to ensure loading into the microdevice reservoir without overflow. We demonstrate that microdevices can be rapidly loaded with high capacities of both small molecule and biological therapeutics with nearly zero drug waste.

4.3. Methods

4.3.1. Materials for device fabrication and drug loading

Topotecan hydrochloride, insulin (recombinant human), hydrochloric acid (HCl), and trichloro(1H,1H,2H,2H-perfluorooctyl)silane were purchased from Sigma-Aldrich, USA. Poly(methyl methacrylate) (950 kDa in anisole), Shipley 1818 positive photoresist, Microposit 351 developer, and 1112A photoresist remover were purchased from MicroChem, USA. CyQUANT direct cell proliferation assay kit was purchased from Thermo Fisher Scientific, USA. Silicon wafers were purchased from Addison Engineering Inc, USA.

4.3.2. Microdevice fabrication

Microdevices with reservoirs were fabricated as previously described.[263] Briefly, a silicon wafer was spin-coated with poly(methyl methacrylate) (PMMA) followed by a baking step. This process was repeated for two layers of PMMA. The hardened PMMA was spin-coated with positive photoresist followed with another baking step. The wafer was then exposed to UV light under a positive mask to form the device body features. The exposed wafer was developed and post-baked. The PMMA surrounding the masked region was dry etched with oxygen plasma in a Surface Technology PE1000 AC Plasma Source Reactive ion etcher. Remaining photoresist was removed by incubation in photoresist remover. To fabricate the reservoirs, the microdevice bodies were spin-coated with photoresist followed by UV exposure with a positive photomask aligned over the microdevice bodies with reservoir pattern. The microdevices were then developed, dry etched, and excess photoresist was removed to form microdevices with reservoirs.

The final microdevices were disc-shaped, 200 μm in diameter and 8 μm in height. Each device contained a central reservoir 100 μm in diameter and 5.5 μm in depth, which corresponds to a volume of 43.2 pL. Each 3'' silicon wafer contained a 4 × 4 array of 20 × 20 microdevice subarrays for a total device count of 6400.

4.3.3. Microdevice surface modification

Prior to drug printing, the silicon wafer with fabricated microdevices was silanized with trichloro(1H,1H,2H,2H-perfluorooctyl)silane via vapor deposition under vacuum at room temperature for 30 min. Wafers were printed the same day as silanization.

4.3.4. Drug loading into microdevices

Drug printing was performed using the sciFLEXARRAYER S3 (Figure 4.1). This system is an automated drop-on-demand piezoelectric printing system suitable for deposition of 50-800 pL drops at up to 1000 Hz with positional accuracy of +/-20 μm. The printer is composed of a XYZ movable head with a mounted piezo-driven dispenser. Topotecan and insulin solutions were prepared fresh at 10 mg/mL in 10 mM HCl and filtered through a 100 kDa centrifuge tube for 10 min at 5000 RCF. The freshly prepared drug solutions were then loaded into a microtiter plate. Prior to printing, drug solution was aspirated into the dispenser nozzle. During setup, the printer's control unit was aligned to the fiduciaries on the silicon wafer, which enabled programmable automatic dispensing. The printer is equipped with a camera to visualize drop volume, stability, and trajectory, which can be adjusted by changing the piezo voltage, pulse width, and frequency. These parameters were optimized to obtain drops with volumes of ~400

pL. An increasing number of single 400 pL drops of either drug solution were printed into device reservoirs. The printing process was performed in multiple cycles to allow the solvent to completely evaporate between each cycle, preventing solution spillover.

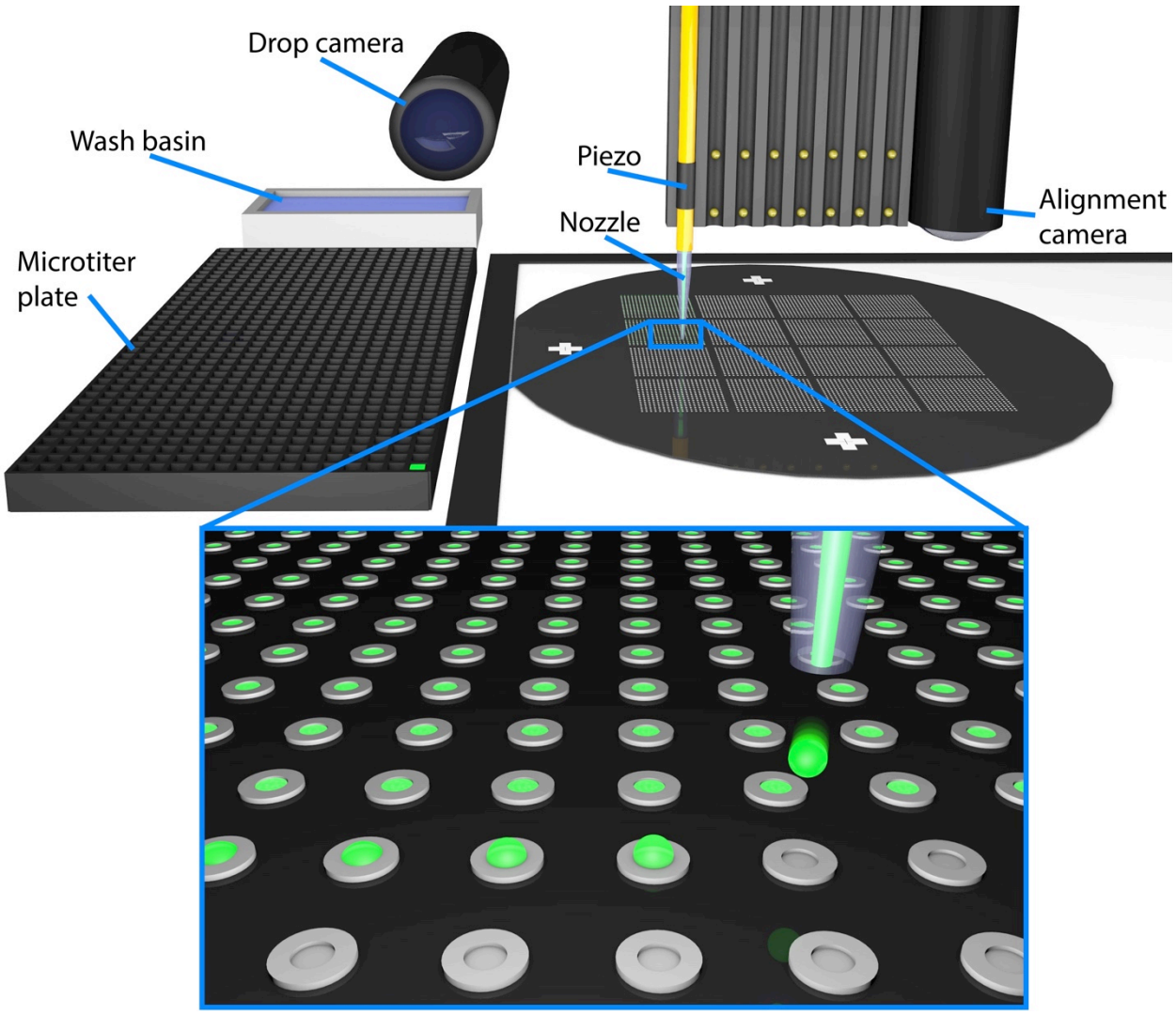

Figure 4.1. Schematic of picoliter-volume printer configuration. Prior to each run, drug is drawn from the microtiter plate into the nozzle, and the fiduciary markers on the wafer are recognized by automated recognition of images taken by the alignment camera. Drug is then printed into microdevice reservoirs in an automated sequence. For each printing pass, the nozzle is dipped into the wash basin, and the drop camera is used to confirm successful formation of 400 pL droplets for the specified piezo settings. The printer then dispenses a single droplet into the reservoir of each microdevice on the wafer. Droplets quickly dry, and additional drug solution is printed over solidified drug in future passes. Finally, the alignment camera captures quality-control images of all devices.

4.3.5. Scanning electron microscopy

Samples were prepared for SEM by sputter coating with 8 nm of gold followed by mounting onto carbon tape. The samples were imaged with a Carl Zeiss Ultra 55 field emission scanning electron microscope.

4.3.6. Cellular toxicity studies

To determine the cytotoxicity of silanized microdevices, samples were analyzed using a proliferation assay using the CyQUANT direct cell proliferation assay kit. Caco-2 cells were grown to confluency in 12-well tissue culture plates. All media was aspirated from wells and one of the following were added in triplicate: media containing 400 silanized and insulin filled microdevices, media only, or 20% DMSO in media. The cells were then incubated at 37 °C, 5% CO_2 for 4 hours. At the end of the incubation, cells were trypsinized and subsequently spun down to pellets via centrifugation. The supernatant was discarded, and the cells were resuspended in PBS. Detection reagent with background suppressor was then added to each tube. The samples were incubated at 37 °C for one hour and then plated in a 96-well plate in triplicate. Fluorescence of samples was measured using a spectrophotometer with cells in suspension.

4.4. Results

Because planar microdevices are applied for oral delivery of both small molecule drugs and biological therapeutics, drug loading techniques will ideally be compatible with both small molecules and biologics. We chose topotecan, an inhibitor of DNA enzyme topoisomerase I used as a chemotherapeutic, as a model small molecule drug.[269, 270] Orally administered chemotherapy could reduce hospital admissions or visits to outpatient infusion centers for parenteral administration. However, oral formulations require higher amounts of drug to be delivered compared to the intravenous route, which can lead to higher off-target effects and toxicity. Preparing chemotherapeutic agents in microdevice form can potentially reduce the dosage needed.

We wanted to expand the utility of this platform by using insulin as our model biologic. Insulin is an important peptide hormone that is secreted by the beta cells in the Islets of Langerhans within the pancreas to signal for glucose uptake from the bloodstream by cells. Current administration of insulin is frequently done by multiple subcutaneous injections per day or via insulin pumps. This is not ideal due to issues such as non-compliance, cost, and tissue damage at injection sites. Previous research investigating insulin for oral drug delivery has not been able to translate clinically.[271]

The shape and size of the drug delivery vehicle are important parameters to consider in oral drug delivery. We fabricated planar microdevices 200 μm in diameter and 8 μm in height. This low aspect ratio is necessary to resist shear flow from peristalsis and increase residence time. Each microdevice possessed an inner reservoir measuring 100 μm in diameter and 5.5 μm in depth. Furthermore, the reservoir is etched into only one side of the device, allowing for

unidirectional drug release toward intestinal tissue and high local drug concentration at the epithelium.

The ability to load relatively large amounts of drug with minimal drug waste holds many advantages. The inkjet printer enables printing of drug directly into the reservoir and obviates the need of other methods such as spin-casting or supercritical impregnation which can result in significant drug loss and does not guarantee uniform loading conditions.

Surface energy is an important consideration when spotting into the shallow wells of microdevices. Before printing, the microdevices were silanized via vapor deposition using trichloro(1H,1H,2H,2H-perfluorooctyl)silane, a silane commonly used to render surfaces hydrophobic.[272, 273] The presence of a hydrophobic surface on the microdevices allowed printed drops to collect inside the reservoir (Figure 4.2). When loading microdevices without the silane treatment, the drops would collect outside the reservoir, which compromised loading efficiency. Following silane treatment, the drops can be spotted directly into the reservoir without overflow. Silanized microdevices were used henceforth for topotecan and insulin loading.

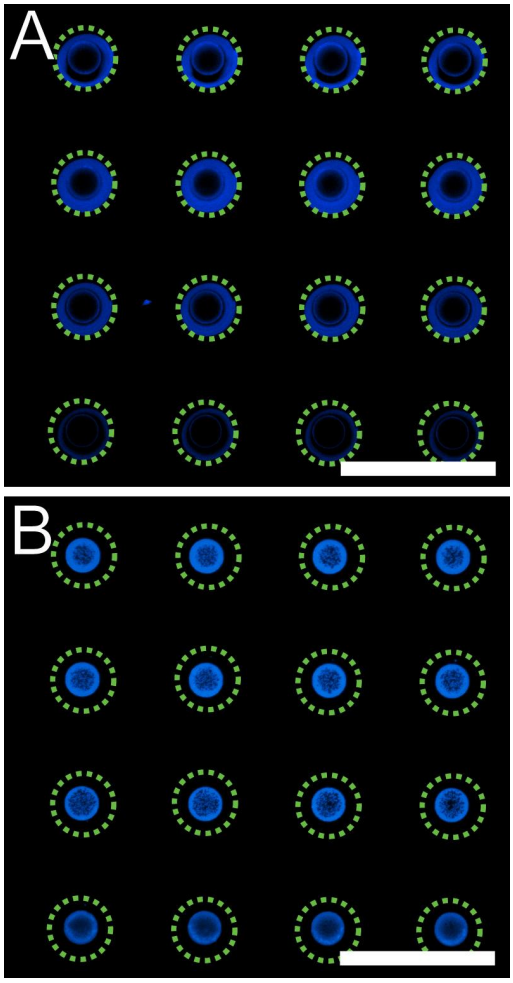

Figure 4.2. Microdevice silanization enhances drug localization into device reservoirs. A. Fluorescence microscopy of devices (outlined in green dashed lines) loaded with topotecan (blue) indicates that drug spotting size was too large in non-silanized devices, with drug being deposited both with device reservoirs and onto the device body outside of the drug reservoirs. B. Devices silanized with trichloro(1H,1H,2H,2H-perfluoro-octly)silane became more hydrophobic which demonstrated efficient loading into device reservoirs. Scale bars are 500 μm.

Drug delivery systems must also display a favorable toxicological profile in addition to demonstrating efficacy. Although we have tested microdevices in animal models before, this is the first time we have utilized silane deposition on microdevices. Silane in large quantities can be toxic to cells. However, previous studies using silanized nanoparticles did not show cell

cytotoxicity suggesting the silanization process uses volumes small enough to be biocompatible.[274] To confirm that silanized microdevices do not cause cytotoxicity, we conducted a CyQUANT assay using Caco-2 cells, a heterogeneous human epithelial colorectal adenocarcinoma cell line that is used as a model for the gastrointestinal tract.[275] Here, we show that silanized microdevices do not significantly decrease live cell counts compared to cells incubated in media alone (Figure 4.3). The DMSO group showed an expected decrease in cell viability. The results indicate that the silanized microdevices display cell biocompatibility and negligible cytotoxicity, a necessary feature when translating to animal models.

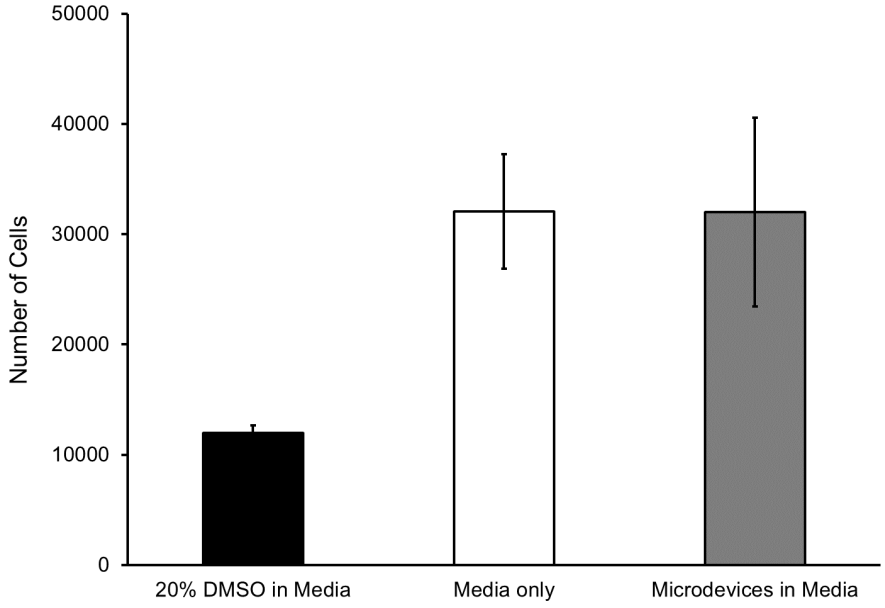

Figure 4.3. Microdevices do not exhibit significant cytotoxicity. *In vitro* CyQUANT viability data showing that silane-coated microdevices do not show significant toxicity to Caco-2 intestinal epithelial cells.

As low-viscosity solutions (<10 cP) are most compatible with the printer, we sought to find suitable solvents for both drugs. Topotecan is soluble in aqueous solutions and is most stable at low pH values.[276] Insulin is not soluble at neutral pH but increases solubility in acidic solutions. Thus, we dissolved topotecan and insulin at 10 mg/mL in 10 mM HCl. The measured viscosity was found to be less than 10 cP (data not shown). A silicon wafer with silanized microdevices was then placed into the printer and aligned via image recognition of the fiducial markers on the wafer before use.

Following loading of solution into the nozzle, the size of the topotecan and insulin drops was tracked by the camera and software of the printer. Before printing, 100 drops were dispensed at 200 Hz to calculate the average volume. The average drop size was determined to be ~400 pL. Camera images taken post-printing revealed that one 400 pL drop was sufficient to fill the entirety of the microdevice reservoir (Figure 4.4). When more than one drop was printed at a time, we observed overflow beyond the reservoir. Thus, one drop per microdevice was used during a single printing run. In order to fill the entirety of the microdevice reservoir with dry, packed drug, multiple runs were conducted with drying steps between each pass.

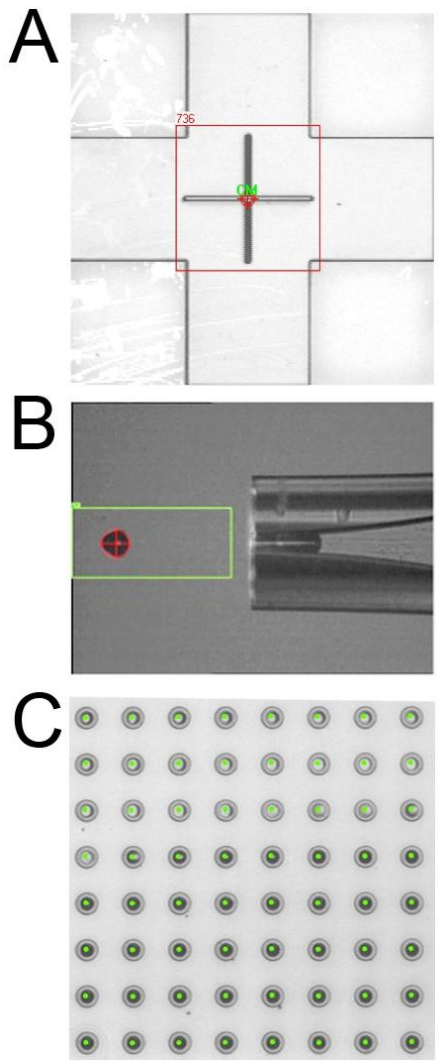

Figure 4.4. Drug printing quality-control images. A. Recognition of fiduciary markers for alignment to microdevices. B. Droplet detection to confirm proper formation of droplets at the desired volume. C. Quality-control images of devices immediately after printing confirm accurate localization of drug droplets within device reservoirs.

To determine the optimal number of single drops that can be loaded into each microdevice, we systematically increased the number of drops up to 16 total drops per microdevice and characterized loading efficiency via SEM (Figure 4.5). For both topotecan and insulin, we observed gradual filling of the reservoir with increasing cycles. Imaging revealed that

approximately 10 drops was the ideal number for loading topotecan while 12 drops was ideal for insulin. Topotecan loading beyond 10 drops began to overfill the microdevice reservoir until the topotecan pellet delaminated from the reservoir. Insulin loading beyond 12 drops showed overflow but no delamination was observed. Loading drug by printing 400 pL droplets in multiple passes allowed for significantly higher loading capacity than previous loading approaches utilizing spin casting and photolithography. For example, spin-casting and UV-crosslinking a 10 mg/mL insulin hydrogel solution to fill the 43.2 pL device reservoir volume would allow for loading of 0.432 ng of insulin per device. However, with inkjet printing, twelve 400 pL drops of 10 mg/mL insulin were printed into each device for a total of 48 ng insulin per device, a >100-fold increase in loading capacity.

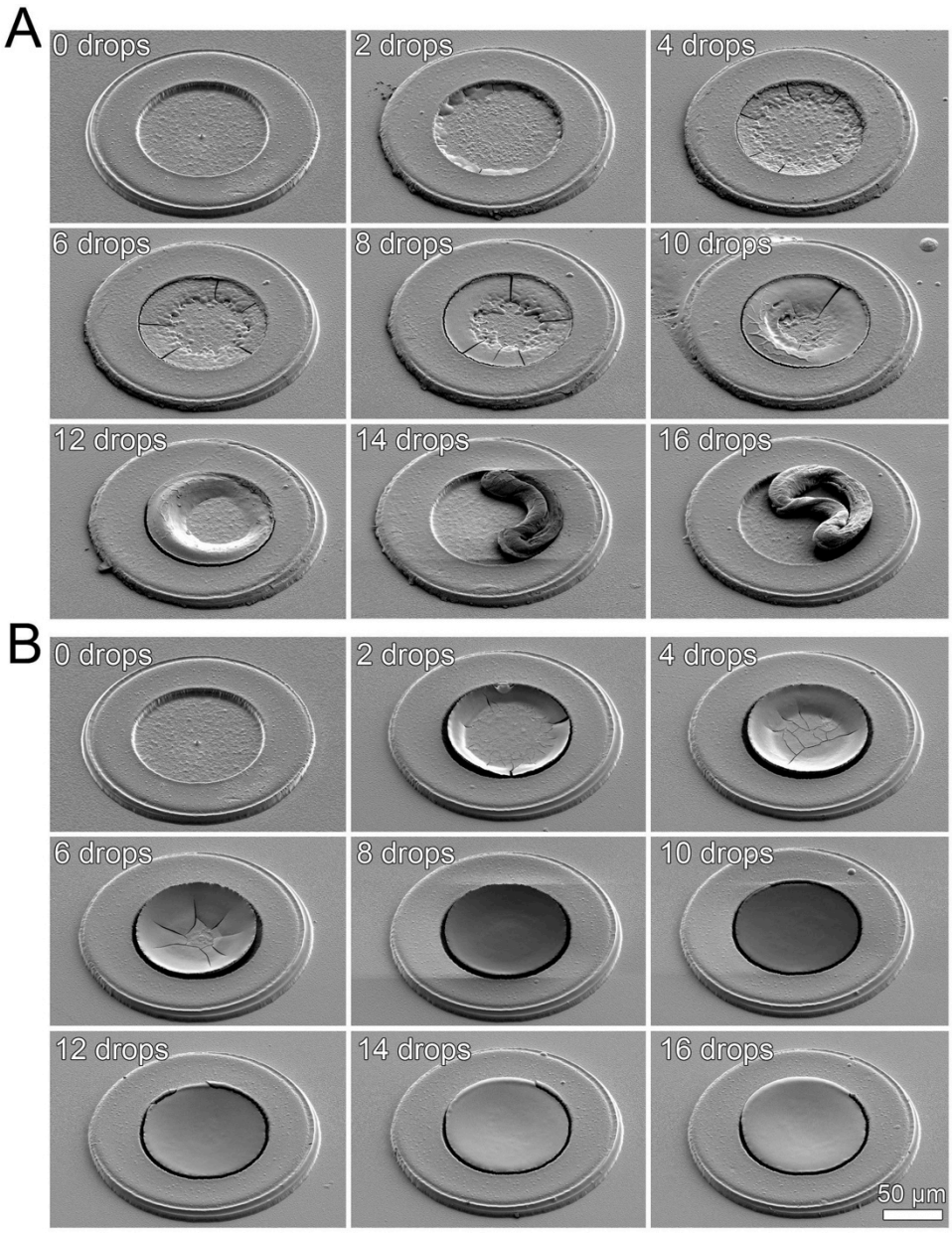

Figure 4.5. SEM images of devices loaded with increasing numbers of topotecan and insulin drops. SEM images of representative microdevices loaded with increasing number of 400 pL drops of (A) 10 mg/mL topotecan and (B) 10 mg/mL insulin.

4.5. Conclusion

In this work, we demonstrate the use of inkjet printing to efficiently load two different drugs, topotecan and insulin, into microdevices. The advantages of the inkjet printer system lie in its high-throughput loading efficiency, accuracy, and programmability. Spotting drug directly into the reservoir minimizes drug waste. Additionally, multiple printing and drying cycles allow for significantly higher drug loading capacity than that achieved by currently available techniques limited to loading drug at its solubility limit. Furthermore, this method does not require UV light or heat which can damage sensitive therapeutics. Surface functionalization increased surface hydrophobicity, which allowed printed drug solution to localize into the microdevice reservoir and did not show significant cytotoxicity. Future studies will assess the stability and storage conditions of the drugs after printing and investigate microdevice capping and drug formulation to control drug release. This inkjet printing approach could be adapted for low-waste, high capacity loading of a number of drugs and drug formulations into planar microdevices for oral drug delivery.

4.6. Acknowledgements

This work was partially supported by the Z Cube Zambon Research Venture and NIH Grant R01EB018842. C.B.F. was supported by NIH Training Grant 5T32GM007175-37 and an ARCS Fellowship. C.L.N. was supported by NSF Graduate Research Fellowship DGE-1106400. R.W.C. was supported by NIH Training Grant 5T32DK007762-38. Microfabrication was performed at the UCSF Biomedical Micro & Nanotechnology Core and the UC Berkeley Biomolecular Nanotechnology Center. We gratefully acknowledge the UCSF Center for Advanced Technology for use of the sciFLEXARRAYER S3 and the San Francisco State University Electron

Microscopy Facility for use of the Carl Zeiss Ultra FE-SEM for SEM imaging. The FE-SEM and supporting facilities were obtained under NSF-MRI award no. 0821619 and NSF-EAR award no. 0949176.

Chapter 5 – Summary and Conclusions

The work presented here describes approaches to incorporate nanoscale features into oral drug delivery microdevice technology. Specifically, PMMA microdevices were coated with PCL nanowires in one device design and sealed with polycarbonate membranes with interspersed aluminum oxide nanostraws in a second device design. For both designs, the nanostructures serve to increase device bioadhesion and provide a facile drug loading approach. The nanostraw devices, while fabricated though a lower throughput approach than the nanowire devices, have the advantages of providing tunable drug release rates and limiting exposure of loaded drug to outside biomolecules. Notably, the advantages provided by the nanoscale features do not compromise the planar, asymmetric design of the devices, allowing the devices to retain geometries that reduce force from fluid flow on the devices and provide unidirectional release of drug toward GI tissue.

Previously, the scalability of microdevice technology has been limited by a lack of techniques to load drugs into devices in a rapid, low-waste approach. Furthermore, the drug capacity of the devices was limited by the solubility of the drug in the hydrogel matrix that the drugs were loaded in, dramatically reducing scalability for drugs with low solubility in the release matrix or requiring relatively high doses. By loading drugs by printing high-concentration drug solutions directly into devices with multiple passes, the throughput and drug capacity of microdevices can be dramatically increased, expanding the number of drugs that could be incorporated into microdevices.

These studies lay the groundwork for future pre-clinical work testing microdevice efficacy. While the advantages of the nanoscale features have been demonstrated here through *in vitro* and *ex vivo* studies investigating individual mechanisms by which they may enhance drug

delivery, future *in vivo* studies will demonstrate how these mechanisms may work together to increase the oral bioavailability of a wide range of drugs. Given their differing advantages and disadvantages, nanowire and nanostraw microdevices may be used for different applications. Specifically, because nanowire devices are surface-loaded with drug, resulting in relatively rapid drug release rates, these devices may most beneficial for esophageal drug delivery. Nanostraw devices, with lower throughput fabrication, tunable drug release, and ability to limit exposure of loaded drug to outside biomolecules, may be most beneficial for delivery of fragile and expensive biological therapeutics to various regions of the GI tract. Finally, the drug printing approach presented here may be applied to allow drugs with solubility limitations or high required dosages to be incorporated into microdevices and tested in pre-clinical studies.

References

1. Moeller, E. H.; Jorgensen, L. Alternative Routes of Administration for Systemic Delivery of Protein Pharmaceuticals. *Drug Discov Today Technol* **2008**, *5*, e89-94.

2. Garrido-Siles, M.; Arenas-Villafranca, J. J.; Perez-Ruiz, E.; de Linares Fernandez, M. F.; Tortajada, B.; Rivas-Ruiz, F.; Faus, V.; Rueda, A. New Cutaneous Toxicities with Generic Docetaxel: Are the Excipients Guilty? *Support Care Cancer* **2015**, *23*, 1917-23.

3. Gelderblom, H.; Verweij, J.; Nooter, K.; Sparreboom, A. Cremophor El: The Drawbacks and Advantages of Vehicle Selection for Drug Formulation. *Eur J Cancer* **2001**, *37*, 1590-8.

4. Thiel, G.; Hermle, M.; Brunner, F. P. Acutely Impaired Renal Function During Intravenous Administration of Cyclosporine A: A Cremophore Side-Effect. *Clin Nephrol* **1986**, *25 Suppl 1*, S40-2.

5. Hua, S.; Marks, E.; Schneider, J. J.; Keely, S. Advances in Oral Nano-Delivery Systems for Colon Targeted Drug Delivery in Inflammatory Bowel Disease: Selective Targeting to Diseased Versus Healthy Tissue. *Nanomedicine* **2015**.

6. Chirra, H. D.; Desai, T. A. Emerging Microtechnologies for the Development of Oral Drug Delivery Devices. *Adv. Drug Deliv. Rev.* **2012**, *64*, 1569-78.

7. Keely, S.; Ryan, S. M.; Haddleton, D. M.; Limer, A.; Mantovani, G.; Murphy, E. P.; Colgan, S. P.; Brayden, D. J. Dexamethasone-Pdmaema Polymeric Conjugates Reduce Inflammatory Biomarkers in Human Intestinal Epithelial Monolayers. *J Control Release* **2009**, *135*, 35-43.

8. Stegemann, S.; Leveiller, F.; Franchi, D.; de Jong, H.; Linden, H. When Poor Solubility Becomes an Issue: From Early Stage to Proof of Concept. *Eur J Pharm Sci* **2007**, *31*, 249-61.

9. Li, P.; Zhao, L. Developing Early Formulations: Practice and Perspective. *Int J Pharm* **2007**, *341*, 1-19.

10. Agrawal, U.; Sharma, R.; Gupta, M.; Vyas, S. P. Is Nanotechnology a Boon for Oral Drug Delivery? *Drug Discov Today* **2014**, *19*, 1530-46.

11. Schwarz, U. I.; Gramatte, T.; Krappweis, J.; Oertel, R.; Kirch, W. P-Glycoprotein Inhibitor Erythromycin Increases Oral Bioavailability of Talinolol in Humans. *Int J Clin Pharmacol Ther* **2000**, *38*, 161-7.

12. Ponchel, G.; Irache, J. Specific and Non-Specific Bioadhesive Particulate Systems for Oral Delivery to the Gastrointestinal Tract. *Adv Drug Deliv Rev* **1998**, *34*, 191-219.

13. Pawar, V. K.; Meher, J. G.; Singh, Y.; Chaurasia, M.; Surendar Reddy, B.; Chourasia, M. K. Targeting of Gastrointestinal Tract for Amended Delivery of Protein/Peptide Therapeutics: Strategies and Industrial Perspectives. *J Control Release* **2014**, *196*, 168-83.

14. Lehr, C. M. Lectin-Mediated Drug Delivery: The Second Generation of Bioadhesives. *J Control Release* **2000**, *65*, 19-29.

15. Hunter, A. C.; Elsom, J.; Wibroe, P. P.; Moghimi, S. M. Polymeric Particulate Technologies for Oral Drug Delivery and Targeting: A Pathophysiological Perspective. *Nanomedicine* **2012**, *8 Suppl 1*, S5-20.

16. Hassan, N.; Ahad, A.; Ali, M.; Ali, J. Chemical Permeation Enhancers for Transbuccal Drug Delivery. *Expert Opin Drug Deliv* **2010**, *7*, 97-112.

17. Felton, L. A.; Porter, S. C. An Update on Pharmaceutical Film Coating for Drug Delivery. *Expert Opin Drug Deliv* **2013**, *10*, 421-35.

18. Fasano, A.; Uzzau, S. Modulation of Intestinal Tight Junctions by Zonula Occludens Toxin Permits Enteral Administration of Insulin and Other Macromolecules in an Animal Model. *J Clin Invest* **1997**, *99*, 1158-64.

19. Bernkop-Schnurch, A.; Kast, C. E.; Guggi, D. Permeation Enhancing Polymers in Oral Delivery of Hydrophilic Macromolecules: Thiomer/Gsh Systems. *J Control Release* **2003**, *93*, 95-103.

20. Ainslie, K. M.; Desai, T. A. Microfabricated Implants for Applications in Therapeutic Delivery, Tissue Engineering, and Biosensing. *Lab Chip* **2008**, *8*, 1864-78.

21. Ahmed, A.; Bonner, C.; Desai, T. A. Bioadhesive Microdevices with Multiple Reservoirs: A New Platform for Oral Drug Delivery. *Journal of controlled release : official journal of the Controlled Release Society* **2002**, *81*, 291-306.

22. Siegel, R. A.; Gu, Y.; Lei, M.; Baldi, A.; Nuxoll, E. E.; Ziaie, B. Hard and Soft Micro- and Nanofabrication: An Integrated Approach to Hydrogel-Based Biosensing and Drug Delivery. *J Control Release* **2010**, *141*, 303-13.

23. Sant, S.; Tao, S. L.; Fisher, O. Z.; Xu, Q.; Peppas, N. A.; Khademhosseini, A. Microfabrication Technologies for Oral Drug Delivery. *Adv Drug Deliv Rev* **2012**, *64*, 496-507.

24. Nuxoll, E. Biomems in Drug Delivery. *Adv Drug Deliv Rev* **2013**, *65*, 1611-25.

25. Nguyen, N. T.; Shaegh, S. A.; Kashaninejad, N.; Phan, D. T. Design, Fabrication and Characterization of Drug Delivery Systems Based on Lab-on-a-Chip Technology. *Adv Drug Deliv Rev* **2013**, *65*, 1403-19.

26. Kararli, T. T. Comparison of the Gastrointestinal Anatomy, Physiology, and Biochemistry of Humans and Commonly Used Laboratory Animals. *Biopharmaceutics & drug disposition* **1995**, *16*, 351-80.

27. Allen, A.; Flemstrom, G.; Garner, A.; Kivilaakso, E. Gastroduodenal Mucosal Protection. *Physiological reviews* **1993**, *73*, 823-57.

28. Atuma, C.; Strugala, V.; Allen, A.; Holm, L. The Adherent Gastrointestinal Mucus Gel Layer: Thickness and Physical State in Vivo. *American journal of physiology. Gastrointestinal and liver physiology* **2001**, *280*, G922-9.

29. Gustafsson, J. K.; Ermund, A.; Johansson, M. E.; Schutte, A.; Hansson, G. C.; Sjovall, H. An Ex Vivo Method for Studying Mucus Formation, Properties, and Thickness in Human Colonic Biopsies and Mouse Small and Large Intestinal Explants. *American journal of physiology. Gastrointestinal and liver physiology* **2012**, *302*, G430-8.

30. Pries, A. R.; Secomb, T. W.; Gaehtgens, P. The Endothelial Surface Layer. *Pflugers Archiv : European journal of physiology* **2000**, *440*, 653-66.

31. van den Berg, B. M.; Nieuwdorp, M.; Stroes, E. S.; Vink, H. Glycocalyx and Endothelial (Dys) Function: From Mice to Men. *Pharmacological reports : PR* **2006**, *58 Suppl*, 75-80.

32. Lipinski, C. A.; Lombardo, F.; Dominy, B. W.; Feeney, P. J. Experimental and Computational Approaches to Estimate Solubility and Permeability in Drug Discovery and Development Settings. *Advanced drug delivery reviews* **2001**, *46*, 3-26.

33. Mayor, S.; Pagano, R. E. Pathways of Clathrin-Independent Endocytosis. *Nature reviews. Molecular cell biology* **2007**, *8*, 603-12.

34. Le Roy, C.; Wrana, J. L. Clathrin- and Non-Clathrin-Mediated Endocytic Regulation of Cell Signalling. *Nature reviews. Molecular cell biology* **2005**, *6*, 112-26.

35. International Transporter, C.; Giacomini, K. M.; Huang, S. M.; Tweedie, D. J.; Benet, L. Z.; Brouwer, K. L.; Chu, X.; Dahlin, A.; Evers, R.; Fischer, V.; Hillgren, K. M.; Hoffmaster, K. A.; Ishikawa, T.; Keppler, D.; Kim, R. B.; Lee, C. A.; Niemi, M.; Polli, J. W.; Sugiyama, Y.; Swaan, P. W.; Ware, J. A.; Wright, S. H.; Yee, S. W.; Zamek-Gliszczynski, M. J.; Zhang, L. Membrane Transporters in Drug Development. *Nature reviews. Drug discovery* **2010**, *9*, 215-36.

36. Pantzar, N.; Lundin, S.; Wester, L.; Westrom, B. R. Bidirectional Small-Intestinal Permeability in the Rat to Some Common Marker Molecules in Vitro. *Scandinavian journal of gastroenterology* **1994**, *29*, 703-9.

37. Salama, N. N.; Eddington, N. D.; Fasano, A. Tight Junction Modulation and Its Relationship to Drug Delivery. *Advanced drug delivery reviews* **2006**, *58*, 15-28.

38. Tang, R.; Li, W. X.; Huang, W.; Yan, F.; Chai, W. M.; Yang, G. Y.; Chen, K. M. Co2-Based in-Line Phase Contrast Imaging of Small Intestine in Mice. *Scientific reports* **2013**, *3*, 2313.

39. Ainslie, K. M.; Lowe, R. D.; Beaudette, T. T.; Petty, L.; Bachelder, E. M.; Desai, T. A. Microfabricated Devices for Enhanced Bioadhesive Drug Delivery: Attachment to and Small-Molecule Release through a Cell Monolayer under Flow. *Small* **2009**, *5*, 2857-63.

40. Tachibana, T.; Kato, M.; Takano, J.; Sugiyama, Y. Predicting Drug-Drug Interactions Involving the Inhibition of Intestinal Cyp3a4 and P-Glycoprotein. *Current drug metabolism* **2010**, *11*, 762-77.

41. Besheer, A.; Wood, K. M.; Peppas, N. A.; Mader, K. Loading and Mobility of Spin-Labeled Insulin in Physiologically Responsive Complexation Hydrogels Intended for Oral Administration. *Journal of controlled release : official journal of the Controlled Release Society* **2006**, *111*, 73-80.

42. Kim, B.; Peppas, N. A. In Vitro Release Behavior and Stability of Insulin in Complexation Hydrogels as Oral Drug Delivery Carriers. *International journal of pharmaceutics* **2003**, *266*, 29-37.

43. Lowman, A. M.; Morishita, M.; Kajita, M.; Nagai, T.; Peppas, N. A. Oral Delivery of Insulin Using Ph-Responsive Complexation Gels. *Journal of pharmaceutical sciences* **1999**, *88*, 933-7.

44. Al-Hilal, T. A.; Alam, F.; Byun, Y. Oral Drug Delivery Systems Using Chemical Conjugates or Physical Complexes. *Advanced drug delivery reviews* **2013**, *65*, 845-64.

45. Chirra, H. D.; Desai, T. A. Multi-Reservoir Bioadhesive Microdevices for Independent Rate-Controlled Delivery of Multiple Drugs. *Small* **2012**, *8*, 3839-46.

46. Tao, S. L.; Desai, T. A. Micromachined Devices: The Impact of Controlled Geometry from Cell-Targeting to Bioavailability. *Journal of controlled release : official journal of the Controlled Release Society* **2005**, *109*, 127-38.

47. Tao, S. L.; Popat, K.; Desai, T. A. Off-Wafer Fabrication and Surface Modification of Asymmetric 3d Su-8 Microparticles. *Nature protocols* **2006**, *1*, 3153-8.

48. Harris, L. A.; Hansel, S.; DiBaise, J.; Crowell, M. D. Irritable Bowel Syndrome and Chronic Constipation: Emerging Drugs, Devices, and Surgical Treatments. *Current gastroenterology reports* **2006**, *8*, 282-90.

49. Wald, A. Irritable Bowel Syndrome--Diarrhoea. *Best practice & research. Clinical gastroenterology* **2012**, *26*, 573-80.

50. Wilson, D. S.; Dalmasso, G.; Wang, L.; Sitaraman, S. V.; Merlin, D.; Murthy, N. Orally Delivered Thioketal Nanoparticles Loaded with Tnf-Alpha-Sirna Target Inflammation and Inhibit Gene Expression in the Intestines. *Nature materials* **2010**, *9*, 923-8.

51. Foraker, A. B.; Walczak, R. J.; Cohen, M. H.; Boiarski, T. A.; Grove, C. F.; Swaan, P. W. Microfabricated Porous Silicon Particles Enhance Paracellular Delivery of Insulin across Intestinal Caco-2 Cell Monolayers. *Pharmaceutical research* **2003**, *20*, 110-6.

52. Hiebl, B.; Hopperdietzel, C.; Hunigen, H.; Jung, F.; Scharnagl, N. Influence of a Silicon (Si14)-Based Coating Substrate for Biomaterials on Fibroblast Growth and Human C5a. *Clinical hemorheology and microcirculation* **2013**, *55*, 491-9.

53. Peng, F.; Su, Y.; Zhong, Y.; Fan, C.; Lee, S. T.; He, Y. Silicon Nanomaterials Platform for Bioimaging, Biosensing, and Cancer Therapy. *Accounts of chemical research* **2014**, *47*, 612-23.

54. Santos, H. A.; Makila, E.; Airaksinen, A. J.; Bimbo, L. M.; Hirvonen, J. Porous Silicon Nanoparticles for Nanomedicine: Preparation and Biomedical Applications. *Nanomedicine* **2014**, *9*, 535-54.

55. Fubini, B.; Hubbard, A. Reactive Oxygen Species (Ros) and Reactive Nitrogen Species (Rns) Generation by Silica in Inflammation and Fibrosis. *Free radical biology & medicine* **2003**, *34*, 1507-16.

56. Tungjai, M.; Whorton, E. B.; Rithidech, K. N. Persistence of Apoptosis and Inflammatory Responses in the Heart and Bone Marrow of Mice Following Whole-Body Exposure to (2)(8)Silicon ((2)(8)Si) Ions. *Radiation and environmental biophysics* **2013**, *52*, 339-50.

57. Food; Drug Administration, H. H. S. Medical Devices; Reclassification of Polymethylmethacrylate (Pmma) Bone Cement. Final Rule. *Federal register* **2002**, *67*, 46852-5.

58. Xu, Y.; Xie, F.; Qiu, T.; Xie, L.; Xing, W.; Cheng, J. Rapid Fabrication of a Microdevice with Concave Microwells and Its Application in Embryoid Body Formation. *Biomicrofluidics* **2012**, *6*, 16504-1650411.

59. Reedy, C. R.; Price, C. W.; Sniegowski, J.; Ferrance, J. P.; Begley, M.; Landers, J. P. Solid Phase Extraction of DNA from Biological Samples in a Post-Based, High Surface Area Poly(Methyl Methacrylate) (Pmma) Microdevice. *Lab on a chip* **2011**, *11*, 1603-11.

60. Tao, S. L.; Lubeley, M. W.; Desai, T. A. Bioadhesive Poly(Methyl Methacrylate) Microdevices for Controlled Drug Delivery. *J Control Release* **2003**, *88*, 215-28.

61. Wei, S.; Vaidya, B.; Patel, A. B.; Soper, S. A.; McCarley, R. L. Photochemically Patterned Poly(Methyl Methacrylate) Surfaces Used in the Fabrication of Microanalytical Devices. *The journal of physical chemistry. B* **2005**, *109*, 16988-96.

62. Ainslie, K. M.; Kraning, C. M.; Desai, T. A. Microfabrication of an Asymmetric, Multi-Layered Microdevice for Controlled Release of Orally Delivered Therapeutics. *Lab Chip* **2008**, *8*, 1042-7.

63. Kotzar, G.; Freas, M.; Abel, P.; Fleischman, A.; Roy, S.; Zorman, C.; Moran, J. M.; Melzak, J. Evaluation of Mems Materials of Construction for Implantable Medical Devices. *Biomaterials* **2002**, *23*, 2737-50.

64. Voskerician, G.; Shive, M. S.; Shawgo, R. S.; von Recum, H.; Anderson, J. M.; Cima, M. J.; Langer, R. Biocompatibility and Biofouling of Mems Drug Delivery Devices. *Biomaterials* **2003**, *24*, 1959-67.

65. Vernekar, V. N.; Cullen, D. K.; Fogleman, N.; Choi, Y.; Garcia, A. J.; Allen, M. G.; Brewer, G. J.; LaPlaca, M. C. Su-8 2000 Rendered Cytocompatible for Neuronal Biomems Applications. *Journal of biomedical materials research. Part A* **2009**, *89*, 138-51.

66. Guan, J.; He, H.; Lee, L. J.; Hansford, D. J. Fabrication of Particulate Reservoir-Containing, Capsulelike, and Self-Folding Polymer Microstructures for Drug Delivery. *Small* **2007**, *3*, 412-8.

67. Tao, S. L.; Desai, T. A. Microfabrication of Multilayer, Asymmetric, Polymeric Devices for Drug Delivery. *Advanced Materials* **2005**, *17*, 1625-+.

68. Ryu, W. H.; Vyakarnam, M.; Greco, R. S.; Prinz, F. B.; Fasching, R. J. Fabrication of Multi-Layered Biodegradable Drug Delivery Device Based on Micro-Structuring of Plga Polymers. *Biomedical microdevices* **2007**, *9*, 845-53.

69. Guan, J. J.; Chakrapani, A.; Hansford, D. J. Polymer Microparticles Fabricated by Soft Lithography. *Chem Mater* **2005**, *17*, 6227-6229.

70. Guan, J.; He, H.; Hansford, D. J.; Lee, L. J. Self-Folding of Three-Dimensional Hydrogel Microstructures. *J Phys Chem B* **2005**, *109*, 23134-7.

71. He, H.; Cao, X.; Lee, L. J. Design of a Novel Hydrogel-Based Intelligent System for Controlled Drug Release. *Journal of controlled release : official journal of the Controlled Release Society* **2004**, *95*, 391-402.

72. Ito, Y.; Hasuda, H.; Morimatsu, M.; Takagi, N.; Hirai, Y. A Microfabrication Method of a Biodegradable Polymer Chip for a Controlled Release System. *Journal of biomaterials science. Polymer edition* **2005**, *16*, 949-55.

73. Norman, J. J.; Desai, T. A. Methods for Fabrication of Nanoscale Topography for Tissue Engineering Scaffolds. *Annals of biomedical engineering* **2006**, *34*, 89-101.

74. Qian, T.; Wang, Y. Micro/Nano-Fabrication Technologies for Cell Biology. *Medical & biological engineering & computing* **2010**, *48*, 1023-32.

75. Ziaie, B.; Baldi, A.; Lei, M.; Gu, Y.; Siegel, R. A. Hard and Soft Micromachining for Biomems: Review of Techniques and Examples of Applications in Microfluidics and Drug Delivery. *Advanced drug delivery reviews* **2004**, *56*, 145-72.

76. Chirra, H. D.; Shao, L.; Ciaccio, N.; Fox, C. B.; Wade, J. M.; Ma, A.; Desai, T. A. Planar Microdevices for Enhanced in Vivo Retention and Oral Bioavailability of Poorly Permeable Drugs. *Advanced healthcare materials* **2014**.

77. Tao, S. L.; Desai, T. A. Gastrointestinal Patch Systems for Oral Drug Delivery. *Drug discovery today* **2005**, *10*, 909-15.

78. Guan, J.; Ferrell, N.; James Lee, L.; Hansford, D. J. Fabrication of Polymeric Microparticles for Drug Delivery by Soft Lithography. *Biomaterials* **2006**, *27*, 4034-41.

79. Jackman, R. J.; Duffy, D. C.; Ostuni, E.; Willmore, N. D.; Whitesides, G. M. Fabricating Large Arrays of Microwells with Arbitrary Dimensions and Filling Them Using Discontinuous Dewetting. *Analytical chemistry* **1998**, *70*, 2280-7.

80. Ferrell, N.; Woodard, J.; Hansford, D. Fabrication of Polymer Microstructures for Mems: Sacrificial Layer Micromolding and Patterned Substrate Micromolding. *Biomedical microdevices* **2007**, *9*, 815-21.

81. Geipel, A.; Goldschmidtboeing, F.; Jantscheff, P.; Esser, N.; Massing, U.; Woias, P. Design of an Implantable Active Microport System for Patient Specific Drug Release. *Biomedical microdevices* **2008**, *10*, 469-78.

82. Husler, R.; Schlittler, F. L.; Kreutziger, J.; Streit, M.; Banic, A.; Schoni-Affolter, F.; Hunger, R. E.; Constaninescu, M. A. Staged Surgical Therapy of Basal Cell Carcinoma of the Head and Neck Region: An Evaluation of 500 Procedures. *Swiss medical weekly* **2008**, *138*, 746-51.

83. Lu, X.; Kim-Han, J. S.; O'Malley, K. L.; Sakiyama-Elbert, S. E. A Microdevice Platform for Visualizing Mitochondrial Transport in Aligned Dopaminergic Axons. *Journal of neuroscience methods* **2012**, *209*, 35-9.

84. Park, J.; Li, J.; Han, A. Micro-Macro Hybrid Soft-Lithography Master (Mmhsm) Fabrication for Lab-on-a-Chip Applications. *Biomedical microdevices* **2010**, *12*, 345-51.

85. Fischer, K. E.; Nagaraj, G.; Hugh Daniels, R.; Li, E.; Cowles, V. E.; Miller, J. L.; Bunger, M. D.; Desai, T. A. Hierarchical Nanoengineered Surfaces for Enhanced Cytoadhesion and Drug Delivery. *Biomaterials* **2011**, *32*, 3499-506.

86. Uskokovic, V.; Lee, K.; Lee, P. P.; Fischer, K. E.; Desai, T. A. Shape Effect in the Design of Nanowire-Coated Microparticles as Transepithelial Drug Delivery Devices. *ACS Nano* **2012**, *6*, 7832-41.

87. Uskokovic, V.; Lee, P. P.; Walsh, L. A.; Fischer, K. E.; Desai, T. A. Pegylated Silicon Nanowire Coated Silica Microparticles for Drug Delivery across Intestinal Epithelium. *Biomaterials* **2012**, *33*, 1663-72.

88. Kam, K. R.; Walsh, L. A.; Bock, S. M.; Koval, M.; Fischer, K. E.; Ross, R. F.; Desai, T. A. Nanostructure-Mediated Transport of Biologics across Epithelial Tissue: Enhancing Permeability Via Nanotopography. *Nano Lett* **2013**, *13*, 164-71.

89. Lohmuller, T.; Aydin, D.; Schwieder, M.; Morhard, C.; Louban, I.; Pacholski, C.; Spatz, J. P. Nanopatterning by Block Copolymer Micelle Nanolithography and Bioinspired Applications. *Biointerphases* **2011**, *6*, MR1-12.

90. Marmiroli, B.; Amenitsch, H. X-Ray Lithography and Small-Angle X-Ray Scattering: A Combination of Techniques Merging Biology and Materials Science. *European biophysics journal : EBJ* **2012**, *41*, 851-61.

91. Betancourt, T.; Brannon-Peppas, L. Micro- and Nanofabrication Methods in Nanotechnological Medical and Pharmaceutical Devices. *International journal of nanomedicine* **2006**, *1*, 483-95.

92. Chen, Y.; Pepin, A. Nanofabrication: Conventional and Nonconventional Methods. *Electrophoresis* **2001**, *22*, 187-207.

93. Hu, W. C.; Sarveswaran, K.; Lieberman, M.; Bernstein, G. H. Sub-10 Nm Electron Beam Lithography Using Cold Development of Poly(Methylmethacrylate). *J Vac Sci Technol B* **2004**, *22*, 1711-1716.

94. Pulsifer, D. P.; Lakhtakia, A. Background and Survey of Bioreplication Techniques. *Bioinspiration & biomimetics* **2011**, *6*, 031001.

95. Wu, C. C.; Reinhoudt, D. N.; Otto, C.; Subramaniam, V.; Velders, A. H. Strategies for Patterning Biomolecules with Dip-Pen Nanolithography. *Small* **2011**, *7*, 989-1002.

96. Chou, S. Y.; Krauss, P. R. Imprint Lithography with Sub-10 Nm Feature Size and High Throughput. *Microelectron Eng* **1997**, *35*, 237-240.

97. Chou, S. Y.; Krauss, P. R.; Renstrom, P. J. Imprint Lithography with 25-Nanometer Resolution. *Science* **1996**, *272*, 85-87.

98. Lan, H.; Liu, H. Uv-Nanoimprint Lithography: Structure, Materials and Fabrication of Flexible Molds. *Journal of nanoscience and nanotechnology* **2013**, *13*, 3145-72.

99. Truskett, V. N.; Watts, M. P. Trends in Imprint Lithography for Biological Applications. *Trends in biotechnology* **2006**, *24*, 312-7.

100. Fischer, K. E.; Aleman, B. J.; Tao, S. L.; Hugh Daniels, R.; Li, E. M.; Bunger, M. D.; Nagaraj, G.; Singh, P.; Zettl, A.; Desai, T. A. Biomimetic Nanowire Coatings for Next Generation Adhesive Drug Delivery Systems. *Nano Lett.* **2009**, *9*, 716-20.

101. Porter, J. R.; Henson, A.; Popat, K. C. Biodegradable Poly(Epsilon-Caprolactone) Nanowires for Bone Tissue Engineering Applications. *Biomaterials* **2009**, *30*, 780-8.

102. He, H.; Guan, J.; Lee, J. L. An Oral Delivery Device Based on Self-Folding Hydrogels. *J Control Release* **2006**, *110*, 339-46.

103. Gao, W.; Dong, R.; Thamphiwatana, S.; Li, J.; Gao, W.; Zhang, L.; Wang, J. Artificial Micromotors in the Mouse's Stomach: A Step toward in Vivo Use of Synthetic Motors. *ACS Nano* **2015**, *9*, 117-23.

104. Chirra, H. D.; Shao, L.; Ciaccio, N.; Fox, C. B.; Wade, J. M.; Ma, A.; Desai, T. A. Planar Microdevices for Enhanced in Vivo Retention and Oral Bioavailability of Poorly Permeable Drugs. *Adv Healthc Mater* **2014**, *3*, 1648-54.

105. Wood, K. M.; Stone, G. M.; Peppas, N. A. The Effect of Complexation Hydrogels on Insulin Transport in Intestinal Epithelial Cell Models. *Acta Biomater* **2010**, *6*, 48-56.

106. Wood, K. M.; Stone, G. M.; Peppas, N. A. Wheat Germ Agglutinin Functionalized Complexation Hydrogels for Oral Insulin Delivery. *Biomacromolecules* **2008**, *9*, 1293-8.

107. Wood, K. M.; Stone, G.; Peppas, N. A. Lectin Functionalized Complexation Hydrogels for Oral Protein Delivery. *J Control Release* **2006**, *116*, e66-8.

108. Carreno-Gomez, B.; Woodley, J. F.; Florence, A. T. Studies on the Uptake of Tomato Lectin Nanoparticles in Everted Gut Sacs. *Int J Pharm* **1999**, *183*, 7-11.

109. Fox, C. B.; Chirra, H. D.; Desai, T. A. Planar Bioadhesive Microdevices: A New Technology for Oral Drug Delivery. *Curr Pharm Biotechnol* **2014**, *15*, 673-83.

110. Pennisi, E. Biomechanics. Geckos Climb by the Hairs of Their Toes. *Science* **2000**, *288*, 1717-8.

111. Crosby, A. J.; Hageman, M.; Duncan, A. Controlling Polymer Adhesion with "Pancakes". *Langmuir* **2005**, *21*, 11738-43.

112. Autumn, K.; Sitti, M.; Liang, Y. A.; Peattie, A. M.; Hansen, W. R.; Sponberg, S.; Kenny, T. W.; Fearing, R.; Israelachvili, J. N.; Full, R. J. Evidence for Van Der Waals Adhesion in Gecko Setae. *Proc Natl Acad Sci U S A* **2002**, *99*, 12252-6.

113. Autumn, K.; Liang, Y. A.; Hsieh, S. T.; Zesch, W.; Chan, W. P.; Kenny, T. W.; Fearing, R.; Full, R. J. Adhesive Force of a Single Gecko Foot-Hair. *Nature* **2000**, *405*, 681-5.

114. Traverso, G.; Schoellhammer, C. M.; Schroeder, A.; Maa, R.; Lauwers, G. Y.; Polat, B. E.; Anderson, D. G.; Blankschtein, D.; Langer, R. Microneedles for Drug Delivery Via the Gastrointestinal Tract. *J Pharm Sci* **2015**, *104*, 362-7.

115. Fischer, K. E.; Jayagopal, A.; Nagaraj, G.; Daniels, R. H.; Li, E. M.; Silvestrini, M. T.; Desai, T. A. Nanoengineered Surfaces Enhance Drug Loading and Adhesion. *Nano Lett* **2011**, *11*, 1076-81.

116. Fox, C. B.; Kim, J.; Schlesinger, E. B.; Chirra, H. D.; Desai, T. A. Fabrication of Micropatterned Polymeric Nanowire Arrays for High-Resolution Reagent Localization and Topographical Cellular Control. *Nano Lett* **2015**, *15*, 1540-6.

117. Shimko, D. A.; Nauman, E. A. Development and Characterization of a Porous Poly(Methyl Methacrylate) Scaffold with Controllable Modulus and Permeability. *J Biomed Mater Res B Appl Biomater* **2007**, *80*, 360-9.

118. Rohner, D.; Hutmacher, D. W.; Cheng, T. K.; Oberholzer, M.; Hammer, B. In Vivo Efficacy of Bone-Marrow-Coated Polycaprolactone Scaffolds for the Reconstruction of Orbital Defects in the Pig. *J Biomed Mater Res B Appl Biomater* **2003**, *66*, 574-80.

119. Patil, S. B.; Kaul, A.; Babbar, A.; Mathur, R.; Mishra, A.; Sawant, K. K. In Vivo Evaluation of Alginate Microspheres of Carvedilol for Nasal Delivery. *J Biomed Mater Res B Appl Biomater* **2012**, *100*, 249-55.

120. Pal, D.; Nayak, A. K. Novel Tamarind Seed Polysaccharide-Alginate Mucoadhesive Microspheres for Oral Gliclazide Delivery: In Vitro-in Vivo Evaluation. *Drug Deliv* **2012**, *19*, 123-31.

121. Thanou, M.; Verhoef, J. C.; Junginger, H. E. Oral Drug Absorption Enhancement by Chitosan and Its Derivatives. *Adv Drug Deliv Rev* **2001**, *52*, 117-26.

122. Sogias, I. A.; Williams, A. C.; Khutoryanskiy, V. V. Why Is Chitosan Mucoadhesive? *Biomacromolecules* **2008**, *9*, 1837-42.

123. Chen, M. C.; Mi, F. L.; Liao, Z. X.; Hsiao, C. W.; Sonaje, K.; Chung, M. F.; Hsu, L. W.; Sung, H. W. Recent Advances in Chitosan-Based Nanoparticles for Oral Delivery of Macromolecules. *Adv Drug Deliv Rev* **2013**, *65*, 865-79.

124. Uccello-Barretta, G.; Balzano, F.; Vanni, L.; Sanso, M. Mucoadhesive Properties of Tamarind-Seed Polysaccharide/Hyaluronic Acid Mixtures: A Nuclear Magnetic Resonance Spectroscopy Investigation. *Carbohydr Polym* **2013**, *91*, 568-72.

125. Sandri, G.; Rossi, S.; Ferrari, F.; Bonferoni, M. C.; Zerrouk, N.; Caramella, C. Mucoadhesive and Penetration Enhancement Properties of Three Grades of Hyaluronic Acid Using Porcine Buccal and Vaginal Tissue, Caco-2 Cell Lines, and Rat Jejunum. *J Pharm Pharmacol* **2004**, *56*, 1083-90.

126. Wang, J.; Tauchi, Y.; Deguchi, Y.; Morimoto, K.; Tabata, Y.; Ikada, Y. Positively Charged Gelatin Microspheres as Gastric Mucoadhesive Drug Delivery System for Eradication of H. Pylori. *Drug Deliv* **2000**, *7*, 237-43.

127. Wang, J.; Tabata, Y.; Bi, D.; Morimoto, K. Evaluation of Gastric Mucoadhesive Properties of Aminated Gelatin Microspheres. *J Control Release* **2001**, *73*, 223-31.

128. Rahmat, D.; Muller, C.; Barthelmes, J.; Shahnaz, G.; Martien, R.; Bernkop-Schnurch, A. Thiolated Hydroxyethyl Cellulose: Design and in Vitro Evaluation of Mucoadhesive and Permeation Enhancing Nanoparticles. *Eur J Pharm Biopharm* **2013**, *83*, 149-55.

129. Mazoniene, E.; Joceviciute, S.; Kazlauske, J.; Niemeyer, B.; Liesiene, J. Interaction of Cellulose-Based Cationic Polyelectrolytes with Mucin. *Colloids Surf B Biointerfaces* **2011**, *83*, 160-4.

130. Sosnik, A.; das Neves, J.; Sarmento, B. Mucoadhesive Polymers in the Design of Nano-Drug Delivery Systems for Administration by Non-Parenteral Routes: A Review. *Progress in Polymer Science* **2014**, *39*, 2030-2075.

131. Shrestha, N.; Shahbazi, M. A.; Araujo, F.; Zhang, H.; Makila, E. M.; Kauppila, J.; Sarmento, B.; Salonen, J. J.; Hirvonen, J. T.; Santos, H. A. Chitosan-Modified Porous

Silicon Microparticles for Enhanced Permeability of Insulin across Intestinal Cell Monolayers. *Biomaterials* **2014**, *35*, 7172-9.

132. Sajeesh, S.; Bouchemal, K.; Marsaud, V.; Vauthier, C.; Sharma, C. P. Cyclodextrin Complexed Insulin Encapsulated Hydrogel Microparticles: An Oral Delivery System for Insulin. *J Control Release* **2010**, *147*, 377-84.

133. Liao, Z. X.; Chuang, E. Y.; Hsiao, C. W.; Sung, H. W. 21. Ph-Sensitive Chitosan-Based Nanoparticles for Protein Drug Delivery: Oral Approaches: Original Research Article: A Novel Ph-Sensitive Hydrogel Composed of Carboxymethyl Chitosan and Alginate Cross-Linked by Genipin for Protein Drug Delivery, 2004. *J Control Release* **2014**, *190*, 68-70.

134. Gradauer, K.; Barthelmes, J.; Vonach, C.; Almer, G.; Mangge, H.; Teubl, B.; Roblegg, E.; Dunnhaupt, S.; Frohlich, E.; Bernkop-Schnurch, A.; Prassl, R. Liposomes Coated with Thiolated Chitosan Enhance Oral Peptide Delivery to Rats. *J Control Release* **2013**, *172*, 872-8.

135. Gadalla, H. H.; Soliman, G. M.; Mohammed, F. A.; El-Sayed, A. M. Development and in Vitro/in Vivo Evaluation of Zn-Pectinate Microparticles Reinforced with Chitosan for the Colonic Delivery of Progesterone. *Drug Deliv* **2015**, 1-14.

136. Fan, B.; Xing, Y.; Zheng, Y.; Sun, C.; Liang, G. Ph-Responsive Thiolated Chitosan Nanoparticles for Oral Low-Molecular Weight Heparin Delivery: In Vitro and in Vivo Evaluation. *Drug Deliv* **2014**, 1-10.

137. Dunnhaupt, S.; Barthelmes, J.; Iqbal, J.; Perera, G.; Thurner, C. C.; Friedl, H.; Bernkop-Schnurch, A. In Vivo Evaluation of an Oral Drug Delivery System for Peptides Based on S-Protected Thiolated Chitosan. *J Control Release* **2012**, *160*, 477-85.

138. Ahn, S.; Lee, I. H.; Lee, E.; Kim, H.; Kim, Y. C.; Jon, S. Oral Delivery of an Anti-Diabetic Peptide Drug Via Conjugation and Complexation with Low Molecular Weight Chitosan. *J Control Release* **2013**, *170*, 226-32.

139. Xu, J.; Strandman, S.; Zhu, J. X.; Barralet, J.; Cerruti, M. Genipin-Crosslinked Catechol-Chitosan Mucoadhesive Hydrogels for Buccal Drug Delivery. *Biomaterials* **2015**, *37*, 395-404.

140. Tang, C.; Guan, Y. X.; Yao, S. J.; Zhu, Z. Q. Preparation of Ibuprofen-Loaded Chitosan Films for Oral Mucosal Drug Delivery Using Supercritical Solution Impregnation. *Int J Pharm* **2014**, *473*, 434-41.

141. Liang, Y.; Liu, W.; Han, B.; Yang, C.; Ma, Q.; Zhao, W.; Rong, M.; Li, H. Fabrication and Characters of a Corneal Endothelial Cells Scaffold Based on Chitosan. *J Mater Sci Mater Med* **2011**, *22*, 175-83.

142. Koev, S. T.; Dykstra, P. H.; Luo, X.; Rubloff, G. W.; Bentley, W. E.; Payne, G. F.; Ghodssi, R. Chitosan: An Integrative Biomaterial for Lab-on-a-Chip Devices. *Lab Chip* **2010**, *10*, 3026-42.

143. Lopez-Leon, T.; Carvalho, E. L.; Seijo, B.; Ortega-Vinuesa, J. L.; Bastos-Gonzalez, D. Physicochemical Characterization of Chitosan Nanoparticles: Electrokinetic and Stability Behavior. *J Colloid Interface Sci* **2005**, *283*, 344-51.

144. Zakharchenko, S.; Ionov, L. Anisotropic Liquid Microcapsules from Biomimetic Self-Folding Polymer Films. *ACS Appl Mater Interfaces* **2015**.

145. Stoychev, G.; Puretskiy, N.; Ionov, L. Self-Folding All-Polymer Thermoresponsive Microcapsules. *Soft Matter* **2011**, *7*, 3277-3279.

146. Bassik, N.; Abebe, B. T.; Laflin, K. E.; Gracias, D. H. Photolithographically Patterned Smart Hydrogel Based Bilayer Actuators. *Polymer* **2010**, *51*, 6093-6098.

147. Wu, Z.; Wu, Y.; He, W.; Lin, X.; Sun, J.; He, Q. Self-Propelled Polymer-Based Multilayer Nanorockets for Transportation and Drug Release. *Angew Chem Int Ed Engl* **2013**, *52*, 7000-3.

148. Wilson, D. A.; Nolte, R. J.; van Hest, J. C. Autonomous Movement of Platinum-Loaded Stomatocytes. *Nat Chem* **2012**, *4*, 268-74.

149. Paxton, W. F.; Kistler, K. C.; Olmeda, C. C.; Sen, A.; St Angelo, S. K.; Cao, Y.; Mallouk, T. E.; Lammert, P. E.; Crespi, V. H. Catalytic Nanomotors: Autonomous Movement of Striped Nanorods. *J Am Chem Soc* **2004**, *126*, 13424-31.

150. Mirkovic, T.; Zacharia, N. S.; Scholes, G. D.; Ozin, G. A. Fuel for Thought: Chemically Powered Nanomotors out-Swim Nature's Flagellated Bacteria. *ACS Nano* **2010**, *4*, 1782-9.

151. Guix, M.; Mayorga-Martinez, C. C.; Merkoci, A. Nano/Micromotors in (Bio)Chemical Science Applications. *Chem Rev* **2014**, *114*, 6285-322.

152. Gao, W.; Uygun, A.; Wang, J. Hydrogen-Bubble-Propelled Zinc-Based Microrockets in Strongly Acidic Media. *J Am Chem Soc* **2012**, *134*, 897-900.

153. Dingal, P. C.; Discher, D. E. Combining Insoluble and Soluble Factors to Steer Stem Cell Fate. *Nature materials* **2014**, *13*, 532-7.

154. Dalby, M. J.; Gadegaard, N.; Oreffo, R. O. Harnessing Nanotopography and Integrin-Matrix Interactions to Influence Stem Cell Fate. *Nature materials* **2014**, *13*, 558-69.

155. Ramsay, G. DNA Chips: State-of-the Art. *Nature biotechnology* **1998**, *16*, 40-4.

156. Ganau, M.; Bosco, A.; Palma, A.; Corvaglia, S.; Parisse, P.; Fruk, L.; Beltrami, A. P.; Cesselli, D.; Casalis, L.; Scoles, G. A DNA-Based Nano-Immunoassay for the Label-Free Detection of Glial Fibrillary Acidic Protein in Multicell Lysates. *Nanomedicine* **2014**, *14*, 207-15.

157. Cai, Y.; Ocko, B. M. Large-Scale Fabrication of Protein Nanoarrays Based on Nanosphere Lithography. *Langmuir* **2005**, *21*, 9274-9.

158. Tao, S. L.; Popat, K.; Desai, T. A. Off-Wafer Fabrication and Surface Modification of Asymmetric 3d Su-8 Microparticles. *Nature protocols* **2006**, *1*, 3153-8.

159. Siegel, R. A.; Gu, Y.; Lei, M.; Baldi, A.; Nuxoll, E. E.; Ziaie, B. Hard and Soft Micro- and Nanofabrication: An Integrated Approach to Hydrogel-Based Biosensing and Drug Delivery. *Journal of controlled release : official journal of the Controlled Release Society* **2010**, *141*, 303-13.

160. Sheridan, C. Proof of Concept for Next-Generation Nanoparticle Drugs in Humans. *Nature biotechnology* **2012**, *30*, 471-3.

161. Quake, S. R.; Scherer, A. From Micro- to Nanofabrication with Soft Materials. *Science* **2000**, *290*, 1536-40.

162. Norman, J. J.; Desai, T. A. Methods for Fabrication of Nanoscale Topography for Tissue Engineering Scaffolds. *Annals of biomedical engineering* **2006**, *34*, 89-101.

163. Lee, K. W.; Yoon, S. M.; Lee, S. C.; Lee, W.; Kim, I. M.; Lee, C. E.; Kim, D. H. Secondary Electron Generation in Electron-Beam-Irradiated Solids: Resolution Limits to Nanolithography. *J. Korean Phys. Soc.* **2009**, *55*, 1720-1723.

164. Truskett, V. N.; Watts, M. P. Trends in Imprint Lithography for Biological Applications. *Trends in biotechnology* **2006**, *24*, 312-7.

165. Biswas, A.; Bayer, I. S.; Biris, A. S.; Wang, T.; Dervishi, E.; Faupel, F. Advances in Top-Down and Bottom-up Surface Nanofabrication: Techniques, Applications & Future Prospects. *Advances in colloid and interface science* **2012**, *170*, 2-27.

166. Torres, C. M. S.; Zankovych, S.; Seekamp, J.; Kam, A. P.; Cedeno, C. C.; Hoffmann, T.; Ahopelto, J.; Reuther, F.; Pfeiffer, K.; Bleidiessel, G.; Gruetzner, G.; Maximov, M. V.; Heidari, B. Nanoimprint Lithography: An Alternative Nanofabrication Approach. *Mat. Sci. Eng. C* **2003**, *23*, 23-31.

167. Zhang, J.; Li, Y.; Zhang, X.; Yang, B. Colloidal Self-Assembly Meets Nanofabrication: From Two-Dimensional Colloidal Crystals to Nanostructure Arrays. *Advanced materials* **2010**, *22*, 4249-69.

168. Tao, S. L.; Desai, T. A. Aligned Arrays of Biodegradable Poly(Epsilon-Caprolactone) Nanowires and Nanofibers by Template Synthesis. *Nano letters* **2007**, *7*, 1463-8.

169. Mai, Y.; Eisenberg, A. Self-Assembly of Block Copolymers. *Chemical Society reviews* **2012**, *41*, 5969-85.

170. Chen, W.; Villa-Diaz, L. G.; Sun, Y.; Weng, S.; Kim, J. K.; Lam, R. H.; Han, L.; Fan, R.; Krebsbach, P. H.; Fu, J. Nanotopography Influences Adhesion, Spreading, and Self-Renewal of Human Embryonic Stem Cells. *ACS Nano* **2012**, *6*, 4094-103.

171. Yang, K.; Jung, K.; Ko, E.; Kim, J.; Park, K. I.; Kim, J.; Cho, S. W. Nanotopographical Manipulation of Focal Adhesion Formation for Enhanced Differentiation of Human Neural Stem Cells. *ACS applied materials & interfaces* **2013**, *5*, 10529-40.

172. Yang, K.; Jung, H.; Lee, H. R.; Lee, J. S.; Kim, S. R.; Song, K. Y.; Cheong, E.; Bang, J.; Im, S. G.; Cho, S. W. Multiscale, Hierarchically Patterned Topography for Directing Human Neural Stem Cells into Functional Neurons. *ACS Nano* **2014**, *8*, 7809-22.

173. Tan, J.; Saltzman, W. M. Biomaterials with Hierarchically Defined Micro- and Nanoscale Structure. *Biomaterials* **2004**, *25*, 3593-601.

174. Muthusubramaniam, L.; Zaitseva, T.; Paukshto, M.; Martin, G.; Desai, T. Effect of Collagen Nanotopography on Keloid Fibroblast Proliferation and Matrix Synthesis: Implications for Dermal Wound Healing. *Tissue engineering. Part A* **2014**, *20*, 2728-36.

175. Muthusubramaniam, L.; Peng, L.; Zaitseva, T.; Paukshto, M.; Martin, G. R.; Desai, T. A. Collagen Fibril Diameter and Alignment Promote the Quiescent Keratocyte Phenotype. *Journal of biomedical materials research. Part A* **2012**, *100*, 613-21.

176. Kim, H. N.; Hong, Y.; Kim, M. S.; Kim, S. M.; Suh, K. Y. Effect of Orientation and Density of Nanotopography in Dermal Wound Healing. *Biomaterials* **2012**, *33*, 8782-92.

177. Chua, J. S.; Chng, C. P.; Moe, A. A.; Tann, J. Y.; Goh, E. L.; Chiam, K. H.; Yim, E. K. Extending Neurites Sense the Depth of the Underlying Topography During Neuronal Differentiation and Contact Guidance. *Biomaterials* **2014**, *35*, 7750-61.

178. Riveline, D.; Zamir, E.; Balaban, N. Q.; Schwarz, U. S.; Ishizaki, T.; Narumiya, S.; Kam, Z.; Geiger, B.; Bershadsky, A. D. Focal Contacts as Mechanosensors: Externally Applied Local Mechanical Force Induces Growth of Focal Contacts by an Mdia1-Dependent and Rock-Independent Mechanism. *The Journal of cell biology* **2001**, *153*, 1175-86.

179. Reig, G.; Pulgar, E.; Concha, M. L. Cell Migration: From Tissue Culture to Embryos. *Development* **2014**, *141*, 1999-2013.

180. Fu, J.; Wang, Y. K.; Yang, M. T.; Desai, R. A.; Yu, X.; Liu, Z.; Chen, C. S. Mechanical Regulation of Cell Function with Geometrically Modulated Elastomeric Substrates. *Nature methods* **2010**, *7*, 733-6.

181. Marizza, P.; Keller, S. S.; Boisen, A. Inkjet Printing as a Technique for Filling of Micro-Wells with Biocompatible Polymers. *Microelectron Eng* **2013**, *111*, 391-395.

182. Marizza, P.; Keller, S. S.; Mullertz, A.; Boisen, A. Polymer-Filled Microcontainers for Oral Delivery Loaded Using Supercritical Impregnation. *Journal of controlled release : official journal of the Controlled Release Society* **2014**, *173*, 1-9.

183. Chirra, H. D.; Desai, T. A. Emerging Microtechnologies for the Development of Oral Drug Delivery Devices. *Advanced drug delivery reviews* **2012**, *64*, 1569-78.

184. Fox, C. B.; Chirra, H. D.; Desai, T. A. Planar Bioadhesive Microdevices: A New Technology for Oral Drug Delivery. *Current pharmaceutical biotechnology* **2014**, *15*, 673-83.

185. Yuan, J.; Liu, X.; Akbulut, O.; Hu, J.; Suib, S. L.; Kong, J.; Stellacci, F. Superwetting Nanowire Membranes for Selective Absorption. *Nature nanotechnology* **2008**, *3*, 332-6.

186. Kim, B. S.; Shin, S.; Shin, S. J.; Kim, K. M.; Cho, H. H. Control of Superhydrophilicity/Superhydrophobicity Using Silicon Nanowires Via Electroless Etching Method and Fluorine Carbon Coatings. *Langmuir* **2011**, *27*, 10148-56.

187. Yuan, W.; Lu, Z.; Liu, J.; Wang, H.; Li, C. M. Zno Nanowire Array-Templated Lbl Self-Assembled Polyelectrolyte Nanotube Arrays and Application for Charged Drug Delivery. *Nanotechnology* **2013**, *24*, 045605.

188. Garcia-Gradilla, V.; Sattayasamitsathit, S.; Soto, F.; Kuralay, F.; Yardimci, C.; Wiitala, D.; Galarnyk, M.; Wang, J. Ultrasound-Propelled Nanoporous Gold Wire for Efficient Drug Loading and Release. *Small* **2014**, *10*, 4154-9.

189. Fischer, K. E.; Jayagopal, A.; Nagaraj, G.; Daniels, R. H.; Li, E. M.; Silvestrini, M. T.; Desai, T. A. Nanoengineered Surfaces Enhance Drug Loading and Adhesion. *Nano letters* **2011**, *11*, 1076-81.

190. Mikos, A. G.; Peppas, N. A. Bioadhesive Analysis of Controlled-Release Systems .4. An Experimental-Method for Testing the Adhesion of Microparticles with Mucus. *J. Control. Release* **1990**, *12*, 31-37.

191. Jeyachandran, Y. L.; Mielczarski, E.; Rai, B.; Mielczarski, J. A. Quantitative and Qualitative Evaluation of Adsorption/Desorption of Bovine Serum Albumin on Hydrophilic and Hydrophobic Surfaces. *Langmuir* **2009**, *25*, 11614-20.

192. Porter, J. R.; Henson, A.; Ryan, S.; Popat, K. C. Biocompatibility and Mesenchymal Stem Cell Response to Poly(Epsilon-Caprolactone) Nanowire Surfaces for Orthopedic Tissue Engineering. *Tissue engineering. Part A* **2009**, *15*, 2547-59.

193. Popat, K. C.; Daniels, R. H.; Dubrow, R. S.; Hardev, V.; Desai, T. A. Nanostructured Surfaces for Bone Biotemplating Applications. *Journal of orthopaedic research : official publication of the Orthopaedic Research Society* **2006**, *24*, 619-27.

194. Bechara, S.; Popat, K. C. Micro-Patterned Nanowire Surfaces Encourage Directional Neural Progenitor Cell Adhesion and Proliferation. *Journal of biomedical nanotechnology* **2013**, *9*, 1698-706.

195. Shimko, D. A.; Nauman, E. A. Development and Characterization of a Porous Poly(Methyl Methacrylate) Scaffold with Controllable Modulus and Permeability. *Journal of biomedical materials research. Part B, Applied biomaterials* **2007**, *80*, 360-9.

196. Ainslie, K. M.; Tao, S. L.; Popat, K. C.; Daniels, H.; Hardev, V.; Grimes, C. A.; Desai, T. A. In Vitro Inflammatory Response of Nanostructured Titania, Silicon Oxide, and Polycaprolactone. *Journal of biomedical materials research. Part A* **2009**, *91*, 647-55.

197. Bechara, S. L.; Judson, A.; Popat, K. C. Template Synthesized Poly(Epsilon-Caprolactone) Nanowire Surfaces for Neural Tissue Engineering. *Biomaterials* **2010**, *31*, 3492-501.

198. Huang, T. K.; Chen, Y. C.; Ko, H. C.; Huang, H. W.; Wang, C. H.; Lin, H. K.; Chen, F. R.; Kai, J. J.; Lee, C. Y.; Chiu, H. T. Growth of High-Aspect-Ratio Gold Nanowires on Silicon by Surfactant-Assisted Galvanic Reductions. *Langmuir* **2008**, *24*, 5647-9.

199. Lundgren, M.; Allan, N. L.; Cosgrove, T. Modeling of Wetting: A Study of Nanowetting at Rough and Heterogeneous Surfaces. *Langmuir* **2007**, *23*, 1187-94.

200. Wade, J. S.; Desai, T. A. Planar Microdevices Enhance Transport of Large Molecular Weight Molecules across Retinal Pigment Epithelial Cells. *Biomedical microdevices* **2014**, *16*, 629-38.

201. Chirra, H. D.; Shao, L.; Ciaccio, N.; Fox, C. B.; Wade, J. M.; Ma, A.; Desai, T. A. Planar Microdevices for Enhanced in Vivo Retention and Oral Bioavailability of Poorly Permeable Drugs. *Advanced healthcare materials* **2014**, *3*, 1648-54.

202. Meyle, J.; Wolburg, H.; von Recum, A. F. Surface Micromorphology and Cellular Interactions. *Journal of biomaterials applications* **1993**, *7*, 362-74.

203. Ciobanasu, C.; Faivre, B.; Le Clainche, C. Integrating Actin Dynamics, Mechanotransduction and Integrin Activation: The Multiple Functions of Actin Binding Proteins in Focal Adhesions. *European journal of cell biology* **2013**, *92*, 339-48.

204. Kim, H. N.; Jiao, A.; Hwang, N. S.; Kim, M. S.; Kang do, H.; Kim, D. H.; Suh, K. Y. Nanotopography-Guided Tissue Engineering and Regenerative Medicine. *Advanced drug delivery reviews* **2013**, *65*, 536-58.

205. Kam, K. R.; Walsh, L. A.; Bock, S. M.; Ollerenshaw, J. D.; Ross, R. F.; Desai, T. A. The Effect of Nanotopography on Modulating Protein Adsorption and the Fibrotic Response. *Tissue engineering. Part A* **2014**, *20*, 130-8.

206. Ayala, P.; Lopez, J. I.; Desai, T. A. Microtopographical Cues in 3d Attenuate Fibrotic Phenotype and Extracellular Matrix Deposition: Implications for Tissue Regeneration. *Tissue engineering. Part A* **2010**, *16*, 2519-27.

207. Oh, S.; Brammer, K. S.; Li, Y. S.; Teng, D.; Engler, A. J.; Chien, S.; Jin, S. Stem Cell Fate Dictated Solely by Altered Nanotube Dimension. *Proceedings of the National Academy of Sciences of the United States of America* **2009**, *106*, 2130-5.

208. Luo, W.; Jones, S. R.; Yousaf, M. N. Geometric Control of Stem Cell Differentiation Rate on Surfaces. *Langmuir* **2008**, *24*, 12129-33.

209. Celiz, A. D.; Smith, J. G.; Langer, R.; Anderson, D. G.; Winkler, D. A.; Barrett, D. A.; Davies, M. C.; Young, L. E.; Denning, C.; Alexander, M. R. Materials for Stem Cell Factories of the Future. *Nature materials* **2014**, *13*, 570-9.

210. Bauwens, C. L.; Song, H.; Thavandiran, N.; Ungrin, M.; Masse, S.; Nanthakumar, K.; Seguin, C.; Zandstra, P. W. Geometric Control of Cardiomyogenic Induction in Human Pluripotent Stem Cells. *Tissue engineering. Part A* **2011**, *17*, 1901-9.

211. Cheng, C. M.; LeDuc, P. R.; Lin, Y. W. Localized Bimodal Response of Neurite Extensions and Structural Proteins in Dorsal-Root Ganglion Neurons with Controlled Polydimethylsiloxane Substrate Stiffness. *Journal of biomechanics* **2011**, *44*, 856-62.

212. Leszczak, V.; Baskett, D. A.; Popat, K. C. Smooth Muscle Cell Functionality on Collagen Immobilized Polycaprolactone Nanowire Surfaces. *Journal of functional biomaterials* **2014**, *5*, 58-77.

213. Dash, T. K.; Konkimalla, V. B. Polymeric Modification and Its Implication in Drug Delivery: Poly-Epsilon-Caprolactone (Pcl) as a Model Polymer. *Molecular pharmaceutics* **2012**, *9*, 2365-79.

214. Chung, T. W.; Lai, D. M.; Chen, S. D.; Lin, Y. I. Poly (Epsilon-Caprolactone) Scaffolds Functionalized by Grafting Ngf and Grgd Promote Growth and Differentiation of Pc12 Cells. *Journal of biomedical materials research. Part A* **2014**, *102*, 315-23.

215. Wade, J. S.; Desai, T. A. Planar Microdevices Enhance Transport of Large Molecular Weight Molecules across Retinal Pigment Epithelial Cells. *Biomed. microdevices* **2014**, *16*, 629-38.

216. Marizza, P.; Keller, S. S.; Mullertz, A.; Boisen, A. Polymer-Filled Microcontainers for Oral Delivery Loaded Using Supercritical Impregnation. *J Control Release* **2014**, *173*, 1-9.

217. Marizza, P.; Keller, S. S.; Boisen, A. Inkjet Printing as a Technique for Filling of Micro-Wells with Biocompatible Polymers. *Microelectron. Eng.* **2013**, *111*, 391-395.

218. Fox, C. B.; Chirra, H. D.; Desai, T. A. Planar Bioadhesive Microdevices: A New Technology for Oral Drug Delivery. *Curr. Pharm. Biotechnol.* **2014**.

219. Kam, K. R.; Desai, T. A. Nano- and Microfabrication for Overcoming Drug Delivery Challenges. *J. Mater. Chem. B Mater. Biol. Med.* **2013**, *1*, 1878-1884.

220. Lee, M. H.; Lim, N.; Ruebusch, D. J.; Jamshidi, A.; Kapadia, R.; Lee, R.; Seok, T. J.; Takei, K.; Cho, K. Y.; Fan, Z.; Jang, H.; Wu, M.; Cho, G.; Javey, A. Roll-to-Roll Anodization and Etching of Aluminum Foils for High-Throughput Surface Nanotexturing. *Nano letters* **2011**, *11*, 3425-30.

221. Parker, N. W.; Brodie, A. D.; McCoy, J. H. A High Throughput Ngl Electron Beam Direct-Write Lithography System. *P Soc Photo-Opt Ins* **2000**, *3997*, 713-720.

222. Patel, V. F.; Liu, F.; Brown, M. B. Advances in Oral Transmucosal Drug Delivery. *J. Control. Release* **2011**, *153*, 106-16.

223. Chaturvedi, K.; Ganguly, K.; Nadagouda, M. N.; Aminabhavi, T. M. Polymeric Hydrogels for Oral Insulin Delivery. *J. Control. Release* **2013**, *165*, 129-38.

224. Thanki, K.; Gangwal, R. P.; Sangamwar, A. T.; Jain, S. Oral Delivery of Anticancer Drugs: Challenges and Opportunities. *J. Control. Release* **2013**, *170*, 15-40.

225. Park, K.; Kwon, I. C.; Park, K. Oral Protein Delivery: Current Status and Future Prospect. *React. Funct. Polym.* **2011**, *71*, 280-287.

226. Fox, C. B.; Kim, J.; Le, L. V.; Nemeth, C. L.; Chirra, H. D.; Desai, T. A. Micro/Nanofabricated Platforms for Oral Drug Delivery. *J. Control. Release* **2015**, *219*, 431-44.

227. Walsh, L. A.; Allen, J. L.; Desai, T. A. Nanotopography Applications in Drug Delivery. *Expert Opin. Drug Deliv.* **2015**, *12*, 1823-7.

228. Xu, A. M.; Aalipour, A.; Leal-Ortiz, S.; Mekhdjian, A. H.; Xie, X.; Dunn, A. R.; Garner, C. C.; Melosh, N. A. Quantification of Nanowire Penetration into Living Cells. *Nat. Commun.* **2014**, *5*, 3613.

229. Xie, X.; Xu, A. M.; Leal-Ortiz, S.; Cao, Y.; Garner, C. C.; Melosh, N. A. Nanostraw-Electroporation System for Highly Efficient Intracellular Delivery and Transfection. *ACS Nano* **2013**, *7*, 4351-8.

230. Xie, X.; Aalipour, A.; Gupta, S. V.; Melosh, N. A. Determining the Time Window for Dynamic Nanowire Cell Penetration Processes. *ACS Nano* **2015**, *9*, 11667-77.

231. VanDersarl, J. J.; Xu, A. M.; Melosh, N. A. Nanostraws for Direct Fluidic Intracellular Access. *Nano Lett.* **2012**, *12*, 3881-6.

232. Schneider, C. A.; Rasband, W. S.; Eliceiri, K. W. Nih Image to Imagej: 25 Years of Image Analysis. *Nat. Methods* **2012**, *9*, 671-5.

233. Schindelin, J.; Arganda-Carreras, I.; Frise, E.; Kaynig, V.; Longair, M.; Pietzsch, T.; Preibisch, S.; Rueden, C.; Saalfeld, S.; Schmid, B.; Tinevez, J. Y.; White, D. J.; Hartenstein, V.; Eliceiri, K.; Tomancak, P.; Cardona, A. Fiji: An Open-Source Platform for Biological-Image Analysis. *Nat. Methods* **2012**, *9*, 676-82.

234. Wang, B.; Mao, Y. K.; Diorio, C.; Pasyk, M.; Wu, R. Y.; Bienenstock, J.; Kunze, W. A. Luminal Administration Ex Vivo of a Live Lactobacillus Species Moderates Mouse Jejunal Motility within Minutes. *Fed. Am. Soc. Exp. Biol. J.* **2010**, *24*, 4078-88.

235. Mols, R.; Brouwers, J.; Schinkel, A. H.; Annaert, P.; Augustijns, P. Intestinal Perfusion with Mesenteric Blood Sampling in Wild-Type and Knockout Mice: Evaluation of a Novel Tool in Biopharmaceutical Drug Profiling. *Drug Metab. Dispos.* **2009**, *37*, 1334-7.

236. Luo, Z.; Liu, Y.; Zhao, B.; Tang, M.; Dong, H.; Zhang, L.; Lv, B.; Wei, L. Ex Vivo and in Situ Approaches Used to Study Intestinal Absorption. *J. Pharmacol. Toxicol. Methods*. **2013**, *68*, 208-16.

237. Escribano, E.; Sala, X. G.; Salamanca, J.; Navarro, C. R.; Regue, J. Q. Single-Pass Intestinal Perfusion to Establish the Intestinal Permeability of Model Drugs in Mouse. *Int. J. Pharm*. **2012**, *436*, 472-7.

238. Spende, A.; Sobel, N.; Lukas, M.; Zierold, R.; Riedl, J. C.; Gura, L.; Schubert, I.; Moreno, J. M.; Nielsch, K.; Stuhn, B.; Hess, C.; Trautmann, C.; Toimil-Molares, M. E. Tio2, Sio2, and Al2o3 Coated Nanopores and Nanotubes Produced by Ald in Etched Ion-Track Membranes for Transport Measurements. *Nanotechnology* **2015**, *26*, 335301.

239. Chakarvarti, S. K. Track-Etch Membranes Enabled Nano-/Microtechnology: A Review. *Radiat. Meas*. **2009**, *44*, 1085-1092.

240. Williams, W. D.; Giordano, N. Fabrication of 80-a Metal Wires. *Review of Scientific Instruments* **1984**, *55*, 410-412.

241. Wang, Q.; Webster, T. J. Nanostructured Selenium for Preventing Biofilm Formation on Polycarbonate Medical Devices. *J. Biomed. Mater. Res. A* **2012**, *100*, 3205-10.

242. Nyitray, C. E.; Chang, R.; Faleo, G.; Lance, K. D.; Bernards, D. A.; Tang, Q.; Desai, T. A. Polycaprolactone Thin-Film Micro- and Nanoporous Cell-Encapsulation Devices. *ACS Nano* **2015**, *9*, 5675-82.

243. Masson, B. Emergence of the Alumina Matrix Composite in Total Hip Arthroplasty. *Int. Orthop*. **2009**, *33*, 359-63.

244. Jeyachandran, Y. L.; Mielczarski, J. A.; Mielczarski, E.; Rai, B. Efficiency of Blocking of Non-Specific Interaction of Different Proteins by Bsa Adsorbed on Hydrophobic and Hydrophilic Surfaces. *J Colloid Interface Sci* **2010**, *341*, 136-42.

245. Fujie, T.; Desii, A.; Ventrelli, L.; Mazzolai, B.; Mattoli, V. Inkjet Printing of Protein Microarrays on Freestanding Polymeric Nanofilms for Spatio-Selective Cell Culture Environment. *Biomed. Microdevices* **2012**, *14*, 1069-76.

246. Humphrey, S. P.; Williamson, R. T. A Review of Saliva: Normal Composition, Flow, and Function. *J. Prosthet. Dent*. **2001**, *85*, 162-9.

247. Fallingborg, J. Intraluminal Ph of the Human Gastrointestinal Tract. *Dan. Med. Bull*. **1999**, *46*, 183-96.

248. Fallingborg, J.; Christensen, L. A.; Jacobsen, B. A.; Rasmussen, S. N. Very Low Intraluminal Colonic Ph in Patients with Active Ulcerative Colitis. *Dig. Dis. Sci*. **1993**, *38*, 1989-93.

249. Yoshida, T.; Lai, T. C.; Kwon, G. S.; Sako, K. Ph- and Ion-Sensitive Polymers for Drug Delivery. *Expert Opin. Drug Deliv.* **2013**, *10*, 1497-513.

250. Watson, P. M.; Paterson, J. C.; Thom, G.; Ginman, U.; Lundquist, S.; Webster, C. I. Modelling the Endothelial Blood-Cns Barriers: A Method for the Production of Robust in Vitro Models of the Rat Blood-Brain Barrier and Blood-Spinal Cord Barrier. *BMC Neurosci.* **2013**, *14*, 59.

251. Chiu, K.; Agoubi, L. L.; Lee, I.; Limpar, M. T.; Lowe, J. W., Jr.; Goh, S. L. Effects of Polymer Molecular Weight on the Size, Activity, and Stability of Peg-Functionalized Trypsin. *Biomacromolecules* **2010**, *11*, 3688-92.

252. Antosiewicz, J.; Porschke, D. The Nature of Protein Dipole Moments: Experimental and Calculated Permanent Dipole of Alpha-Chymotrypsin. *Biochemistry* **1989**, *28*, 10072-8.

253. Lizarraga, B.; Sanchez-Romero, D.; Gil, A.; Melgar, E. The Role of Ca2+ on Ph-Induced Hydrodynamic Changes of Bovine Pancreatic Deoxyribonuclease A. *J. Biol. Chem.* **1978**, *253*, 3191-5.

254. Marzorati, M.; Vanhoecke, B.; De Ryck, T.; Sadaghian Sadabad, M.; Pinheiro, I.; Possemiers, S.; Van den Abbeele, P.; Derycke, L.; Bracke, M.; Pieters, J.; Hennebel, T.; Harmsen, H. J.; Verstraete, W.; Van de Wiele, T. The Hmi Module: A New Tool to Study the Host-Microbiota Interaction in the Human Gastrointestinal Tract in Vitro. *BMC Microbiol.* **2014**, *14*, 133.

255. Wu, L.; Liu, M.; Zhu, X.; Shan, W.; Huang, Y. Modification Strategies of Lipid-Based Nanocarriers for Mucosal Drug Delivery. *Curr. Pharm. Des.* **2015**, *21*, 5198-211.

256. Ermund, A.; Schutte, A.; Johansson, M. E.; Gustafsson, J. K.; Hansson, G. C. Studies of Mucus in Mouse Stomach, Small Intestine, and Colon. I. Gastrointestinal Mucus Layers Have Different Properties Depending on Location as Well as over the Peyer's Patches. *Am. J. Physiol. Gastrointest. Liver Physiol.* **2013**, *305*, G341-7.

257. Gunther, C.; Buchen, B.; Neurath, M. F.; Becker, C. Regulation and Pathophysiological Role of Epithelial Turnover in the Gut. *Semin Cell Dev Biol* **2014**, *35*, 40-50.

258. Wong, H. M.; Zhao, Y.; Tam, V.; Wu, S.; Chu, P. K.; Zheng, Y.; To, M. K.; Leung, F. K.; Luk, K. D.; Cheung, K. M.; Yeung, K. W. In Vivo Stimulation of Bone Formation by Aluminum and Oxygen Plasma Surface-Modified Magnesium Implants. *Biomaterials* **2013**, *34*, 9863-76.

259. Bolgen, N.; Menceloglu, Y. Z.; Acatay, K.; Vargel, I.; Piskin, E. In Vitro and in Vivo Degradation of Non-Woven Materials Made of Poly(Epsilon-Caprolactone) Nanofibers Prepared by Electrospinning under Different Conditions. *J Biomater Sci Polym Ed* **2005**, *16*, 1537-55.

260. Ayre, W. N.; Denyer, S. P.; Evans, S. L. Ageing and Moisture Uptake in Polymethyl Methacrylate (Pmma) Bone Cements. *J Mech Behav Biomed Mater* **2014**, *32*, 76-88.

261. Arjun, G. N.; Ramesh, P. Structural Characterization, Mechanical Properties, and in Vitro Cytocompatibility Evaluation of Fibrous Polycarbonate Urethane Membranes for Biomedical Applications. *J. Biomed. Mater. Res. A* **2012**, *100*, 3042-50.

262. Traverso, G.; Langer, R. Perspective: Special Delivery for the Gut. *Nature* **2015**, *519*, S19.

263. Fox, C. B.; Cao, Y.; Nemeth, C. L.; Chirra, H. D.; Chevalier, R. W.; Xu, A. M.; Melosh, N. A.; Desai, T. A. Fabrication of Sealed Nanostraw Microdevices for Oral Drug Delivery. *ACS Nano* **2016**, *10*, 5873-81.

264. Bietsch, A.; Hegner, M.; Lang, H. P.; Gerber, C. Inkjet Deposition of Alkanethiolate Monolayers and DNA Oligonucleotides on Gold: Evaluation of Spot Uniformity by Wet Etching. *Langmuir* **2004**, *20*, 5119-22.

265. Xu, T.; Jin, J.; Gregory, C.; Hickman, J. J.; Boland, T. Inkjet Printing of Viable Mammalian Cells. *Biomaterials* **2005**, *26*, 93-9.

266. Daly, R.; Harrington, T. S.; Martin, G. D.; Hutchings, I. M. Inkjet Printing for Pharmaceutics - a Review of Research and Manufacturing. *Int J Pharm* **2015**, *494*, 554-67.

267. Arrabito, G.; Pignataro, B. Inkjet Printing Methodologies for Drug Screening. *Anal Chem* **2010**, *82*, 3104-7.

268. Marizza, P.; Keller, S. S.; Boisen, A. Inkjet Printing as a Technique for Filling of Micro-Wells with Biocompatible Polymers. Microelectronic Engineering: 2013; Vol. 111, pp 391-395.

269. Pommier, Y.; Pourquier, P.; Fan, Y.; Strumberg, D. Mechanism of Action of Eukaryotic DNA Topoisomerase I and Drugs Targeted to the Enzyme. *Biochim Biophys Acta* **1998**, *1400*, 83-105.

270. Palchaudhuri, R.; Hergenrother, P. J. DNA as a Target for Anticancer Compounds: Methods to Determine the Mode of Binding and the Mechanism of Action. *Curr Opin Biotechnol* **2007**, *18*, 497-503.

271. Iyer, H.; Khedkar, A.; Verma, M. Oral Insulin - a Review of Current Status. *Diabetes Obes Metab* **2010**, *12*, 179-85.

272. Glass, N. R.; Tjeung, R.; Chan, P.; Yeo, L. Y.; Friend, J. R. Organosilane Deposition for Microfluidic Applications. *Biomicrofluidics* **2011**, *5*, 36501-365017.

273. Ikawa, M.; Yamada, T.; Matsui, H.; Minemawari, H.; Tsutsumi, J.; Horii, Y.; Chikamatsu, M.; Azumi, R.; Kumai, R.; Hasegawa, T. Simple Push Coating of Polymer Thin-Film Transistors. *Nat Commun* **2012**, *3*, 1176.

274. Sun, Z.; Yathindranath, V.; Worden, M.; Thliveris, J. A.; Chu, S.; Parkinson, F. E.; Hegmann, T.; Miller, D. W. Characterization of Cellular Uptake and Toxicity of

Aminosilane-Coated Iron Oxide Nanoparticles with Different Charges in Central Nervous System-Relevant Cell Culture Models. *Int J Nanomedicine* **2013**, *8*, 961-70.

275. Hidalgo, I. J.; Raub, T. J.; Borchardt, R. T. Characterization of the Human Colon Carcinoma Cell Line (Caco-2) as a Model System for Intestinal Epithelial Permeability. *Gastroenterology* **1989**, *96*, 736-49.

276. Craig, S. B.; Bhatt, U. H.; Patel, K. Stability and Compatibility of Topotecan Hydrochloride for Injection with Common Infusion Solutions and Containers. *J Pharm Biomed Anal* **1997**, *16*, 199-205.

Publishing Agreement

It is the policy of the University to encourage the distribution of all theses, dissertations, and manuscripts. Copies of all UCSF theses, dissertations, and manuscripts will be routed to the library via the Graduate Division. The library will make all theses, dissertations, and manuscripts accessible to the public and will preserve these to the best of their abilities, in perpetuity.

Please sign the following statement:

I hereby grant permission to the Graduate Division of the University of California, San Francisco to release copies of my thesis, dissertation, or manuscript to the Campus Library to provide access and preservation, in whole or in part, in perpetuity.

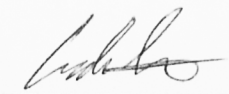

Author Signature

12-19-2016

Date